

# Geochemistry, Geophysics, Geosystems®



## RESEARCH ARTICLE

10.1029/2023GC011126

### Key Points:

- We report age and composition for 119 tephra from sediment cores representing ~6.2 Ma record of explosive volcanism in the NW Pacific
- The tephra have subduction-related origin and mostly originate from volcanic eruptions with magnitude (M) of 5.8–7.8 in Kamchatka
- The data indicates episodes of explosive activity at ~6,200, 5,600–5,000, 4,300–3,700 ka, and almost continuous activity since ~3,000 ka

### Supporting Information:

Supporting Information may be found in the online version of this article.

### Correspondence to:

M. V. Portnyagin,  
[mportnyagin@geomar.de](mailto:mportnyagin@geomar.de)

### Citation:

Ponomareva, V. V., Portnyagin, M. V., Bubenshchikova, N. V., Zelenin, E. A., Derkachev, A. N., Jicha, B., et al. (2023). A 6.2 Ma-long record of major explosive eruptions from the NW Pacific volcanic arcs based on the offshore tephra sequences on the northern tip of the Emperor Seamount Chain. *Geochemistry, Geophysics, Geosystems*, 24, e2023GC011126. <https://doi.org/10.1029/2023GC011126>

Received 10 JUL 2023  
Accepted 28 OCT 2023

### Author Contributions:

**Conceptualization:** V. V. Ponomareva, M. V. Portnyagin

© 2023 The Authors. *Geochemistry, Geophysics, Geosystems* published by Wiley Periodicals LLC on behalf of American Geophysical Union. This is an open access article under the terms of the [Creative Commons Attribution-NonCommercial-NoDerivs License](https://creativecommons.org/licenses/by-nc-nd/4.0/), which permits use and distribution in any medium, provided the original work is properly cited, the use is non-commercial and no modifications or adaptations are made.

## A 6.2 Ma-Long Record of Major Explosive Eruptions From the NW Pacific Volcanic Arcs Based on the Offshore Tephra Sequences on the Northern Tip of the Emperor Seamount Chain

V. V. Ponomareva<sup>1</sup>, M. V. Portnyagin<sup>2</sup> , N. V. Bubenshchikova<sup>3</sup> , E. A. Zelenin<sup>4</sup>, A. N. Derkachev<sup>5</sup>, B. Jicha<sup>6</sup> , S. A. Gorbarenko<sup>5</sup> , E. Cook<sup>7</sup> , D. Garbe-Schönberg<sup>8,9</sup> , and K. Hoernle<sup>2,8</sup>

<sup>1</sup>Institute of Volcanology and Seismology, Petropavlovsk-Kamchatsky, Russia, <sup>2</sup>GEOMAR Helmholtz Center for Ocean Research Kiel, Kiel, Germany, <sup>3</sup>Shirshov Institute of Oceanology, Moscow, Russia, <sup>4</sup>Geological Institute, Moscow, Russia, <sup>5</sup>V.I. Il'ichev Pacific Oceanological Institute, Vladivostok, Russia, <sup>6</sup>Department of Geoscience, University of Wisconsin Madison, Madison, WI, USA, <sup>7</sup>Physics of Ice, Climate and Earth (PICE), Niels Bohr Institute, University of Copenhagen, Copenhagen, Denmark, <sup>8</sup>Kiel University, Kiel, Germany, <sup>9</sup>Department of Physics and Earth Sciences, Jacobs University Bremen, Bremen, Germany

**Abstract** We present a continuous ~6.2 Ma long record of explosive activity from the Northwest Pacific volcanic arcs based on a composite tephra sequence derived from Ocean Drilling Program Sites 882A and 884B, and core MD01-2416 on the Detroit Seamount. Geochemical fingerprinting of tephra glass using major and trace element analyses and correlations of tephra layers between the three cores allowed the identification of 119 unique tephra, suggesting eruptions of magnitude (M) of 5.8–7.8. Age estimates for all the identified eruptions were obtained with the help of published and further refined age models for the studied cores, direct <sup>40</sup>Ar/<sup>39</sup>Ar dating of four ash layers, and Bayesian age modeling. The glass compositions vary from low- to high-K<sub>2</sub>O basaltic andesite to rhyolite and exhibit typical subduction-related affinity. The majority of the tephra originated from Kamchatka, only a few tephra—from the neighboring Kuril and Aleutian arcs. The glass compositions revealed no temporal trends but made it possible to identify their source volcanic zones in Kamchatka and, in some cases, to determine their source eruptive centers. Our data indicates episodes of explosive activity recorded in the Detroit tephra sequence at ~6,200, 5,600–5,000, 4,300–3,700 ka, and almost continuous activity since ~3,000 ka. Within the latter episode, the most active intervals can be identified at 1,700–1,600, 1,150–1,050, and 600–50 ka. Geochemically fingerprinted and dated Detroit tephra sequence form a framework for dating and correlating diverse paleoenvironmental archives across the Northwest Pacific and for studies of geochemical evolution of the adjacent volcanic arcs.

**Plain Language Summary** Explosive volcanic eruptions produce defragmented material named tephra, which can be spread over large distances and form layers in sediments on ocean floor and continents. Long continuous tephra sequences preserved in marine sediments provide one of the best chronicles of the explosive eruptions, and allow detailed evaluation of their timing relative to climatic changes. We studied one of such natural records of explosive volcanism preserved in the sediments covering the Detroit Seamount in the Northwest Pacific. We identified 119 tephra layers, which have been buried in the sediments during the last 6.2 Ma and represent volcanic eruptions with  $\geq 7$  km<sup>3</sup> tephra volume. We analyzed geochemical composition and determined age of each tephra. Most tephra were found to originate from volcanoes in Kamchatka, a few from the Kuril and Aleutian volcanoes. We found that the explosive activity recorded in the Detroit tephra sequence was not uniform over time. It peaked at ~6,200, 5,600–5,000, 4,300–3,700, has continued since ~3,000 thousand years ago until present. All tephra layers from our study can be used as unique isochrons for dating and correlating paleoenvironmental archives across the Northwest Pacific and for the reconstruction of the detailed volcanic record in the Earth history.

## 1. Introduction

The recognition of long-term temporal and compositional patterns in the eruptive activity of volcanic systems is important for understanding of their magmatic and tectonic evolution and associated hazard assessment. Long continuous tephra sequences preserved in marine sediments provide one of the best chronicles of the explosive

**Data curation:** V. V. Ponomareva, M. V. Portnyagin, N. V. Bubenshchikova, E. A. Zelenin, A. N. Derkachev

**Formal analysis:** N. V. Bubenshchikova, E. A. Zelenin, B. Jicha

**Funding acquisition:** V. V. Ponomareva, M. V. Portnyagin, K. Hoernle

**Investigation:** V. V. Ponomareva, M. V. Portnyagin, N. V. Bubenshchikova, E. A. Zelenin, B. Jicha

**Methodology:** V. V. Ponomareva, M. V. Portnyagin, N. V. Bubenshchikova, E. A. Zelenin

**Project Administration:** V. V. Ponomareva, M. V. Portnyagin

**Resources:** A. N. Derkachev, S. A. Gorbarenko, E. Cook, K. Hoernle

**Software:** E. A. Zelenin

**Supervision:** V. V. Ponomareva, M. V. Portnyagin

**Validation:** V. V. Ponomareva, M. V. Portnyagin, N. V. Bubenshchikova, E. A. Zelenin, B. Jicha, D. Garbe-Schönberg

**Visualization:** V. V. Ponomareva, M. V. Portnyagin, N. V. Bubenshchikova, E. A. Zelenin, B. Jicha

**Writing – original draft:** V. V. Ponomareva, M. V. Portnyagin, N. V. Bubenshchikova, E. A. Zelenin

**Writing – review & editing:** V. V. Ponomareva, M. V. Portnyagin, N. V. Bubenshchikova, E. A. Zelenin, A. N. Derkachev, B. Jicha, S. A. Gorbarenko, E. Cook, D. Garbe-Schönberg, K. Hoernle

eruptions, and allow detailed evaluation of the timing of these eruptions relative to climatic changes. Excellent examples of the geochemical time-series studies based on long submarine tephra sequences are known for the Central American volcanic arc (e.g., Kutterolf, Freundt, & Peréz, 2008; Kutterolf, Freundt, Peréz, et al., 2008; Schindlbeck, Kutterolf, Freundt, et al., 2018; Schindlbeck, Kutterolf, Straub, et al., 2018; Schindlbeck et al., 2016), Izu-Bonin-Mariana (Bryant et al., 2003; Lee et al., 1995; Straub, 2003; Straub et al., 2015), and Kermadec island arcs (Shane & Wright, 2011). These studies provided novel and unprecedented datasets on the evolution of these arc systems.

The eruptive histories of the Kuril-Kamchatka and Aleutian volcanic arcs (Northwest Pacific) are less well known, although they are arguably the most productive arcs in the world characterized by highly explosive eruptions (e.g., Bindeman et al., 2010; Braitseva et al., 1995; Cook et al., 2018; Derkachev et al., 2018, 2023; Jensen et al., 2021; Larsen et al., 2007; Leonov & Grib, 2004; Miller & Smith, 1987; Ponomareva, Portnyagin, Pevzner et al., 2015; Ponomareva et al., 2004, 2018). At the same time, the complex stratigraphy of their proximal pyroclastic deposits partly removed by erosion makes detailed reconstruction of past explosive activity and assessment of the magnitude of past eruptions difficult.

In Kamchatka, onshore deposits allowed a detailed reconstruction of the Holocene explosive record (e.g., Braitseva et al., 1995, 1997; Krasheninnikov et al., 2020; Ponomareva et al., 2004, 2013a, 2017). Pre-Holocene proximal pyroclastic deposits, however, have been affected by glaciations and tectonic activity and consist of complex, partially eroded and often densely vegetated successions, permitting reconstruction of only disparate fragments of the eruptive history. Therefore, terrestrial record of the late Miocene-Pleistocene explosive activity in Kamchatka includes only ~30 dated ignimbrites (Bergal-Kuvikas et al., 2019; Bindeman et al., 2010, 2019; Seligman et al., 2014) and a continuous but short (~30 ka) tephra record from the Central Kamchatka Depression (Ponomareva et al., 2021).

To reconstruct a longer continuous record of large explosive eruptions from the Kamchatka volcanoes, a number of studies have examined marine cores and off-Kamchatka lacustrine tephra sequences. West of the Kuril-Kamchatka arc, Derkachev et al. (2012, 2016) provided a systematic record of geochemically characterized tephras found in the Okhotsk Sea sediments. However, only five visible tephras were found in the longest, ~1.1 Ma old core MD01-2415 from the central part of the Okhotsk Sea and only four of these were provisionally attributed to Kamchatka volcanoes, and one to the Kuril arc (Derkachev & Portnyagin, 2013). Shorter and younger cores retrieved from different parts of the Okhotsk Sea were found to contain altogether no more than a dozen of presumably Kuril-Kamchatkan tephras (Derkachev et al., 2016). North of Kamchatka, in the ~3.6 Ma old core from the El'gygytyn Lake (Chukotka) only eight visible tephras were detected, seven of which were likely derived from Kamchatka and one—from the Aleutian arc (van den Bogaard et al., 2014).

Marine cores recovered east of Kamchatka, however, contain much longer and more extensive tephra sequences. In particular, Ocean Drilling Program (ODP) Leg 145 Site 881 on abyssal plane and Sites 882–884 on the Detroit Seamount in the Northwest (NW) Pacific were shown to comprise >100 visible tephra layers deposited during the last ~6 Ma (Figure 1; Cao et al., 1995; Prueher & Rea, 2001; Rea et al., 1993). Cao et al. (1995) geochemically characterized tephras from ODP Sites 881–884; however, the compositions obtained did not allow these authors to correlate any of the analyzed tephras between the cores or to specific source volcanoes. At the same time, recent studies of tephra from ~215 ka-old core SO201-2-40 (Meiji Rise) and ~245 ka-old core Lv63-4-2 (Detroit Seamount), ~400 and 600 km east of Kamchatka, respectively (Figure 1a) have allowed Derkachev et al. (2020, 2023) to identify 36 tephra layers and lenses and geochemically link eight of them to their source volcanoes in Kamchatka. Seven of these tephras were identified at several sites and therefore can be used as markers in the NW Pacific region. In addition, a few Kamchatkan and Aleutian tephras found in the Bering Sea and NW Pacific cores have been geochemically fingerprinted and linked to their sources by Ponomareva et al. (2013a, 2013b) and Derkachev et al. (2018).

Since the cores on the Detroit Seamount seemed the most promising in terms of tephra abundance and preservation, we decided to revisit tephra successions in Sites 882 and 884 and to establish tephra record in core MD01-2416. The first result of this project was the identification and precise dating of tephra from the middle Pleistocene Pauzhetka caldera in South Kamchatka (Ponomareva et al., 2018). A special feature of this initial effort was the geochemical correlation of fresh volcanic glass from distal tephra with the altered proximal ignimbrite, a method further developed in Portnyagin et al. (2020).

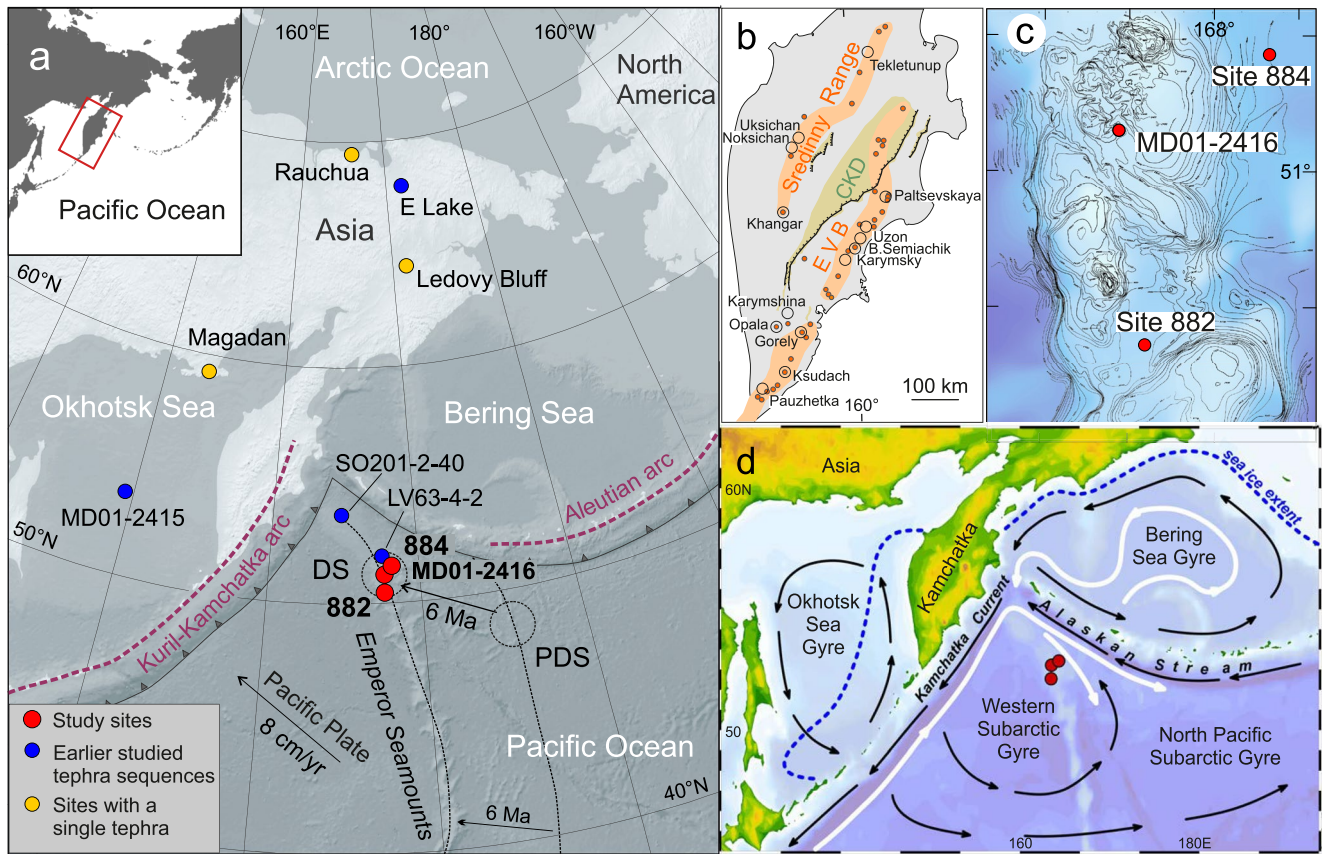


**Figure 1.** Location of the studied sediment cores. (a) Location of the studied ODP Leg 145 Sites 882 and 884 and IMAGES Core MD01-2416 (red circles) on the Detroit Seamount in the NW Pacific. Earlier studied tephra sequences (Derkachev et al., 2016, 2020; van den Bogaard et al., 2014) are shown with blue circles, and sites with a single Kamchatkan tephra—with orange circles. Dashed black lines show modern and ~6 Ma-old positions of the Emperor Seamount Chain: DS—Detroit Seamount, PDS—Paleo-Detroit Seamount. E Lake—El’gygytyn Lake. (b) Position of the Kamchatka volcanic belts (EVB—Eastern Volcanic Belt) and the Central Kamchatka Depression (CKD). Volcanoes are shown with red dots; those mentioned in the text are labeled. (c) Bathymetric chart of the Detroit Seamount area and detailed position of the studied cores. (d) Bathymetric chart of the NW Pacific with mean annual sea ice extent in winter (blue dashed lines), surface (black arrows) and deep (white arrows) circulation patterns (Kawabe & Fujio, 2010; Rostov et al., 2002). The map was created with the ODV 5.0 software (Schlitzer, 2022).

In this paper, we present a continuous ~6.2 Ma record of tephra falls in the NW Pacific “corner” based on three cores on the Detroit Seamount, >600 km downwind from the Kamchatka volcanoes (Figure 1a). Geochemical fingerprinting of tephra glass using ~4,200 electron microprobe analyses along with stratigraphic reasoning and age estimation permitted the correlation of many tephra layers between the sites and the reconstruction of the composite sequence containing 119 unique tephras. About one hundred tephras from this sequence were additionally analyzed with the help of single-shard LA-ICP-MS analysis. For dating of tephras in the three cores, we refined published stable oxygen isotope ( $\delta^{18}\text{O}$ )- and/or paleomagnetic- based age models by using of the up-to-date reference stacks. In addition, we obtained five  $^{40}\text{Ar}/^{39}\text{Ar}$  dates for four tephras. We then determined the ages of tephras in the composite sequence with the help of the Bayesian modeling using relevant tie-points.

The far-western part of the Aleutian arc contains only one young volcanic center—the submarine Piip volcano. For this reason and because of the prevailing westerly winds in this region, we believe that most of the Detroit tephras have been derived from the Kamchatka volcanoes although occasional tephras from the Aleutian or Kuril arcs may also occur. At this stage, we were able to identify source volcanoes for 16 tephra layers, including a tephra layer related to the Pauzhetka caldera and eight layers associated with the Gorely eruptive center in South Kamchatka. Seventeen tephra layers were correlated to their proximal or distal counterparts, which had been dated elsewhere. Trace element composition of the tephras has allowed us to determine the source volcanic zones in Kamchatka. The composite Detroit sequence of geochemically characterized and dated tephra layers is the first ever record of the largest explosive eruptions in the region for the last 6.2 Ma. In addition, it can serve as a reference for regional and even hemispheric tephra correlations across disparate paleoenvironmental archives.

## 2. Northwest Pacific Volcanic Arcs

Our study sites lie in the NW Pacific, near the junction of the Kuril-Kamchatka and Aleutian island arcs (Figure 1a), which owe their existence to the subduction of the Pacific Plate. Overall, the Kuril-Kamchatka and Aleutian arcs host about 150 recently active volcanic centers, more than 75 calderas, and hundreds of monogenetic vents (Global Volcanism Program, 2023, <https://volcano.si.edu/>). The continuous volcanic activity for the Kuril Islands is known since Miocene (Avdeiko et al., 1992) and for most of the Aleutian Islands—for the last 6 Ma (Jicha et al., 2006). The far-western part of the Aleutian arc is almost amagmatic with only one large Late Pleistocene-Holocene submarine Piip volcano and a number of small submarine cones (Seliverstov et al., 1995; Yogodzinski et al., 2015).

The Kamchatka Peninsula is a complex tectonic assemblage of island arc terranes (Konstantinovskaia, 2001; Lander & Shapiro, 2007). Kamchatka hosts two major volcanic belts running NE–SW along the peninsula: Eastern volcanic belt (EVB) and Sredinny Range (SR) (Figure 1b). Prior to the Pliocene, SR extending to the South Kamchatka was the only volcanic belt in Kamchatka. The available data suggest normal subduction-related volcanism and conditions of magma generation similar to the present-day EVB (Avdeiko et al., 2007). During the Neogene, a south to north successive accretion of the paleo-Kronotsky arc to Kamchatka caused shift of the volcanic front from the Sredinny Range to its present position forming the EVB (Avdeiko et al., 2007; Lander & Shapiro, 2007; Volynets, 1994). The current configuration of the volcanic belts has existed since ~2.5 Ma (Avdeiko et al., 2007). The EVB includes the volcanic front (VF), rear-arc (RA) in the southern (51–53°N) and central segments (53–55°N), and the volcanic zone of the Central Kamchatka Depression (CKD) in the north (55–57°N).

The major and trace element compositions of volcanic rocks from the Kuril-Kamchatka and Aleutian arcs generally overlap, which does not allow a clear identification of the origin of distal tephra. The latter can be most reliably identified by Pb isotope ratios (e.g., van den Bogaard et al., 2014). At the same time, the growing body of geochemical data for both arcs allows some insight into possible source zones for specific tephra. The composition of the Aleutian volcanic rocks changes along the arc (Kay & Kay, 1994; Kelemen et al., 2003; Nye et al., 2018; Singer et al., 2007). The composition of the Kuril-Kamchatka volcanic rocks, however, changes across the arc: K<sub>2</sub>O contents in late Pliocene-Quaternary bulk rocks and glasses tend to increase from the volcanic front to the rear of the arc, although there is a significant overlap in major element compositions between the different volcanic zones (Churikova et al., 2001; Portnyagin et al., 2020; Volynets, 1994). Trace elements in rocks and glasses from different volcanic zones show a wider range of concentrations and ratios, which allows a more reliable identification of source zones for distal Kamchatkan tephra (Portnyagin et al., 2020). Data on the composition of pre-Pliocene rocks are limited and their sources uncertain.

## 3. Materials and Methods

### 3.1. Sediment Cores and Tephra Sampling

We examined tephra samples from three sediment cores retrieved at the Detroit Seamount on the northern tip of the Emperor Seamount Chain (NW Pacific) (Figure 1a; Table 1; Table S1). Two of these, Sites 882A and 884B were drilled in 1992 during ODP Leg 145 by the research vessel (R/V) JOIDES Resolution (Rea et al., 1993). The third one—core MD01-2416 was obtained in 2001 during the WEPAMA cruise of the R/V Marion Dufresne (Holbourn et al., 2002).

Core MD01-2416 is located on a summit of the Detroit Seamount at a depth of 2,317 m.b.s.l., while Sites 882A and 884B are located on the southeastern and western flanks of the seamount at deeper depths of 3,244 m.b.s.l. and 3,826 m.b.s.l., respectively (Figure 1c) (Holbourn et al., 2002; Rea et al., 1993). Site 884B is positioned on the Meiji Drift deposit likely formed due to sediment transport by deep ocean currents (Scholl et al., 1977; VanLaningham et al., 2009). The distance between the northernmost Site 884 and southernmost Site 882 is ~130 km. All three cores lie beneath the counterclockwise Western Subarctic gyre (Figure 1d).

For our sampling, we examined the entire cores for Site 882A and core MD01-2416 and the upper 330 m of Site 884B, which have been estimated to correspond to the late Miocene through Quaternary (Table 1; Figure 2). The core MD01-2416 sediments are siliciclastic to diatomaceous-calcareous ooze, which correspond to the past ~1.1 Ma (Figures 2 and 3) (Gebhardt et al., 2008; Holbourn et al., 2002). The ODP cores are dominated by

**Table 1**  
*Sampled Cores and Identified Tephra*

Research cruise	Sampled cores	Coordinates	Initial reports	Core length recovered/ sampled (m)	Time interval sampled (Ma) <sup>a</sup>	Samples taken/ analyzed	Identified tephras	Tephra thickness (cm)		
								Min	Max	Total
Ocean Drilling Program Expedition 145	882A	N 50.3633°	Rea et al. (1993)	398.3	~5.7	159/77	66	0.5	20	396
		E 167.6000°								
MD 122/WEPAMA	MD01-2416	N 51.2680°	Holbourn et al. (2002)	44.75	~1.1	59/59	41	0.5	182	943
		E 167.72550°								
Ocean Drilling Program Expedition 145	884B	N 51.4504°	Rea et al. (1993)	853.9/upper 330	~6.2	143/87	69	0.5	20	273
		E 168.3371°								

<sup>a</sup>refined in this study.

clayey diatom ooze at 0–100 m and by diatom ooze at 100–398.3 m at Site 882A, and by clay and silt at 0–125 m and clayey diatom ooze at 125–330 m at Site 884B; the two intervals at each site correspond to 0–2.6 and 2.6–5.7/6.2 Ma, respectively (Figures 2–5) (Weeks et al., 1995).

Tephra in the studied cores occur as visible layers, pods, and sediment intervals enriched in tephra particles (Figure 6). Tephra from the core MD01-2416 were collected on-board, whereas both ODP cores were sampled in the Gulf Coast Repository, Texas A&M University, College Station (USA). In our sampling of the ODP cores, we relied on the on-board description (Rea et al., 1993) and sampling by Cao et al. (1995). We typically took one sample per layer, but two or three samples from thick layers. Overall, we collected 361 samples and selected 223 of them for geochemical analyses (Table S1).

High-resolution images of the archive halves of the ODP cores can be found at the Gulf Coast Repository site: [http://iodp.tamu.edu/curation/imagerep/legacy\\_core\\_photos/Leg145/](http://iodp.tamu.edu/curation/imagerep/legacy_core_photos/Leg145/).

### 3.2. Geochemical Studies

Geochemical studies included electron probe microanalysis (EPMA) and laser ablation ICP-MS (LA-ICP-MS) microanalyses of volcanic glass. We have obtained ~4,200 EPMA analyses on ~200 tephra samples (Tables S1 and S2). All EPMA analyses were performed at GEOMAR (Kiel, Germany); most of them in 2017, and a half of the core MD01-2416 analyses in 2010. The glasses were analyzed using a JEOL JXA 8200 electron microprobe equipped with five wavelength dispersive spectrometers. The analytical conditions were 15 kV accelerating voltage, 6 nA current, and 5 μm electron beam size for all analyses. Counting times were 5/10 s (peak/background) for Na, 20/10s for Si, Al, Mg, Ca, P, 30/15 s for Fe, K, Ti, Cl, S, 40/20 s for F and 60/20 s for Mn. Short counting times and defocused beam allowed us to minimize Na loss during our microprobe analyses and reproduce reference values for both dry (e.g., Lipari obsidian; Kuhn et al., 2011) and hydrous (e.g., Old Crow rhyolite glass; Kuhn et al., 2011) reference glasses within 5% relative or better using the same analytical conditions as in this study (Portnyagin et al., 2020). Data on EPMA reference materials obtained in the course of this study are listed in Table S2. For a given concentration, two standard deviations (analytical precision at 95% probability) were calculated from replicate analyses of reference glasses in Table S2. For example, SiO<sub>2</sub> in rhyolite glasses is analyzed with uncertainty ±0.5 wt% as calculated from replicate analyses of Lipari obsidian and VG568 rhyolite reference glasses normalized to 100 wt% totals. Further details of the analytical technique and associated analytical uncertainties are provided by Portnyagin et al. (2020).

LA-ICP-MS analyses of major and trace elements in 103 tephra samples were performed at the Institute of Geosciences at Kiel University (Kiel, Germany) mostly in 2017. In addition, we reanalyzed three tephra from the El'gygytgyn Lake core (van den Bogaard et al., 2014). The analyses were obtained using an ICP-MS Agilent 7900s coupled to a Coherent GeoLas HD ArF 193 nm Excimer LA system operated with a fluence of 5 J cm<sup>-2</sup>, at a repetition rate of 10 Hz and a 15–24 μm ablation spot size. The analyses included all major elements (Si, Ti, Al, Fe, Mn, Mg, Ca, Na, K, P), and the data were quantified by adjusting the sum of major elements to 100 wt%, allowing direct comparison with EPMA data and easy identification and rejection of analyses contaminated by mineral phases. Detailed description of the analytical setup, procedures of data quantification, and quality control are provided by Portnyagin et al. (2020). The data for tephra glasses and reference materials obtained during the

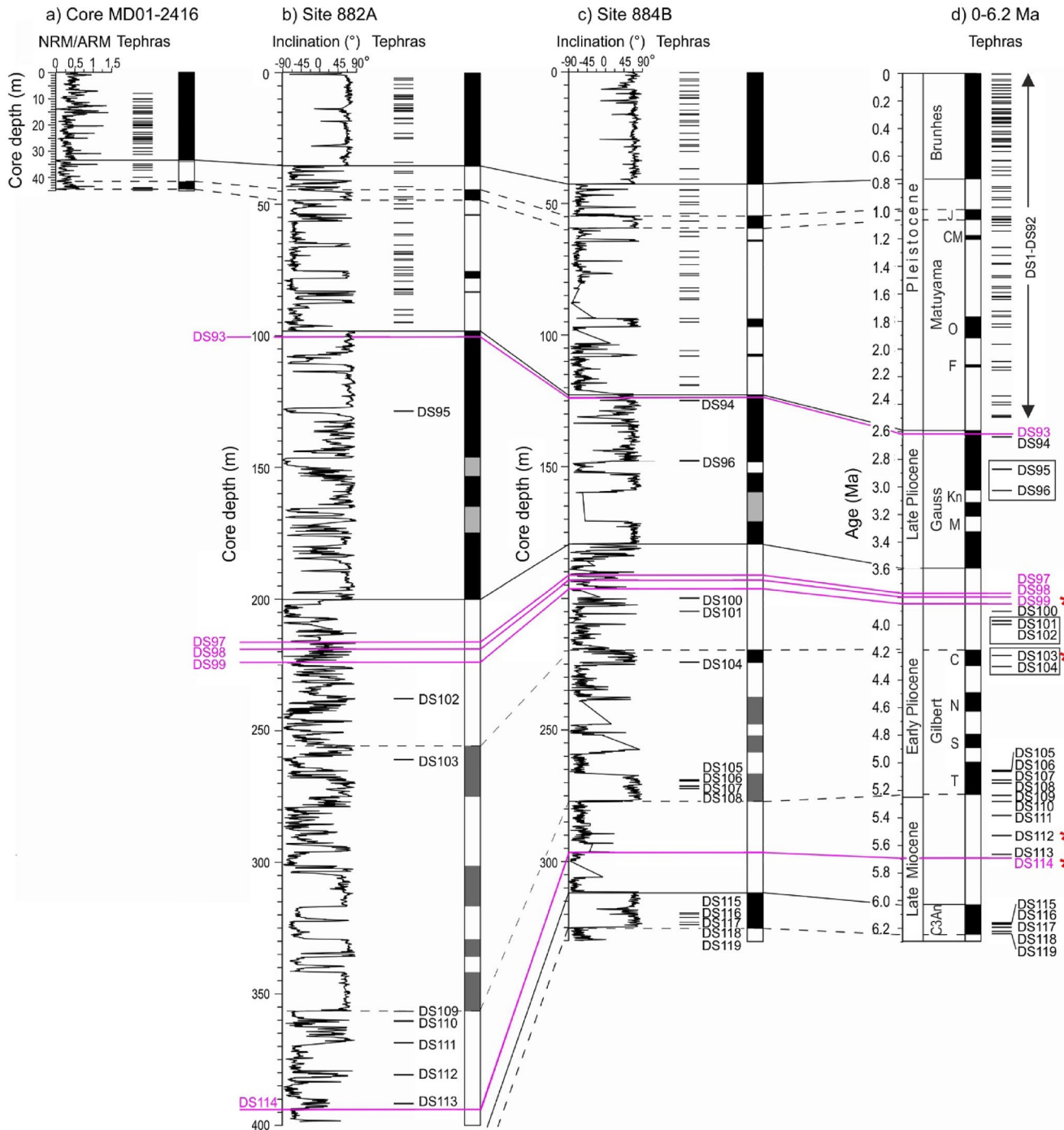


**Figure 2.** An overview of the Detroit tephra sequences. (a–c) Tephra sequences in Core MD01-2416, and Sites 882A and 884B shown with the refined core magnetostratigraphies by the intensity or inclination records (Gebhardt et al., 2008; Rea et al., 1993; Weeks et al., 1995) tied to polarity zones (Lourens et al., 2004; Ogg, 2012); (d) 0–6.2 Ma composite sequence of the Detroit Seamount (DS) tephras with the sedimentation rates (SRs)-based ages (Tables 2 and 3; Table S5). Positions and correlations of the DS93 to DS119 tephras (in magenta) are shown here, and those of the DS1 to DS92 tephras are presented in Figures 3–5. The tephras with uncertain relative stratigraphic positions are shown in boxes. Tephras dated by  $^{40}\text{Ar}/^{39}\text{Ar}$  (Table 4; Table S6) are shown with red asterisks. Normal and reversed polarity zones are shown in black and white, respectively. Black solid and hatched tie lines represent selected magnetostratigraphic datums (all datums are in Table S4). Uncertain paleomagnetic events are marked in gray. J—Jaramillo, CM—Cobb Mountain, O—Olduvai, F—Feni, Kn—Kaena, M—Mammoth, C—Cochiti, N—Nunivak, S—Sidufjall, T—Thvera.

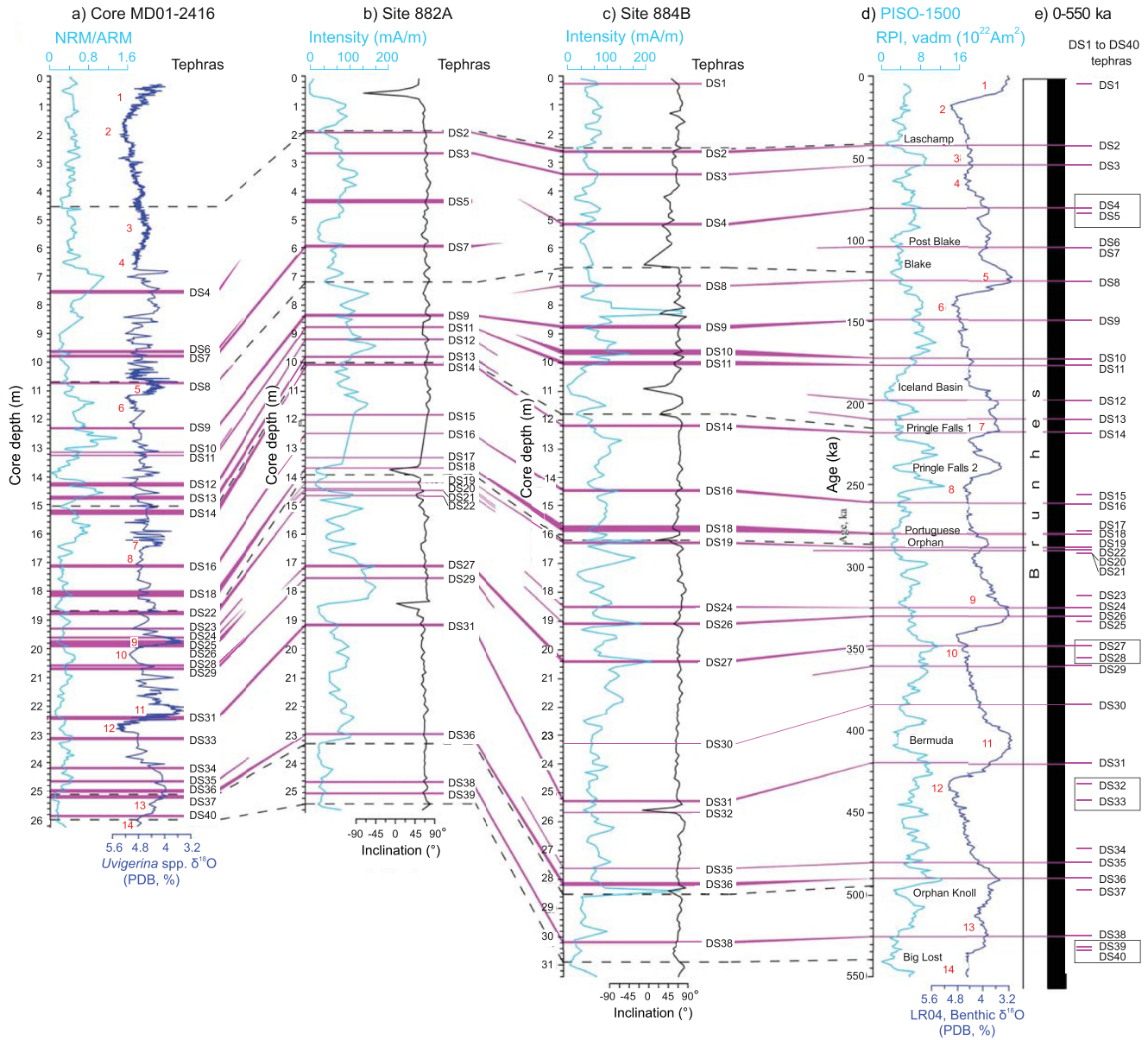


**Figure 3.** Stratigraphic position of tephras *DS1* to *DS40* in Detroit cores. (a) NRM/ARM and *Uvigerina* spp.  $\delta^{18}\text{O}$  records of Core MD01-2416 (0–26 m core depth) (Gebhardt et al., 2008) and (b, c) Intensity and inclination records of Site 882A (0–25.4 m core depth) and Site 884B (0–31 m core depth) (Rea et al., 1993; Weeks et al., 1995) tied to (d) LR04, PISO-1500 and polarity zones (Channell et al., 2020; Lisiecki & Raymo, 2005). Marine isotope stages are shown with red numbers. (e) 0–550 ka sequence of the *DS1* to *DS40* tephras with the sedimentation rates (SRs)-based ages (Table 2; Tables S4 and S5).

same analytical sessions are provided in Table S3. Two standard deviations were calculated from replicate analyses of reference glasses. For most elements, measurement uncertainty is within 5%–13% relative.

Geochemical fingerprinting of tephra glass along with stratigraphic reasoning permitted the correlations of many tephra layers between the three cores and reconstruction of the composite tephra sequence containing 119 unique tephras labeled *DS1*–*DS119* (Section 4.4).

In order to identify source volcanic zones and source volcanoes of the Detroit tephras, we compared their geochemical characteristics to our database of the Kamchatka proximal glass compositions (Portnyagin et al., 2020). However, limited stratigraphic and geochemical data on pre-Holocene proximal Kamchatka pyroclastic deposits rarely permitted direct comparisons between the proximal and distal tephras of the same eruptions in the past. Therefore, we first identified a source volcanic zone and then narrowed the set of possible source volcanoes

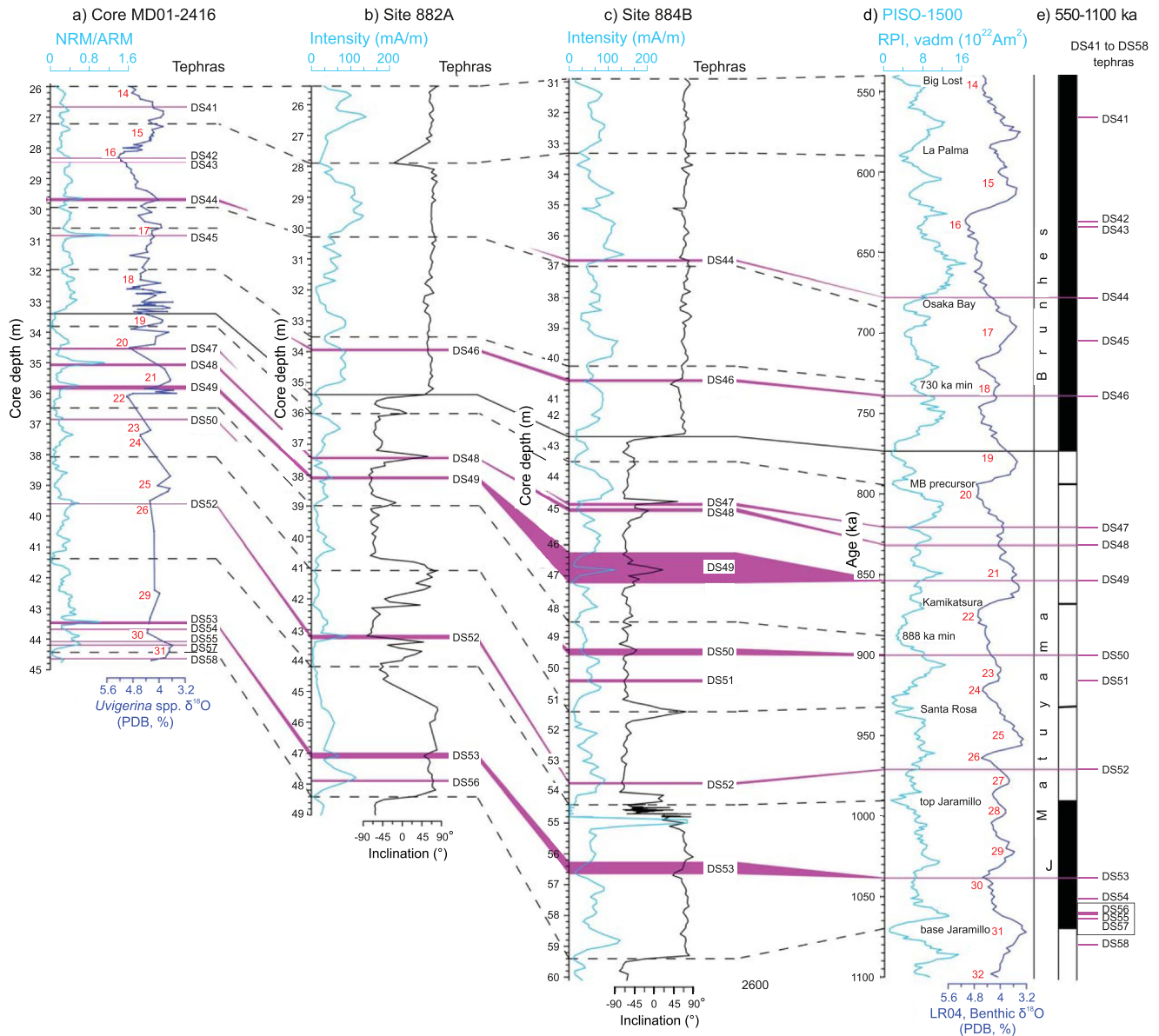


**Figure 4.** Stratigraphic position of tephras *DS41* to *DS58* in Detroit cores. (a) NRM/ARM and *Uvigerina* spp.  $\delta^{18}\text{O}$  records of Core MD01-2416 (26–44.75 m core depth) (Gebhardt et al., 2008), (b, c) Intensity and inclination records of Site 882A (25.4–48.4 m core depth) and Site 884B (31–59.4 m core depth) (Rea et al., 1993; Weeks et al., 1995) tied to (d) LR04, PISO-1500, and polarity zones (Channell et al., 2020; Lisiecki & Raymo, 2005). Marine isotope stages are shown with red numbers. (e) 550–1,100 ka sequence of the *DS41* to *DS58* tephras with the SRs-based ages (Table 2; Tables S4 and S5). See Figure 2 and text for further explanations.

within this zone by comparing tephra trace element compositions with those of the younger rocks from individual eruptive centers. In addition, we compared our data to the available dataset for submarine distal tephra from the NW Pacific (Derkachev et al., 2018, 2020, 2023), Okhotsk Sea (Derkachev et al., 2016), and El'gygytyn Lake (van den Bogaard et al., 2014).

### 3.3. Tephra Ages Assessment

The tephra ages were determined through the refinement of the published core age models, direct dating of four tephras by the  $^{40}\text{Ar}/^{39}\text{Ar}$  technique, and subsequent Bayesian modeling. The youngest tephra in the Detroit tephra sequence and the only Holocene tephra in this study (labeled *DS1*) was found in Site 884B and correlated to the Karymsky caldera ash (KRM), which has also been traced in the Greenland NGRIP ice core and has an age of

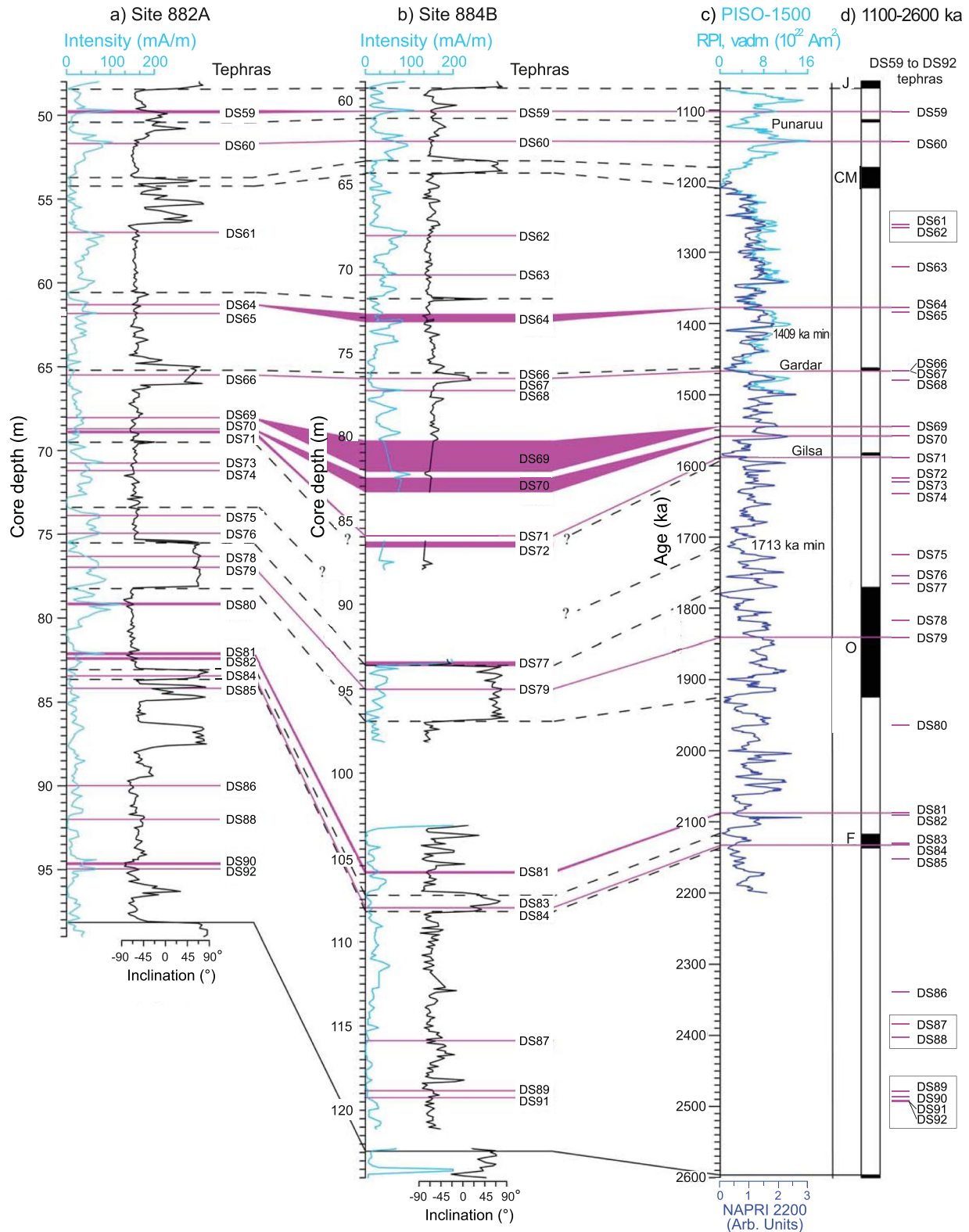


**Figure 5.** Stratigraphic position of tephras *DS59* to *DS92* tephras in Detroit cores and the core magnetostratigraphy. (a, b) Intensity and inclination records of Site 882A (48.4–98 m core depth) and Site 884B (59.4–124 m core depth) (Rea et al., 1993; Weeks et al., 1995) tied to (c) PISO-1500, NARPI-2200 and polarity zones (Channell et al., 2020; Lisiecki & Raymo, 2005); (d) 1,100–2,600 ka sequence of the *DS59* to *DS92* tephras with the SRs-based ages (Table 3; Tables S4 and S5). This part of the sequence lies within the Matuyama reversed magnetic polarity interval.



**Figure 6.** Tephra layers from Site 882A. (a–d)—archive halves, (e)—work half. (a) normal-graded silicic ash *DS9* from the Gorely eruptive center; (b) subvertical ash patch; (c) pumice lapilli likely from a pumice raft; (d, e) the same ash in the archive and working parts of the core; the ash is underlain by compositionally different pumice lapilli seen only in the working half. For each photo, tephra ID, site, hole, core, and section number are provided. High-resolution images of the archive halves of the studied ODP cores can be viewed at [http://iodp.tamu.edu/curation/imagerep/legacy\\_core\\_photos/Leg145/](http://iodp.tamu.edu/curation/imagerep/legacy_core_photos/Leg145/).

$9,045 \pm 64$  b2k (before 2000 CE) (Section 5.3; details of the study of the Karymsky caldera ash in the NGRIP will be published elsewhere).

### 3.3.1. Dating With the Help of Refined Core Age Models

Ages of all tephras from three cores, except the *DS1* tephra from Site 884B, were derived from the refined magnetostratigraphy for Sites 882A and 884B (Rea et al., 1993; Weeks et al., 1995) and combined magneto- and  $\delta^{18}\text{O}$  stratigraphy for core MD01-2416 (Gebhardt et al., 2008). The age data were generated in several steps.

First, all tephra layers were plotted versus the correlative records of inclination and intensity for Sites 882A and 884B, and natural remanent magnetization to anhysteretic remanent magnetization ratio (NRM/ARM) and *Uvigerina* spp.  $\delta^{18}\text{O}$  for core MD01-2416 (Figures 2–5) (Gebhardt et al., 2008; Rea et al., 1993; Weeks et al., 1995). Then, the stratigraphic positions of the geochemically correlated tephras were verified. To minimize inaccuracy in our calculations, we transformed the core depth of the correlative proxies into the corrected depths subtracting the tephra thicknesses. In total, the lengths of Site 882A and core MD01-2416, and the studied interval of Site 884B were reduced by 395.5, 273, and 942.5 cm, respectively (Table 1, Tables S4 and S5). Further, we defined new datum levels by establishing magnetic reversals and relative paleointensity (RPI) events in Sites 882A and 884B, and the RPI and marine isotope stage (MIS) events in core MD01-2416 by using Geomagnetic Polarity Time Scale (GPTS), PICO-1500, NARPI-2200, and LR04 as references (Channell et al., 2020; Lisiecki & Raymo, 2005; Lourens et al., 2004; Ogg, 2012). The tephra ages were calculated assuming linear sedimentation rates (SRs) between the newly obtained datum levels (Table S5). A mean tephra age was calculated if more than one estimate was available (Tables 2 and 3 and Figures 2–5).

### 3.3.2. $^{40}\text{Ar}/^{39}\text{Ar}$ Dating

Detroit tephras are poor in mineral grains and/or fine grained so the direct dating was only possible for four tephras from Site 882A. Five  $^{40}\text{Ar}/^{39}\text{Ar}$  dates were obtained on biotite crystals from these four tephras (Table 4; Table S6; Figure S1 in Supporting Information S1). Mineral separates were irradiated along with the 28.201 Ma Fish Canyon sanidine standard (Kuiper et al., 2008) at the Oregon State University TRIGA reactor in the Cadmium-Lined In-Core Irradiation Tube (CLICIT). Single crystal fusion experiments were performed with a 50 W  $\text{CO}_2$  laser in the WiscAr laboratory at the University of Wisconsin-Madison. Gas was analyzed using a Noblesse multi-collector mass spectrometer following the procedures in Jicha et al. (2016). Because of the extremely low Ar yields ( $\sim 2\times$ – $10\times$  the blank for  $^{40}\text{Ar}$  and  $^{36}\text{Ar}$ ) from the very small biotites ( $\sim 50$ – $60$  microns in diameter), analytical blanks were measured before and after every single crystal fusion. Weighted mean ages are calculated using the decay constants of Min et al. (2000), and are reported with analytical uncertainties at the 95% confidence level.

**Table 2**  
Composite Tephra Sequence Based on the Detroit Seamount Sites 882A and 884B, and Core MD01-2416 (0–1,100 ka)

Detroit tephra ID/alt. ID	Modeled age (ka)	Error 2σ (ka)	SRS-based age (ka)	Volcanic zone	882A #	Thick-ness (cm)	MD01-2416 ID	Alt. MD01-2416 #	Thick-ness (cm)	884B #	Thick-ness (cm)	Source	Marine isotope stage (event)	Paleomagnetic event/interval
DS1/KRM	9	0.2	-	VF				1	0.5			Karymsky eruptive center, Karymsky caldera		
DS2/WP4; D2	50.0	2.8	42.2	RA	1	1.0		2	5.0			Gorely eruptive center	3	Laschamp
DS3	60.3	3.2	54.1	VF	2	0.5		3	1.0			Ksudach?		Blake—Laschamp
DS4/WP5	77.5	9.0	80.5	RA			dt11	1	10.0	4	5.0	Gorely eruptive center	5	Blake—Laschamp
DS5	78.8	2.6	83.5	Aleutian arc?	3	12.0						?		Blake—Laschamp
DS6	96.8	6.8	104.7	VF			dt12	2	6.0			?		Blake—Laschamp
DS7/WP8	101.4	4.4	104.3	VF	4	7.0	dt1	3	8.0			Karymsky eruptive center	5	Blake—Laschamp
DS8/D5	121.8	9.4	125.2	Aleutian arc?			dt2	4	0.5	5	4.0	?		Island Basin—Blake
DS9/DL1	150.9	6.4	149.0	RA	5	8.0	dt3	5	6.0	6	9.0	Gorely eruptive center	6	Island Basin—Blake
DS10/WP9	158.2	7.0	172.6	RA			dt4	6	3.0	7	16.0	Gorely eruptive center	6	Island Basin—Blake
DS11	159.0	6.6	176.6	?	6	0.5	dt13	7	3.0	8	9.0	?		Island Basin—Blake
DS12/DL2	195.0	8.4	198.0	SR	7	0.5	dt14	8	10.0			Khangar	7	Pringle Falls 1—Island Basin
DS13/WP15?	208.4	5.4	209.9	VF	8	2.5	dt5	9	13.0			South Kamchatka?	7	Pringle Falls 1—Island Basin
DS14/D7	213.6	8.4	217.9	VF	9	2.5	dt15	10	15.0	9	6.0	?	7 (TIIIa)	Pringle Falls 2—Pringle Falls 1
DS15	251.7	5.6	255.8	RA	10	4.0						Gorely eruptive center		Portuguese Orphan—Pringle Falls 2
DS16/D8	262.5	6.4	261.2	VF	11	2.0	dt16a,b	11	8.0	10	9.0	Uzon caldera	8	Portuguese Orphan—Pringle Falls 2
DS17	273.2	5.0	277.6	VF or Kuril arc	12	2.0						Ksudach?		Portuguese Orphan—Pringle Falls 2
DS18	278.9	11.8	279.7	RA	13	5.5	dt17a,b,c	12	18.0	11	18.0	Gorely eruptive center	9	Portuguese Orphan
DS19	281.4	11.2	288.1	VF	14	1.5				12	6.0	Uzon caldera	9	Portuguese Orphan
DS20	291.2	8.0	291.7	VF or Kuril arc	15	2.0						?		Bermuda—Portuguese Orphan
DS21	292.1	8.8	291.8	VF	16	3.0						?		Bermuda—Portuguese Orphan
DS22	296.6	13.6	289.6	VF	17	4.0	dt18	13	11.0			Karymsky eruptive center, Polovinka caldera (sample 1999-L9)	9	Bermuda—Portuguese Orphan

**Table 2**  
*Continued*

Detroit tephra ID/alt. ID	Modeled age (ka)	Error $2\sigma$ (ka)	SRS-based age (ka)	Volcanic zone	882A #	Thickness (cm)	MD01-2416 ID	Alt. MD01-2416 #	Thickness (cm)	884B #	Thickness (cm)	Source	Marine isotope stage (event)	Paleomagnetic event/interval
DS23	309.0	16.4	317.5	SR			dt19	14	1.0			Khangar?	9	Bermuda—Portuguese Orphan
DS24	323.0	13.0	324.5	SR			dt20	15	8.0	13	2.0	Khangar	9	Bermuda—Portuguese Orphan
DS25	329.9	9.8	333.3	?			dt6	16	20.0				10-9 (TIV)	Bermuda—Portuguese Orphan
DS26	335.2	10.0	329.8	VF			dt21	17	6.0	14	6.0	Karymsky eruptive center	10-9 (TIV)	Bermuda—Portuguese Orphan
DS27	350.6	10.0	347.7	RA	18	5.0				15	7.5	Gorely eruptive center		Bermuda—Portuguese Orphan
DS28	350.7	5.6	355.6	?			dt22	18	4.0			?	10	Bermuda—Portuguese Orphan
DS29	358.0	5.8	360.4	VF	19	2.0	dt23	19	6.0			?	10	Bermuda—Portuguese Orphan
DS30	390.2	27.8	383.9	?						16	2.5	?		Bermuda—Portuguese Orphan
DS31	418.1	4.8	419.5	RA	20	6.5	dt25	20	8.5	17	4.0	Pauzhetka caldera	12-11 (TV)	Orphan Knoll -Bermuda
DS32	428.4	25.0	432.2	VF						18	4.0	?		Orphan Knoll -Bermuda
DS33	450.0	13.6	442.6	RA			dt26	21	8.0			Gorely eruptive center	12	Orphan Knoll—Bermuda
DS34	470.2	10.2	471.7	?			dt27	22	4.0			?	13	Orphan Knoll—Bermuda
DS35	476.6	6.4	480.2	RA			dt28	23	3.0	19	1.0	Pauzhetka caldera area?	13	Orphan Knoll -Bermuda
DS36	478.3	5.8	489.9	VF	21	1.0	dt29	24	7.0	20	10.0	?	13	Orphan Knoll
DS37	496.0	13.6	497.2	?			dt30	25	8.0			?	13	Orphan Knoll
DS38	523.2	7.0	525.2	VF	22	1.0				21	4.0	Bolshei Semiachik (sample 1990L-8)		Big Lost—Orphan Knoll
DS39	533.9	9.6	532.2	VF	23	2.5						?		Big Lost—Orphan Knoll

**Table 2**  
*Continued*

Detroit tephra ID/alt. ID	Modeled age (ka)	Error 2σ (ka)	SRS-based age (ka)	Volcanic zone	882A #	Thickness (cm)	MD01-2416 ID	Alt. MD01-2416 #	Thickness (cm)	884B #	Thickness (cm)	Source	Marine isotope stage (event)	Paleomagnetic event/interval
DS40	535.6	14.6	534.0	?			dt31	26	3.0			?	14-13 (TVI)	Big Lost—Orphan Knoll
DS41	566.3	16.4	566.1	VF			dt32	27	3.0			?	15-14	La Palma—Big Lost
DS42	627.1	14.4	630.8	?			dt8	28	3.0			?	16 (TVII)	Osaka Bay—La Palma
DS43	637.0	13.2	633.7	?			dt34	29	3.0			?	16 (TVII)	Osaka Bay—La Palma
DS44/T2	677.6	13.2	679.7	VF			dt35	30	10.0	22	7.0	?	17	Osaka Bay
DS45	703.4	16.8	704.8	?			dt9	31	3.0			?	17 (TVIII)	MB—Osaka Bay
DS46	747.9	7.4	739.1	VF	24	6.0	dt36	32	3.0	23	10.0	?	20	MB—Osaka Bay
DS47/T3?	796.9	24.6	820.8	VF								Paltsevskaia (sample 1082-79)		Kamikatsura—MB precursor
DS48	837.8	11.2	831.7	VF	25	5.0	dt10	33	8.0	25	11.5	?	21	Kamikatsura—MB precursor
DS49	853.3	8.2	853.6	Kuril arc?	26	8.5	dt37a,b	34	13.0	26	101.0	?	22-21 (TX)	Kamikatsura—MB precursor
DS50	894.4	13.0	900.0	VF			dt38	35	4.0	27	22.0	Paltsevskaia (samples 1076-79, 1002-79)	23	Santa Rosa—Kamikatsura
DS51	906.9	23.6	915.7	Aleutian arc?						28	11.0	?		Santa Rosa—Kamikatsura
DS52	953.0	8.6	971.0	VF	27	12.0	dt39	36	4.0	29	4.5	?	26-25 (TXII)	Jaramillo—Santa Rosa
DS53	1043.2	8.0	1038.4	VF? RA?	28	19.0	dt40	37	8.0	30	41.0	?	30	Jaramillo
DS54	1049.0	8.6	1051.3	?			dt42	38	3.0			?	30	Jaramillo
DS55	1057.9	9.4	1061.5	?			dt43	39	3.0			?	31	Jaramillo
DS56	1061.3	12.6	1060.1	VF	29	2.5						?		Jaramillo
DS57	1065.2	10.0	1064.0	?			dt44	40	4.0			?	31	Jaramillo
DS58	1078.7	12.8	1079.7	?			dt45	41	3.0			?	32-31 (TXIV)	Punaruu—Jaramillo

*Note.* Column 1 lists DS1 to DS58 tephras from the composite Detroit sequence and alternative (alt.) IDs for geochemically identical tephras from other sites (Braitseva et al., 1997; Derkachev et al., 2020, 2023; van den Bogaard et al., 2014). In columns 2 and 3, modeled ages and associated errors are calculated using Bayesian approach (Text S1 in Supporting Information S1, Model S1 in Supporting Information S2, Table S7). In column 4, sedimentation rate-based (SRS) ages are derived from refined core age models (Tables S4 and S5). Kamchatka volcanic zones: VF—volcanic front, RA—rear-arc and SR—Sredinny Range. Tephra layers correlated between two or three cores are highlighted in gray. In column 13, matching samples of proximal pyroclastic deposits based on Portnyagin et al. (2020). In column 14, marine isotope stages and terminations follow LR04; a Termination (T) is a period of rapid transition from full glacial to full interglacial climates during a glacial cycle (Lisiecki & Raymo, 2005). In column 15, paleomagnetic events/intervals follow PICO-1500 (Channell et al., 2020).

**Table 3**

*Composite Tephra Sequence Based on the Detroit Seamount Sites 882A and 884B (~1,100–6,235 ka)*

Detroit tephra ID/alt. ID	Modeled age (ka)	Error 2σ (ka)	SRs-based age (ka)	Volcanic zone	882A #	Thick-ness (cm)	884B #	Thick-ness (cm)	Source	Paleomagnetic event/interval
DS59	1101.3	15.4	1101.9	VF	30	15.0	31	14.0	Paltsevskaia caldera	Punaruu—Jaramillo
DS60	1134.2	31.6	1144.0	VF	31	7.5	32	7.0	Paltsevskaia caldera	Cobb Mountain—Punaruu
DS61	1269.3	93.2	1260.9	VF	32	2.0			?	1409 ka PICO-1500 min—Cobb Mountain
DS62	1294.2	25.6	1264.1	Aleutian arc?			33	3.0	?	1409 ka PICO-1500 min—Cobb Mountain
DS63	1339.0	82.8	1320.0	VF			34	3.0	Paltsevskaia caldera	1409 ka PICO-1500 min—Cobb Mountain
DS64	1422.1	19.2	1377.2	VF	33	9.0	35	46.0	?	Gardar—1409 ka PICO-1500 min
DS65/T4	1432.6	13.6	1383.4	VF	34	6.5			?	Gardar—1409 ka PICO-1500 min
DS66	1542.3	13.0	1467.0	SR	35	1.5	36	3.0	Pauzhetka area?	Gardar
DS67	1543.1	14.2	1466.0	Aleutian arc			37	3.0	pumice raft?	Gardar
DS68	1551.9	22.4	1479.7	VF? RA?			38	5.0	?	Gilsa—Gardar
DS69	1614.2	13.2	1544.4	VF? RA?	36	1.0	39	182.0	?	Gilsa—Gardar
DS70	1620.3	15.0	1557.8	VF? Aleutian arc?	37	6.0	40	84.0	Karymsky eruptive center? Aleutian arc?	Gilsa—Gardar
DS71	1633.3	12.8	1588.0	RA	38	10.5	41	8.0	?	Gilsa—Gardar
DS72	1652.4	44.8	1616.6	Aleutian arc?			42	30.0	?	1713 ka NARPI-2200min—Gilsa
DS73	1666.4	21.8	1622.8	VF? RA?	39	5.5			?	1713 ka NARPI-2200min—Gilsa
DS74	1677.0	18.4	1639.1	VF	40	2.0			?	1713 ka NARPI-2200min—Gilsa
DS75	1725.7	12.8	1724.7	VF? RA?	41	6.0			?	Olduvai –1713 ka NARPI-2200 min
DS76	1746.2	22.0	1754.1	Aleutian arc?	42	5.0			?	Olduvai –1713 ka NARPI-2200 min
DS77	1853.0	14.6	1765.6	VF	43	2.0			?	Olduvai
DS78	1855.9	72.0	1817.5	VF			43	24.0	?	Olduvai
DS79	1896.3	46.8	1840.6	VF	44	7.0	44	3.0	?	Olduvai
DS80	1994.2	16.0	1964.3	VF? RA?	45	10.0			?	Feni—Olduvai
DS81	2084.9	24.2	2087.1	VF? RA?	46	12.0	45	6.0	?	Feni—Olduvai
DS82	2090.7	22.6	2090.7	VF	47	11.0			?	Feni—Olduvai
DS83	2125.4	30.0	2132.7	?			46	2.0	?	Feni
DS84	2126.7	29.4	2130.5	VF	48	4.0	47	1.5	Paltsevskaia caldera?	Feni
DS85	2155.8	28.2	2152.5	VF	49	4.0			?	Gauss/Matuyama—Feni
DS86	2323.6	25.4	2339.8	SR	50	1.0			?	Gauss/Matuyama—Feni
DS87	2391.0	124.0	2384.7	VF			48	3.0	Paltsevskaia caldera?	Gauss/Matuyama—Feni
DS88	2396.7	23.8	2403.8	?			49	3.0	?	Gauss/Matuyama—Feni
DS89	2490.7	107.4	2479.7	Aleutian arc?	51	4.0			pumice raft	Gauss/Matuyama—Feni
DS90	2492.8	19.2	2487.8	RA			50	1.5	?	Gauss/Matuyama—Feni
DS91	2502.8	30.6	2492.4	VF	52	15.0			Paltsevskaia caldera?	Gauss/Matuyama—Feni
DS92	2504.6	103.2	2493.6	VF	53	3.0			?	Gauss/Matuyama—Feni

**Table 3**  
Continued

Detroit tephra ID/alt. ID	Modeled age (ka)	Error 2σ (ka)	SRs-based age (ka)	Volcanic zone	882A #	Thick-ness (cm)	884B #	Thick-ness (cm)	Source	Paleomagnetic event/interval
DS93	2653.6	17.4	2615.2	VF	54	11.0	51	5.0	?	Kaena—Gauss/Matuyama
DS94	2671.3	36.4	2636.1	Aleutian arc?			52	3.0	?	Kaena
DS95	2933.9	15.0	2871.0	VF	55	7.0			?	Kaena
DS96	3031.8	68.8	3026.7	RA			53	22.0	?	Kaena
DS97	3692.1	20.0	3768.4	VF	56	16.0	54	13.0	?	Cochiti—Gauss/Gilbert
DS98	3730.1	19.6	3795.3	VF	57	5.5	55	8.0	?	Cochiti—Gauss/Gilbert
DS99	3773.1	20.6	3843.9	RA	58	6.0	56	7.0	Karymshina caldera	Cochiti—Gauss/Gilbert
DS100	3839.2	68.0	3895.7	Aleutian arc?			57	5.0	?	Cochiti—Gauss/Gilbert
DS101	3912.4	19.8	3967.9	VF	59	2.0			?	Cochiti—Gauss/Gilbert
DS102	3928.9	95.0	3992.9	VF?			58	3.0	Avachinsky area?	Cochiti—Gauss/Gilbert
DS103	4142.5	59.8	4217.5	RA	60	6.0			?	Cochiti
DS104	4284.3	138.0	4297.5	VF? RA?			59	8.0	?	Cochiti
DS105	5067.5	119.8	5053.8	VF			60	12.0	?	Thvera
DS106	5074.9	120.2	5058.9	?			61	15.0	Tekletunup?	Thvera
DS107	5113.6	119.8	5104.4	RA			62	4.0	?	Thvera
DS108	5132.5	119.0	5124.4	?			63	11.0	Tekletunup?	Thvera
DS109	5218.7	40.6	5235.3	RA	61	7.0			?	Thvera
DS110	5259.1	55.0	5280.3	VF	62	5.0			?	C3n—Thvera
DS111	5346.5	76.0	5381.3	VF? RA?	63	10.0			?	C3n—Thvera
DS112	5472.6	92.6	5528.1	RA	64	15.0			?	C3n—Thvera
DS113	5587.0	107.2	5663.2	VF?	65	3.0			?	C3n—Thvera
DS114	5608.6	109.2	5688.8	RA	66	20.0	64	4.0	?	C3n—Thvera
DS115	6149.8	99.6	6163.8	RA			65	24.0	?	C3n
DS116	6158.5	99.2	6169.5	SR?			66	11.0	?	C3n
DS117	6182.2	97.8	6189.7	RA			67	4.0	?	C3n
DS118	6218.1	94.0	6220.6	VF? RA?			68	4.0	?	C3n
DS119	6235.1	91.6	6235.0	RA			69	4.0	?	C3n

Note. Column 1 lists DS59 to DS119 tephras from the composite Detroit sequence and alternative (alt.) IDs for geochemically identical tephras from other sites (van den Bogaard et al., 2014). In column 11, paleomagnetic events/intervals follow PICO-1500 for 1100 for 1100 to 1500 ka, NARPI-2200 for 1500 to 2200 ka, and GPTS from 2200 to 6235 ka (Lourens et al., 2004; Ogg, 2012; Channell et al., 2020). For other explanations see note to Table 2.

### 3.3.3. Bayesian Age Modeling

Relying on the published stratigraphy, newly obtained datum levels, and  $^{40}\text{Ar}/^{39}\text{Ar}$  dates, we have constructed a Bayesian age model that tied together all known data on stratigraphy and ages. In the Bayesian analysis of paleoenvironmental archives, initial dates are considered as likelihood functions and stratigraphic constraints—as a prior knowledge, which allows stochastic calculation of posterior probabilities of ages using Monte Carlo Markov chains (Blaauw & Christen, 2011; Bronk Ramsey, 2009a).

Tephrochronological correlations of independently dated paleoenvironmental archives provide a good basis for the Bayesian approach; therefore, it is widely accepted in tephrochronological studies (e.g., Blockley et al., 2008; Bronk Ramsey et al., 2015; Ponomareva et al., 2017). Following this approach, our Detroit age model comprised the published age-depth data for the individual sites, datum levels (see Section 3.3.1), and new  $^{40}\text{Ar}/^{39}\text{Ar}$  dates:

- Site 882A: 4–5.7 Ma published data and age model (Janus web database: <http://www-odp.tamu.edu/database/>; Rea et al., 1993; Weeks et al., 1995) refined in our study (Figure 2 and Table 3; Tables S4 and S5);

**Table 4**

Summary of  $^{40}\text{Ar}/^{39}\text{Ar}$  Data for the Detroit Seamount Site 882A

Detroit tephra ID	Sample ID Leg-site-Section_Interval (cm)	Material	n/N	MSWD	K/Ca	Weighted mean age (Ma)	Error ( $2\sigma$ )
DS99	145-882A-24A-4_143-144	biotite	22/27	0.71	8.68	3.90	0.09
DS103	145-882A-28H-4_72-73	biotite	16/16	0.66	39.02	3.96	0.29
DS112	145-882A-41H-1_109-110	biotite	19/19	0.88	10.86	5.48	0.51
	145-882A-41H-1_127-128	biotite	20/20	1.21	34.86	5.52	0.14
DS114	145-882A-42H_56-57	biotite	9/16	0.64	49.01	5.10	0.15

Note. Ages calculated relative to the 28.201 Ma Fish Canyon sanidine standard (Kuiper et al., 2008) using the decay constants of Min et al. (2000). n/N:  $n = \#$  of dates used in weighted mean calculation;  $N =$  total  $\#$  of single crystal fusions per sample.

- Sites 882 A and B composite section: 0–800 ka (Jaccard et al., 2010); 0–4 Ma (Tiedemann and Haug, 1995);
- MD01-2416: 0–1,275 ka published data and age model (Gebhardt et al., 2008; [www.pangea.de https://doi.org/10.1594/PANGAEA.626599](https://doi.org/10.1594/PANGAEA.626599); M. Sarnthein, personal communication, 2017); 0–1,100 ka data and age model, cited above, refined in our study (Figure 4 and Tables 2; Tables S4 and S5);
- Site 884B: published data and age model (Janus web database <http://www-odp.tamu.edu/database/>; Rea et al., 1993; Weeks et al., 1995) refined in our study for 0–6.2 Ma (Figures 2 and 5 and Tables 3; Tables S4 and S5);
- Ar/Ar dates (Table 4);
- Age of  $9,045 \pm 64$  b2k for KRM tephra (DSI tephra found in Site 884B).

For the published data, we have investigated reference chronologies to assign dating uncertainties. For the refined age models of the individual cores (Section 3.3.1), accuracies of the datum levels was set according to the reference chronologies (Channell et al., 2020; Lisiecki & Raymo, 2005; Lourens et al., 2004; Ogg, 2012). The Bayesian model was calculated in OxCal 4.3 (Bronk Ramsey, 2009a) with a Poisson process assumed for sedimentation rates (P\_Sequence() function). To cover the possible underestimation of error, we considered a 5% outlier probability for any date in it by setting an Outlier() option (Bronk Ramsey, 2009b). Details of the model design and the source code are given in Text S1 in Supporting Information S1 and Supporting Information S2, respectively. The output of the model is provided in Table S7.

## 4. Results

### 4.1. Tephra Layers

We identified 41 tephra layers in the shorter core MD01-2416, and 66 and 69 tephra layers in the longer Sites 882A and 884B, respectively (Tables 1–3; Table S1; Figures 2–5). In each of the cores, all tephra layers were numbered consecutively from top to bottom (Tables 2 and 3; Table S1). Tephra thickness varies from 0.5 to 20 cm in Site 882A and core MD01-2416 located directly on the Detroit Seamount and shows markedly higher variations from 0.5 to 182 cm in Site 884B on the Meiji Drift deposit (Table 1; Table S1; Figures 1a and 2–5). Most of the layers have a sharp lower contact with host sediments suggesting instant (relative to pelagic sedimentation rate) deposition from a primary tephra fall (Figure 6a). Some tephra layers form patches or pods, or even sub-vertical lenses (Figure 6b). Most tephra layers are composed of light-colored fine to very fine ash; some are normally graded from medium to fine sand (Figure 6a). Two tephra layers consist of pumice lapilli (Figures 6c and 6e). In some cases, working and archive halves of the core differ. For example, pumice lapilli are present in the working half of the core but absent from the archive half of Site 882A (Figures 6d and 6e).

Most of tephra layers are ash-sized with particles of  $<250 \mu\text{m}$  (Figures 7a and 7b); some tephra layers are composed of cindery (Figure 7c) or pumiceous (Figures 7d, 7f, and 7g) lapilli fragments. Two layers originally sampled as tephra appeared to contain mostly terrigenous particles with only minor amounts of compositionally different glasses. These layers might be a result of accumulation of debris carried by sea ice or ocean currents, which is typical for the NW Pacific pelagic sedimentation (Figure 7h; McCarron et al., 2021; Wang et al., 2021). In addition to tephra layers and pods, we sampled a few sediment intervals, which seemed enriched in tephra particles. However, these samples appeared to contain terrigenous or biogenic particles and very few glass shards.

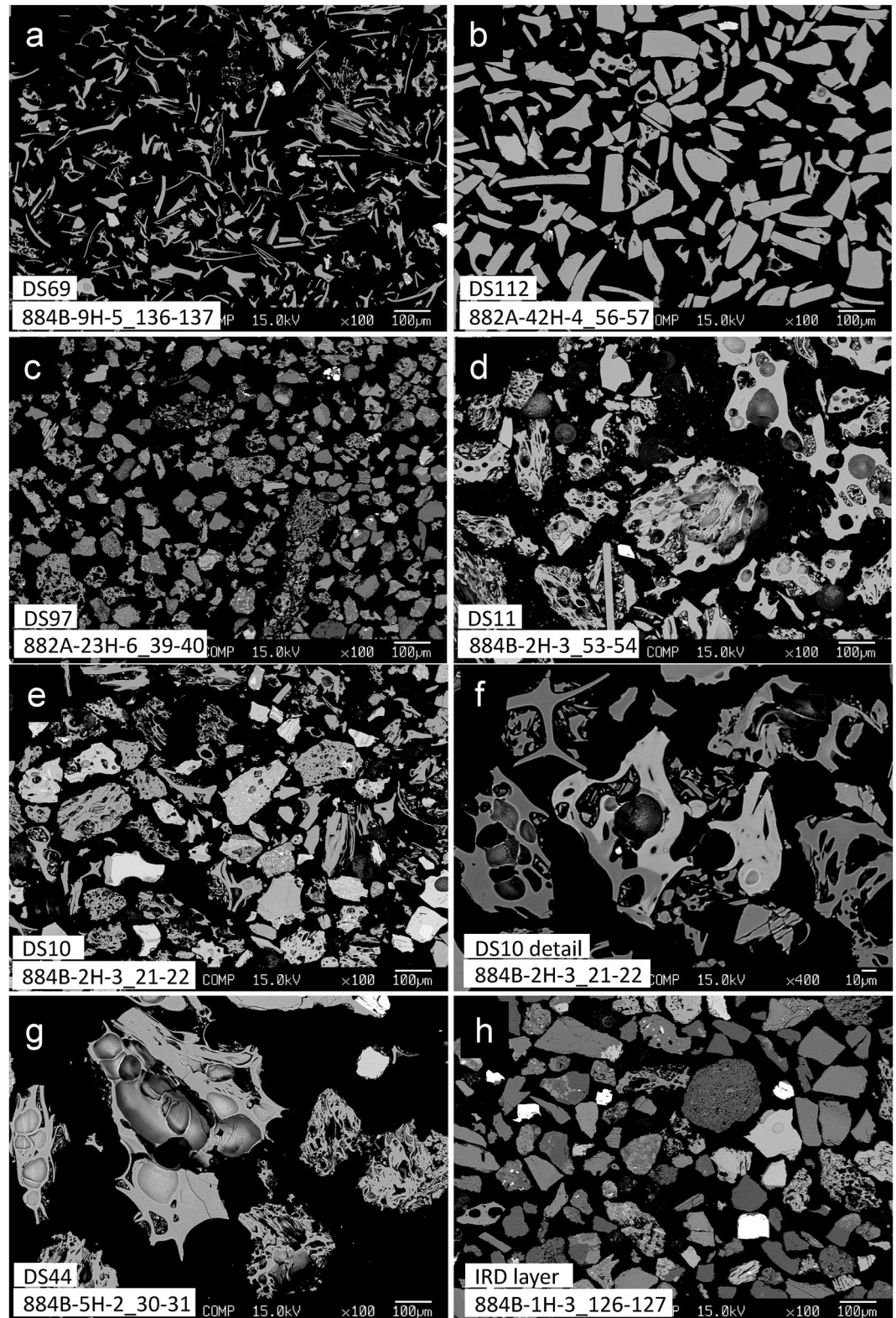


**Figure 7.** Back-scattered electron images of representative tephras showing different glass morphologies. (a, b) silicic glasses, (c) andesitic glasses, (d) pumice, (e, f) one of the heterogeneous Gorely tephras, (g) pumice with “pasta-like” fragments resembling those in ignimbrites, analog of tephra T2 from the El’gygytyn Lake core in Chukotka (Figure 1a; van den Bogaard et al., 2014), (h) ice-rafted debris (IRD) layer. For each photo, tephra ID, site, section number, and interval (cm) are provided.

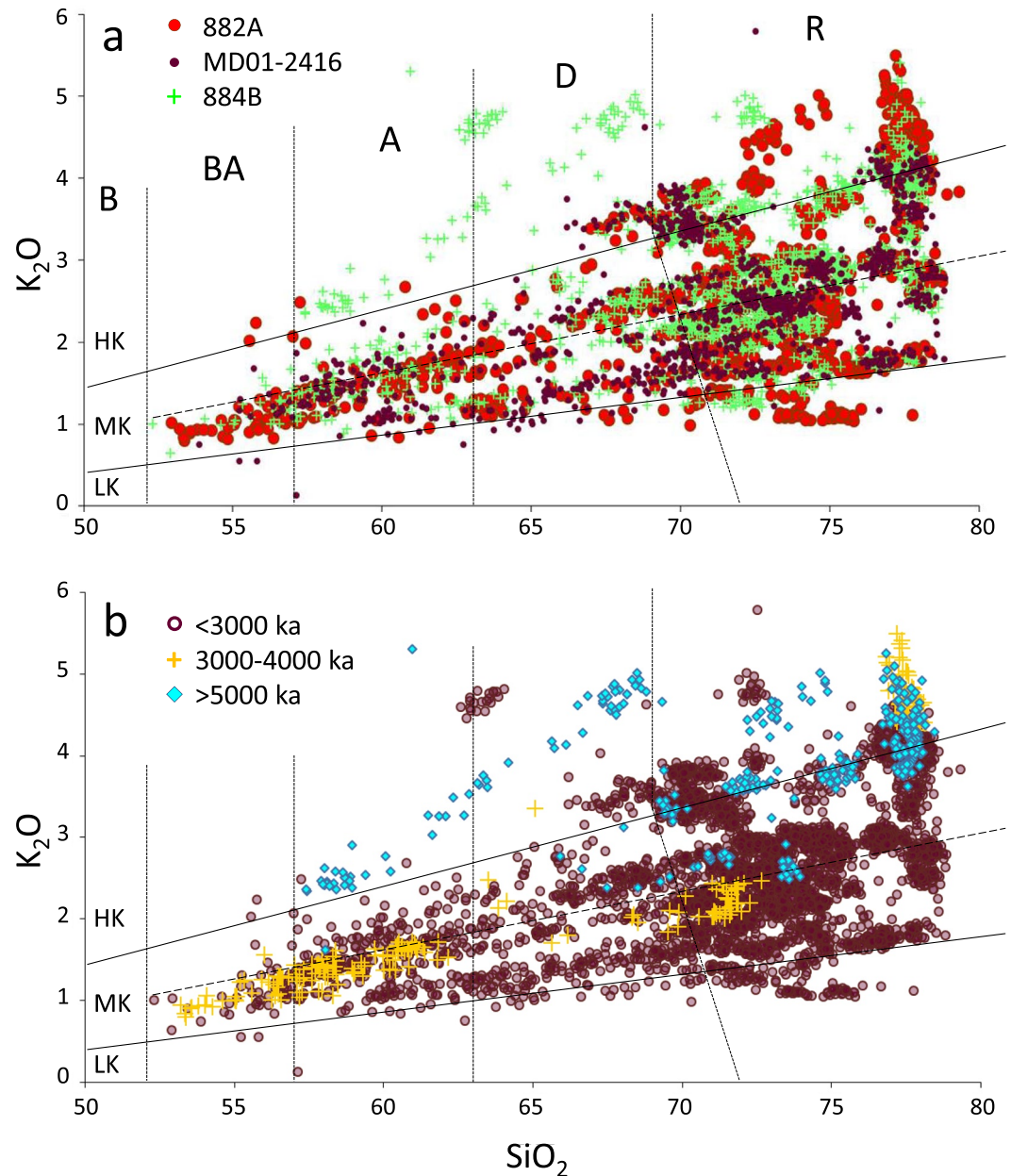


**Figure 8.** An overview of the major element data for the Detroit sequence tephra. (a) all glasses from the Detroit tephra sequence split by individual cores; (b) all glasses from the Detroit tephra sequence split by age intervals. Solid lines divide fields of low- $K_2O$  (LK), medium- $K_2O$  (MK), and high- $K_2O$  (HK) basalts (B), basaltic andesites (BA), andesites (A), dacites (D), and rhyolites (R) at  $Na_2O = 5$  wt% following Le Maitre et al. (2002). Dashed line divides the field of medium-K compositions into the upper and lower ranges for more convenient description of glass compositions. Oxide concentrations are given in wt%.

#### 4.2. Tephra Glass Composition

All studied tephra layers contain fresh glass (Figures 7a–7g). Electron microprobe major element data includes ~4,200 individual analyses on 207 samples from 119 tephra (~19 analyses per sample on average). Trace elements are available for 105 samples from 103 tephra and include 860 single-shard analyses (~8 analyses per sample). An overview of major element data on glasses from all three cores is provided in Figures 8a and 8b. Glass compositions vary from basaltic andesite to rhyolite (52–80 wt%  $SiO_2$ ) and from low- to high- $K_2O$  series. Most of glasses fall into medium- $K_2O$  field while low- $K_2O$  glasses are rare. The rhyolitic field is most densely

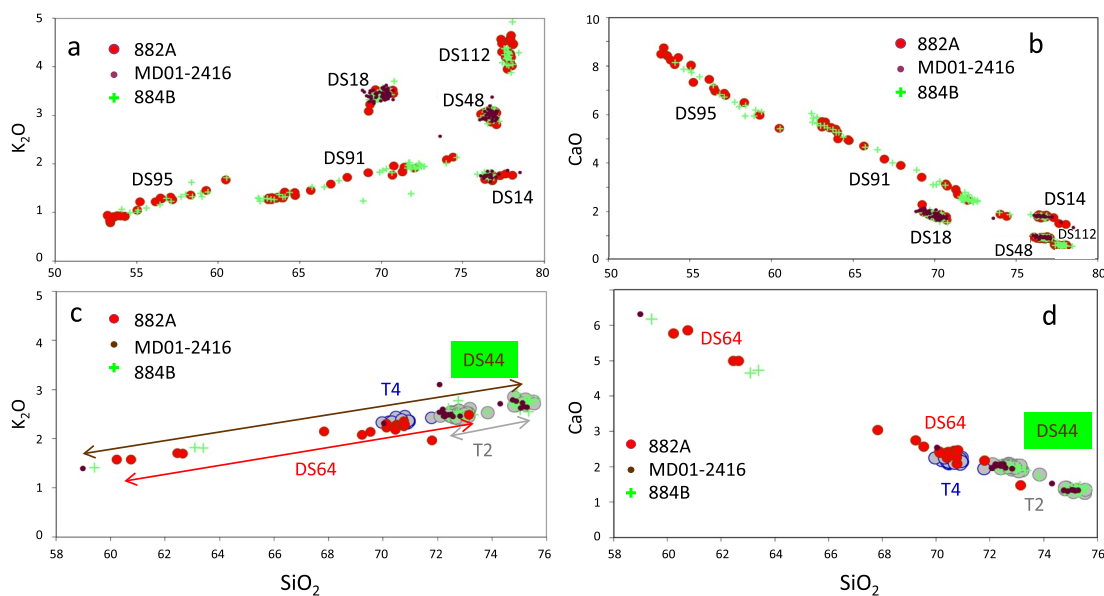


**Figure 9.** Major element composition of glasses from various Detroit tephras. (a, b) examples of homogeneous and heterogeneous tephras. (c, d) examples of heterogeneous tephras and their correlations to the El'gygytyn Lake (EL) core (van den Bogaard et al., 2014). *DS44* tephra found in Core MD01-2416 and Site 884B contains two glass populations matching those from the T2 tephra from the EL core. Prevailing silicic glass population from heterogeneous *DS64* tephra (Site 882A) matches glasses from the T4 tephra from the EL core. Colors of tephra IDs match those of their data points. Color-coded lines show the extent of heterogeneous glass trends. Oxide concentrations are given in wt%.

populated. Tephras from different cores are broadly similar and overlap in the binary plots (Figure 8a). Glasses with the highest  $K_2O$  contents, especially within the andesitic-dacitic field, occur in Site 884B while those with the lowest  $K_2O$  contents were found at Site 882A. Glasses from the oldest analyzed interval of 5,000–6,000 ka tend to be more  $K_2O$ -rich than most of the younger tephras (Figure 8b).

A number of tephra layers exhibit heterogeneous glass composition well discerned in the back-scattered electron images based on different shades of the shards (Figures 7e and 7f). Tephras with homogeneous and heterogeneous glass compositions occur in approximately equal amounts. In some cases, the latter exhibit tight long trends with  $SiO_2$  ranging up to 12 wt% (Figures 9a and 9b). A few tephras (e.g., *DS44* and *DS64*) contain two glass populations, which occur in all the cores where such tephras are present so both populations likely belong to the same eruption (Figures 9c and 9d). The most  $SiO_2$ - and  $K_2O$ -rich glasses often form short vertical trends between 77 and 79 wt%  $SiO_2$  (e.g., *DS112* in Figure 9a). About 20% of the tephras are contaminated with a minor amount of compositionally variable glasses suggesting an admixture of background glasses from the sediments; contaminated samples commonly come from thin ash lenses or the upper parts of thick tephra layers mixed with the sediments (“cloudy tops”).

All the tephras exhibit typical trace element characteristics of magmas formed in subduction-related settings expressed by variable enrichment of elements mobile in subduction zones (e.g., Ba, Th, U, etc.) relative to immobile elements (e.g., Nb, Ta, Zr) (Figure 10). On the diagram for discrimination of granitic magmas, which is likely applicable to tephra glasses with some reservations, formed in different tectonic settings, the glass compositions plot mostly within the field of volcanic arc granites, but some samples plot within the field of within-plate granites (Pearce, 1996). These compositions are also similar to granites formed in post-collisional settings, which do not exhibit distinctive compositional features but rather have compositions similar to some volcanic arc, within-plate, and syn-collisional granites (Figure 10).

### 4.3. Tephra Ages

We determined about 60 new datum levels in each core age models (Figures 2–5 and Table S4). We used a Laschamp excursion at 41 ka as the uppermost datum in all the models. In core MD01-2416, the RPI and MIS events were obtained via comparison of the NRM/ARM and *Uvigerina* spp.  $\delta^{18}O$  records (Gebhardt et al., 2008) to PICO-1500 and LR04 stacks, respectively (Figures 3–5) (Channell et al., 2020; Lisiecki & Raymo, 2005).

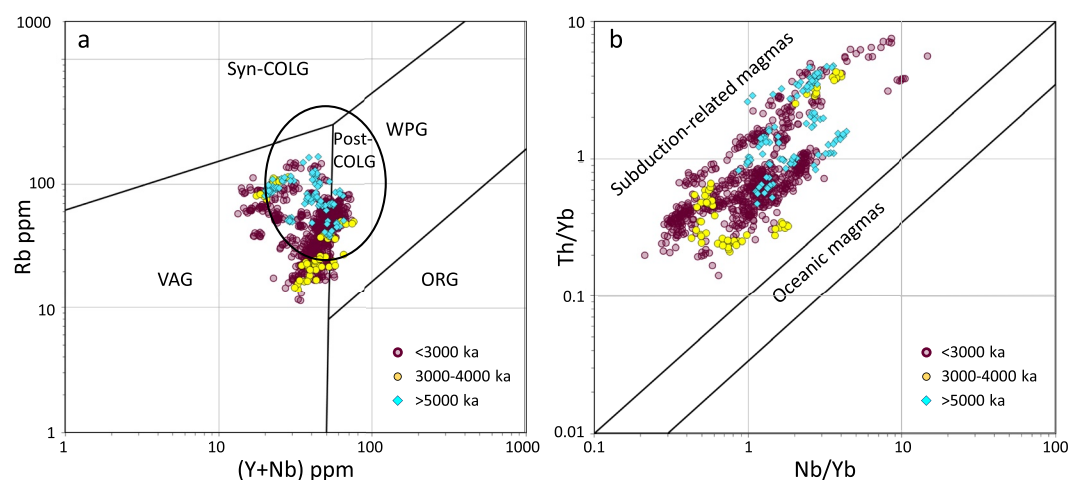


**Figure 10.** Compositions of the Detroit tephras on diagrams for discrimination of different tectonic settings of magmatism. (a)  $(Y + Nb)$  versus Rb diagram for granitic magmas after Pearce et al. (1984) and Pearce (1996). Abbreviations: VAG—volcanic arc granites, Syn-COLG—syncollisional granites, WPG—within-plate granites, ORG—ocean ridge granites; Post-COLG—post-collisional granites. (b) Nb/Yb versus Th/Yb diagram after Pearce and Peate (1995). Subduction-related magmas have  $Th/Nb > 0.1$  due to addition of Th-rich slab-derived component to the mantle wedge source. Tephras are color-coded according to their time intervals <3,000, 3,000–5,000 and >5,000 ka. Element contents are in ppm.

Previously, for the upper 38 m of core MD01-2416, the *Uvigerina* spp.  $\delta^{18}O$  data have been correlated back to MIS 24 (Gebhardt et al., 2008). We found that *DS52* and *DS53* tephras, geochemically tied between three cores, occur above Jaramillo and within this subchron in the ODP cores, respectively (Figure 4). It allowed us to stretch the core MD01-2416 records from 38 to 45 m core depth back to base of Jaramillo and to MIS 31 (Figure 4). Thus, we could date the oldest sediments of core MD01-2416 at 1,100 ka.

From 41 to 2600 ka in Sites 882A and 884B, the new datums were derived from correlation of the paleointensity and inclination records (Rea et al., 1993; Weeks et al., 1995) to PICO-1500 and NARPI-2200 stacks (Channell et al., 2020). The new datums from 2600 to 5,700 ka in Site 882A and 2,600 to 6,300 ka in Site 884B were based on magnetic reversals by Weeks et al. (1995) tied the GPTS (Lourens et al., 2004; Ogg, 2012) (Figure 2). The identification of some reversals during Pliocene in the ODP cores remained uncertain because of the known noisiness of the inclination data (Figure 2) (Rea et al., 1993; Weeks et al., 1995). The geochemically correlated *DS94* and *DS97-DS99* tephras confirmed the recognition of the Gilbert/Gauss (3,600 ka) and Gauss/Matuyama (2,600 ka) boundaries (Figure 2). However, *DS95*, *DS96* and *DS100-DS113* tephras found in one of the cores did not help to improve the core age models. Because of the lack of paleomagnetic events below the Thvera (5,330 ka) event in Site 882A (Figure 2), we used the SRs-based age of *DS114* tephra in Site 884B as the lowest datum in the Site 882A age model (Table S4).

The calculated sedimentation rates between new datum levels vary in the range between 0.7 and 16.9 cm/kyr (Table S4). We applied linear interpolation to calculate the SRs-based ages for *DS2* to *DS119* tephras (Table 2; Table S5). The variations of the SRs-based ages for the same tephras in different cores are less than 8.6 ka (Table S5) that supports our refinement of the core age models. The largest age variations ranging from 12.6 to 29.3 ka were calculated for *DS53*, *DS64*, *DS71*, and *DS79* tephras and caused by the presence of core breaks in Site 884B (Figure 4), which increased uncertainties in determination of the datum levels and sedimentation rates.

The newly obtained five  $^{40}Ar/^{39}Ar$  dates from tephra layers with the weighted mean range from  $3.90 \pm 0.09$  Ma to  $5.52 \pm 0.14$  Ma (Table 4; Table S6, Figure S1 in Supporting Information S1). Three of the samples did not contain any outliers, whereas the other two samples contained  $^{40}Ar/^{39}Ar$  dates that were both younger and older than the main population of dates. The younger dates often have very low radiogenic  $^{40}Ar^*$  yields, which we tentatively attribute to alteration of the biotite. Older dates are likely the result of xenocrysts incorporated into the explosive eruptions or may be due to excess  $^{40}Ar$  in the biotite (e.g., Hora et al., 2010).

The Detroit Bayesian age model includes  $\sim 800$  tie-points to reference chronologies, 24 geomagnetic events, and five  $^{40}Ar/^{39}Ar$  dates tied together by 119 tephra layers. The top of the Detroit age model is the *DS1* (KRM)

tephra with an age of  $9,045 \pm 6$  ka. The model covers the time span from  $\sim 9$  to 6,235 ka (Table 2). Outlier analysis rejected one  $^{40}\text{Ar}/^{39}\text{Ar}$  date and some tie-points that were incompatible with the rest of the model. The resulting ages and error estimates for all tephra layers are provided in Table S7. The model accuracy generally decreases from thousands of years in the Late Pleistocene to tens of thousands of years in the Late Miocene to Pliocene, reproducing the accuracies of the reference chronologies. The largest error reaches 70 ka and occurs when reference chronologies contradict each other. The modeled ages generally converge with the SRs-based ages (Tables 2 and 3). Once new dates or correlations are available, the Detroit Bayesian model will easily incorporate them and permit the update of all the ages.

#### 4.4. Composite Tephra Sequence

Based on geochemical and stratigraphic correlations, we obtained a composite tephra sequence for the Detroit Seamount sediments comprising 119 unique tephra layers labeled consecutively *DS1* to *DS119*. Figures 2–5, Tables 2 and 3; Table S1 provide detailed information on the ages, stratigraphic positions, and provenance of the tephra. The sequence goes back to the late Miocene covering the time span from  $\sim 9$  to 6,235 ka.

The Detroit tephra sequence for the last  $\sim 1,100$  ka is based on all three cores (MD01-2416, 882A and 884B) and consists of 58 tephra (*DS1* to *DS58*). From  $\sim 1,100$  to 5,600 ka, the sequence relies on Sites 882A and 884B and includes 56 tephra (*DS59* to *DS114*). The oldest part of the sequence from 5,700 to 6,235 ka is based on Site 884B and presented by five tephra (*DS115* to *DS119*) (Figures 2–5; Tables 2 and 3). Correlations of tephra layers between the cores were constrained by geochemical compositions of glass. Comparison of major element compositions of tephra from different cores was based on Harker diagrams, that is, plots showing all elements versus  $\text{SiO}_2$ . We accepted correlations of tephra from two or three cores only when their glasses matched in all the elements (examples of comparison can be seen in Figures 9a–9d). In some cases, these correlations were checked with the help of trace element binary plots and spidergrams (a complete set of correlation diagrams is provided in Figure S2 in Supporting Information S1).

All tephra layers, which provide correlations between the cores, are presented in Figures 2–5, and in Tables 2 and 3; Table S1. Eleven tephra from 58 deposited within the last 1,100 ka were found in all three cores. Additionally, within the same interval, 20 tephra were found in two of the cores. The remaining 27 tephra within this interval were only well expressed in one of the cores. From 1,100 to 6,235 ka, 61 tephra were deposited and 15 of those were found both in Sites 882A and 884B. For *DS1–DS119* tephra, the modeled ages are used in geochemical diagrams and in the text hereafter (Tables 2 and 3).

## 5. Discussion

### 5.1. Comparison of the Detroit Tephra Glasses to Those From the Kamchatka and Aleutian Volcanic Arcs

In general, the glass compositions of the Detroit tephra overlap with the Kamchatka proximal dataset (Figure 11; Portnyagin et al., 2020), but there are a few exceptions. These include the most and the least K-rich glasses as well as the field of lower-medium-K compositions being surprisingly rare in the available proximal data (Figure 11a). These discrepancies are most readily explained by insufficient data for the pre-late Pleistocene proximal deposits in Kamchatka. However, the occurrence of some tephra from adjacent volcanic arcs among the Detroit tephra is also possible.

Currently, no reliable geochemical criteria are known that allow discrimination of tephra from Kamchatka and the adjacent Aleutian and Kuril volcanic arcs, located at distances  $\leq 2,000$  km from the Detroit Seamount. Lead isotopes provide one potential possibility as recent Kamchatkan rocks have distinctively less radiogenic Pb isotope composition ( $^{206}\text{Pb}/^{204}\text{Pb} = 18.05\text{--}18.40$ ,  $^{207}\text{Pb}/^{204}\text{Pb} = 15.42\text{--}15.51$ ,  $^{208}\text{Pb}/^{204}\text{Pb} = 37.60\text{--}38.15$ ; Portnyagin et al., 2015 and references therein) compared to the Aleutian emergent volcanoes ( $^{206}\text{Pb}/^{204}\text{Pb} = 18.56\text{--}18.96$ ,  $^{207}\text{Pb}/^{204}\text{Pb} = 15.48\text{--}15.60$ ,  $^{208}\text{Pb}/^{204}\text{Pb} = 38.03\text{--}38.54$ ; Yagodinski et al., 2015). Single-shard Pb isotope analysis may be a future option to define the provenance of the Detroit tephra. At present, we can provide only a very preliminary interpretation based on empirical criteria such as chlorine content in glass and trace element ratios.

Chlorine contents in the Kamchatka proximal volcanic glasses very rarely exceed 0.20 wt% and in only one silicic pumice from Koshelev volcano (South Kamchatka) those exceed 0.25 wt% (Figure 11b; Portnyagin et al., 2020). Our dataset from the Detroit Seamount broadly follows the same pattern but includes also about 10 tephra with

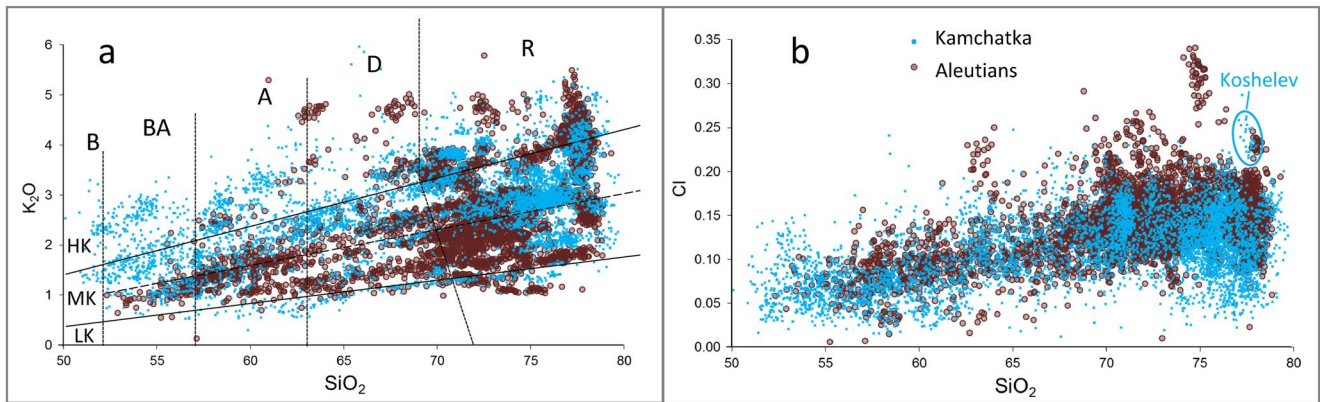


**Figure 11.** Comparison of the Detroit tephra glasses with those in proximal Kamchatka tephra. (a) K<sub>2</sub>O versus SiO<sub>2</sub> and (b) Cl versus SiO<sub>2</sub> contents in the Detroit (dark-brown) and proximal (blue) glasses. The data on proximal glasses exclude those for welded and altered tuffs. Oxide concentrations are given in wt%.

Cl > 0.20 wt%, two of which are characterized with even higher Cl contents of >0.25 wt%. High Cl values often occur in glasses from island arc volcanoes (e.g., Aleutians, Derkachev et al., 2018; Izu arc front, Straub and Layne, 2003), which likely interacted with seawater altered rocks or brines in the magma plumbing system under volcanoes. Based on this criterion, we suggest that tephra where the majority of glasses have Cl contents  $\geq 0.20$  wt% (*DS8*, 17, 20, 62, 67, 70, 72, 76, 94, and 100) might have been derived from the Aleutian or Kuril volcanic arcs rather than Kamchatka. One of the high-Cl tephra (*DS67*; Cl > 0.25 wt%) consists of pumice lapilli likely representing a pumice raft. This example suggests the transport of high-Cl glass and pumice by the currents from the Aleutian Islands (Figure 1d).

Additional constraints on the provenance of Detroit tephra can be obtained using trace element ratios and their comparison to those in tephra glasses and rocks from the potential volcanic source regions. Presently, the data on volcanic glass compositions is abundant for Kamchatka and in contrast rather scarce for the Aleutian and Kuril arcs, where the comparison can be made using only bulk rock compositions. The comparison of tephra glasses with rocks may be compromised by fractionation of trace elements between crystal phases and residual melt that is particularly significant for well crystallized tephra (e.g., Blundy, Cashman, 2008). On the other hand, examples of close coincidence of trace element composition of tephra glasses and bulk rocks are also common (e.g., Ponomareva, Portnyagin, & Davies, 2015; Ponomareva et al., 2013b). Thus, the comparison of Detroit glasses with bulk rocks from the Aleutian and Kuril arcs is justified for the first-order region-scale comparison.

Selected trace element ratios in Detroit tephra are compared to the composition of rocks and tephra glasses from Kamchatka, Aleutian and Kuril arcs in Figure 12. Compared to tephra and welded tuffs from Kamchatka, the compositions of Detroit glasses that fall within a range of Nb/Y > 0.03 and Th/Y > 0.08 closely follow the most densely populated compositional fields of Kamchatkan glasses. For low Nb/Y compositions, Detroit glasses exhibit

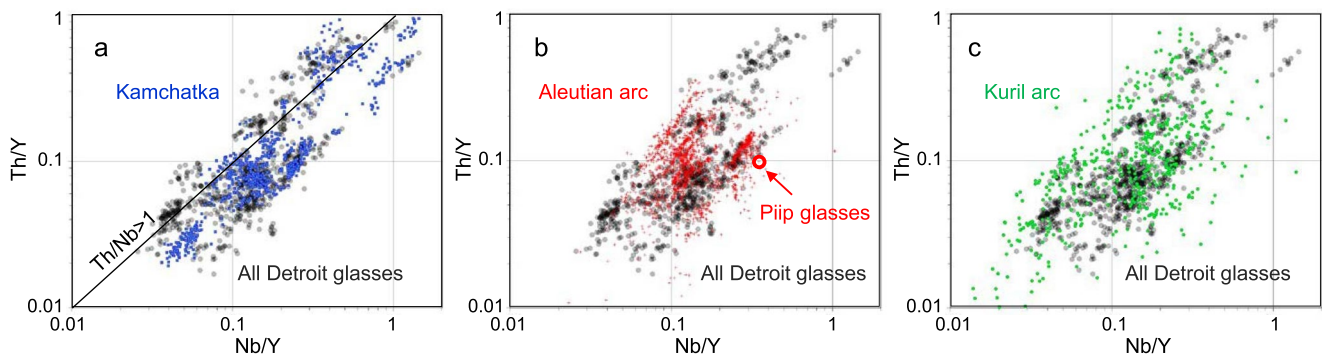


**Figure 12.** Compositions of the Detroit Seamount tephra glasses in comparison with rocks and glasses from Kamchatka (a), Aleutian (b) and Kuril arcs (c). Kamchatka glass compositions are from the TephraKam database (Portnyagin et al., 2020), Aleutian rocks are from compilation by Yagodinski et al. (2015), Kuril Arc rocks are from GEOROC database (accessed December 2021). Ratios were calculated for element contents in ppm.

much more scatter. For example, low-Nb/Y compositions with  $\text{Th/Nb} \geq 1$  are very rare in Kamchatka, but they are relatively abundant in the Detroit sequence. Compositions with low  $\text{Th/Nb} < 0.3$  are also not known in Kamchatka. Most Aleutian rocks have moderately Nb-rich compositions with  $\text{Nb/Y} > 0.05$ . Although the range of these compositions is similar to those from the Detroit cores and Kamchatka, the most common Aleutian compositions tend to have higher  $\text{Th/Nb}$  ratios. Compositions with  $\text{Nb/Y} < 0.05$  and  $\text{Th/Y} > 0.3$  are extremely rare in the Aleutian arc but common among Detroit tephra. The compositions of the Kuril arc rocks are very scattered and some of them are close to high  $\text{Th/Nb}$ —low  $\text{Nb/Y}$  glasses from the Detroit cores. However, these compositions are predominantly found in the southernmost Kuril Islands, Iturup and Kunashir,  $>1,600$  km from the Detroit Seamount.

Thus, the majority of the Detroit tephra have major and trace element compositions compatible with their origin from Kamchatka. However, some tephra may also originate from the Kuril and Aleutian arcs in agreement with conclusions made on the basis of major element and chlorine systematics. The Detroit tephra sequence does not contain any layers related to the submarine Piip volcano located  $\sim 500$  km north of Detroit Seamount although silicic pumice was described at the volcano's slopes (Derkachev et al., 2018; Werner et al., 2016) (Figure 12b).

## 5.2. Geochemical Variations

Variations of selected trace element ratios are shown versus their ages on Figure 13. In general, the compositions reveal no clear geochemical trend, which could be correlated with the regional tectonic evolution or involvement of different magma sources, for example, due to variable subduction input or mantle flow. A similar result was also obtained by Cao et al. (1995) on the basis of smaller dataset of tephra compositions, where trace elements were analyzed by solution ICP-MS technique on bulk samples.

According to the Detroit record, nearly continuous Pleistocene to Holocene explosive volcanism began at  $\sim 2,500$ – $3,000$  ka and can arguably be correlated with volcanism in Kamchatka, where the EVB in its present configuration was formed during the Pliocene to Pleistocene time (Avdeiko et al., 2007).

Portnyagin et al. (2020) proposed that the source volcanic zones of the Pleistocene and Holocene magmas of Kamchatka can be distinguished using discrimination diagrams based on  $\text{Nb/Y}$ ,  $\text{La/Y}$ , and  $\text{Th/Y}$  ratios. However, the Detroit tephra exhibit a much wider range of compositions (Figure 12a). Thus, only a provisional identification of the tephra source zones can be performed using  $\text{Nb/Y}$  ratio in glass—a simplified criteria based on the results of Portnyagin et al. (2020) (Table S3). Kamchatkan tephra originating from the volcanic front have  $\text{Nb/Y} < 0.2$ , rear-arc volcanic centers have  $\text{Nb/Y} = 0.16$ – $0.55$ , and Sredinny Range tephra  $\text{Nb/Y} > 0.4$  (Figure 13a). Tephra from VF and RA, and RA and Sredinny Range overlap within narrow intervals of  $\text{Nb/Y} = 0.16$ – $0.2$  and  $0.4$ – $0.55$ , respectively. For Pliocene and Miocene tephra, it is not possible to distinguish different volcanic zones with the currently available data for proximal rocks because the configuration of active volcanic belts of Kamchatka was different at that time (e.g., Lander & Shapiro, 2007). Neogene Sredinny Range rocks have compositions close to the Holocene–Pleistocene volcanic front and rear-arc magmas (Portnyagin et al., 2020).

It is remarkable that only a few Pleistocene tephra (*DS12*, *24*, *66*, and *86*) have high-Nb/Y compositions with geochemical characteristics of the Sredinny Range magmas. Eruptions of RA volcanoes in Kamchatka were relatively frequent during the last 500 ka (most of them from the Gorely eruptive center as we show in Section 5.3) and rather rare before this. The majority of Pleistocene eruptions likely originated from the Kamchatka VF and have compositions typical for moderately Nb-depleted Kamchatka magmas. Low-Nb Kamchatka magmas with  $\text{Nb/Y} < 0.06$  are rare in the existing database and have been described only for low-K frontal volcanoes (Churikova et al., 2001; Ishikawa et al., 2001; Portnyagin et al., 2020). In the Detroit record, we identified at least 18 such tephra. However, most of them have relatively high  $\text{Th/Nb}$  (Figure 12) and originate from a source, which is presently unknown in Kamchatka.

Pliocene tephra from the age interval of 3,500–4,500 ka display bimodality with one group of high-Nb/Y samples similar to the Pleistocene–Holocene RA volcanics in Kamchatka or those from the Sredinny Range and the second group of low-Nb/Y samples, which are similar to the Pleistocene VF samples. Sample *DS102* from the low-Nb/Y group has a distinctively high  $\text{Ba/Nb} > 30$ , which is typical only for Avachinsky volcano in the EVB in Kamchatka and may indicate a large eruption from this area. The most likely sources of the Pliocene tephra could be located in South Kamchatka and the Sredinny Range, which have been active at least since Miocene, and also from the Pliocene-early Pleistocene volcanic complex of the Eastern Kamchatka, partly overlapping with the modern EVB from  $54.5$  to  $57^\circ\text{N}$  (Avdeiko et al., 2007). The EVB segment between Avachinsky volcano

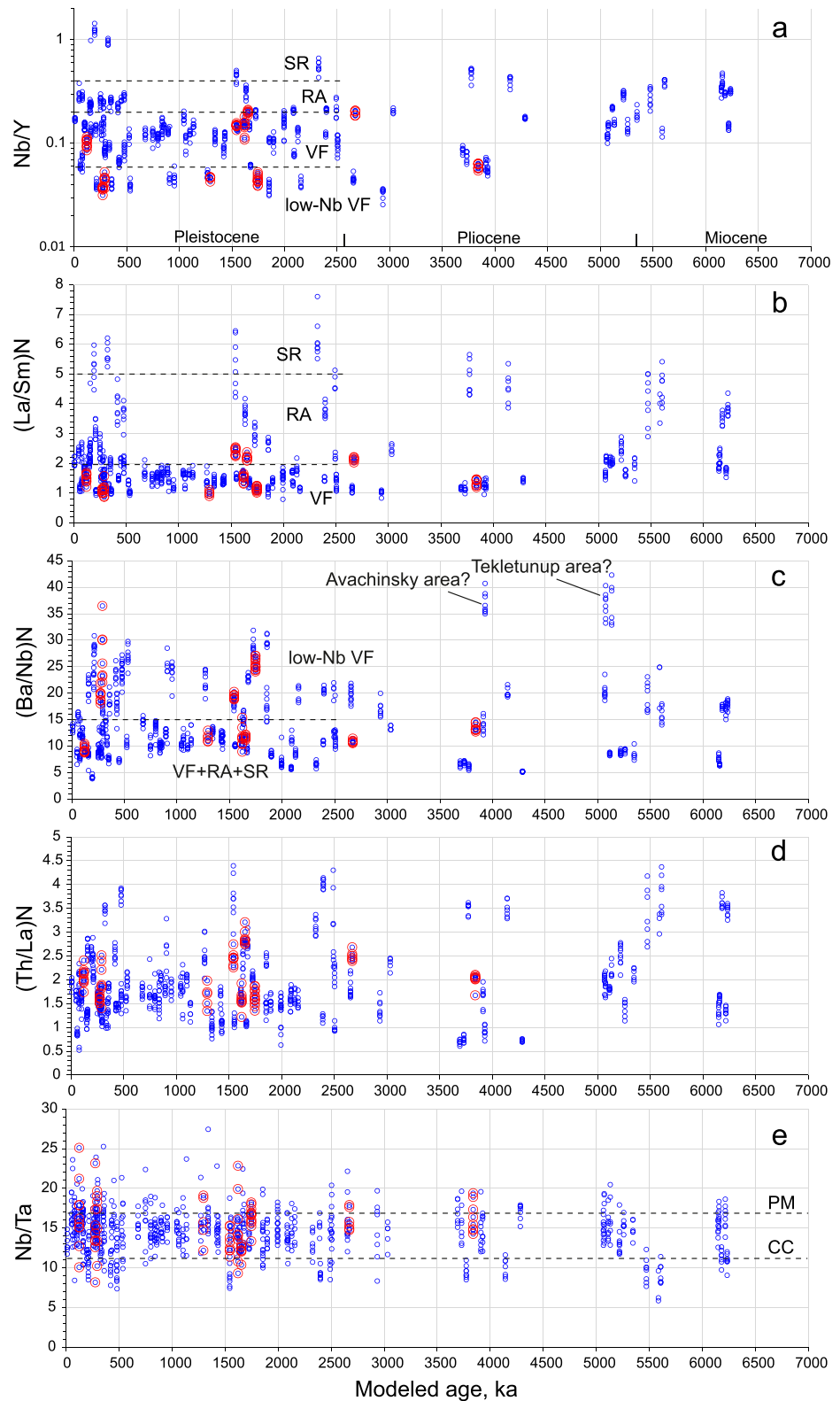


**Figure 13.** Temporal variations of selected trace element ratios in the Detroit tephra glasses shown by individual shard analyses (blue outline). Symbols with additional red outlines refer to tephras with Cl > 0.2 wt%, which can potentially originate from the Aleutian or Kuril island arcs. N—denotes to mantle normalized ratios. The primitive mantle composition is after McDonough and Sun (1995). See text for further details. Ratios were calculated for element contents in ppm.

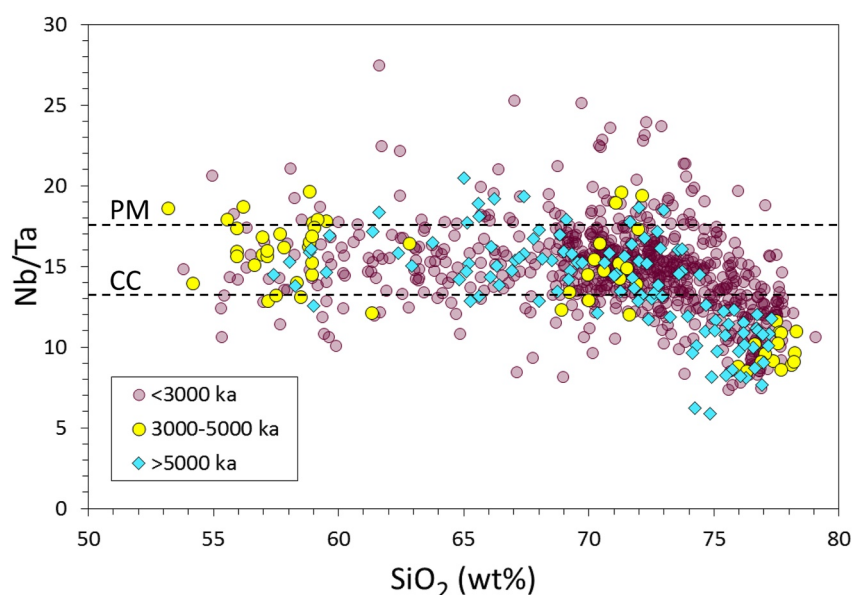


**Figure 14.** Variations of Nb/Ta in the Detroit tephra glasses versus SiO<sub>2</sub> content. Single shard analyses are shown. Characteristic Nb/Ta for the Earth primitive mantle (PM) and bulk continental crust (CC) are shown after McDonough and Sun (1995) and Rudnick and Gao (2003), respectively. Decrease of Nb/Ta in high-Si glasses of all the age groups is most readily explained by crystallization of biotite ± amphibole ± rutile (see text for details).

in the south and Kronotsky volcano in the north was inactive during the Pliocene and was the site of many large caldera-forming eruptions in the Pleistocene.

Miocene tephtras with ages >5 Ma have somewhat distinctive compositions from the other tephtras. They all have relatively high Nb/Y > 0.1, (La/Sm)<sub>N</sub> > 1.5 (Figures 13a and 13b) but variable (Ba/Nb)<sub>N</sub> and (Th/La)<sub>N</sub> overlapping with more recent Kamchatkan tephtras (Figures 13c and 13d). The sources of these magmas are uncertain. Some of them or all could readily originate from the Sredinny Range, where Miocene rocks have typical arc-type compositions and are comparable to the modern RA magmas of Kamchatka (Avdeiko et al., 2007; Portnyagin et al., 2020).

Cao et al. (1995) noticed that Miocene tephtras from the Detroit sequence have distinctively low Nb/Ta ratios, which might suggest a specific source for their parental magmas. Our data (Figures 13e and 14) show that some Miocene samples indeed have Nb/Ta < 10, whereas the majority of other tephtras from all age intervals have Nb/Ta = 15 ± 5. However, the low Nb/Ta ratio appears not to be a unique feature of Miocene tephtras. There are several younger tephtras with low Nb/Ta, which suggest that the low Nb/Ta magma source is not restricted to the Miocene time.

Figure 14 shows relationships between SiO<sub>2</sub> in tephtra glass and Nb/Ta. Apparently, low Nb/Ta is a feature of the most evolved magmas with the highest SiO<sub>2</sub> and the ratio begins decreasing at SiO<sub>2</sub> > 72 wt%. Because Nb/Ta does not correlate with source-sensitive trace element ratios (e.g., Ba/Nb, Th/La, etc.) the most plausible explanation for low Nb/Ta in the most SiO<sub>2</sub>-rich samples is crystal fractionation. Most likely Nb/Ta can be fractionated by crystallization of biotite and amphibole, which have D<sub>Nb</sub>/D<sub>Ta</sub> > 1 (Ballouard et al., 2020). Crystallization of accessory rutile is another possibility because rutile-melt D<sub>Nb</sub>/D<sub>Ta</sub> increases above 1 with decreasing temperature (<900°C) at moderately high H<sub>2</sub>O contents 5–10 wt% (Xiong et al., 2011), which are appropriate for magma storage conditions in the upper crust.

A large compositional variability of studied tephtras makes it possible at least for some of them to identify their source volcanic zones and, in some cases, to precisely determine their source volcano. These results are elaborated in the following chapter.

### 5.3. Identified Source Volcanoes

Kamchatka may have the highest concentration of Quaternary calderas per unit of arc length in the world (Hughes & Mahood, 2008). Most of the calderas are nested so the number of large caldera-forming eruptions is definitely greater than that of the morphologically expressed calderas (e.g., Seligman et al., 2014). Kamchatka calderas are

the first suspected sources of the Detroit tephra, so we began our search for proximal-distal tephra matches from the best studied calderas and their dated pyroclastic deposits (listed below from south to north). The geochemical data for these proximal deposits included the analyses of the dated ignimbrites as well as of many other pyroclastic units (Portnyagin et al., 2020). Many proximal ignimbrites are altered and do not preserve fresh glass, which precludes direct comparison of their composition to that of distal tephra. In this case, we use contents of immobile trace elements (REEs and HFSE = High-Field Strength Elements) in ignimbrite groundmass as those do not change during devitrification (Ponomareva et al., 2018; Portnyagin et al., 2020). We were able to match 14 of 30 dated ignimbrites to their distal counterparts in the Detroit tephra sequence.

Only one tephra from the Detroit sequence, *DS31* has been previously studied and linked to its source eruptive center—*Pauzhetka caldera* in South Kamchatka RA (Figure 1b; Bubenshchikova et al., 2023; Ponomareva et al., 2018). This tephra was found in all three cores on the Detroit Seamount as well as in cores located further south along the Emperor Seamount Chain up to 45°N in the NW Pacific and further west in the Okhotsk Sea. The age of the eruption was estimated at ~418 ka (Bubenshchikova et al., 2023), which coincides with the *DS31* age of 418.1 ka in our Detroit age model (Table 2). Tephra *DS35* and *DS66* are close to *Pauzhetka* tephra in trace element contents (quite distinct among the Detroit tephra due to low Sm and Y contents) and also fall into the RA field (Figures 15a and 15b), which may suggest that their source(s) were located in the same area. However, the *DS35* and *DS66* tephra show higher K<sub>2</sub>O contents, and, in addition, *DS66* tephra has lower Cl and slightly lower CaO contents compared to the *DS31* (*Pauzhetka*) one, which allows their distinction.

Tephra *DS3* (~60 ka), *DS17* (~273 ka), and *DS95* (~2,934 ka) are close in trace element composition to the *Ksudach caldera* eruptives (South Kamchatka) (Figure 15c). However, the oldest *DS95* tephra falls out of the *Ksudach* trend on the SiO<sub>2</sub>-K<sub>2</sub>O diagram (Figure 15d), which indicates a different source. *Ksudach* hosts at least two Pleistocene calderas (Volynets et al., 1999). The only dated pre-Holocene *Ksudach* ignimbrite yielded an age of 162 ± 17 ka (Bindeman et al., 2010), which does not match any of the Detroit tephra with *Ksudach*-like compositions.

*Gorely caldera* in South Kamchatka rear-arc (Figure 1b) is surrounded by an extensive pyroclastic sheet, which comprises layers of pumice and welded tuffs (Selyangin & Ponomareva, 1999). The caldera was originally thought to be the result of a single eruption at ~38 ka BP (calibrated <sup>14</sup>C age from Braitseva et al., 1995), however, five ignimbrite units dated within the range of 38–360 ka and interlayered with pumice horizons suggest a series of large caldera-forming eruptions (Table 5; Bindeman et al., 2010; Seligman et al., 2014).

*Gorely* proximal pyroclastic deposits form a distinct field in the lower part of the RA area in the discrimination trace element diagrams (Figure 15e). Comparisons of the compositions and ages of proximal ignimbrites (Portnyagin et al., 2020) with the Detroit tephra sequence have allowed us to identify eight distal tephra from the *Gorely* eruptive center with ages between ~50 and 450 ka and to correlate seven of them with specific proximal units (Table 5, Figure 15f). The uppermost *Gorely* tephra on the Detroit Seamount, *DS2*, matches the proximal “dacite pumice” (Selyangin & Ponomareva, 1999). Its age near the volcano has been estimated at ~34 ka (Ponomareva et al., 2021), but it goes back to ~50 ka in our age model (more about this tephra in Section 5.4).

Second *Gorely* tephra, *DS4* (~77.5 ka), is compositionally rather similar to *DS2* (Figures 15f and 16a), however, it is still slightly different and significantly older. It might match proximal welded tuff dated at <100 ka but underlying the “dacite pumice” (Table 5; Seligman et al., 2014). *DS9* (~151 ka) and *DS10* (158 ka) tephra are rather close to each other in age and composition (Table 5) and correlate to the ignimbrite-pumice fall package exposed north of *Gorely*, in *Spokoyny Creek* (Portnyagin et al., 2020). Glasses from these tephra exhibit distinctive long trends in SiO<sub>2</sub> contents (Figure 15f). *DS15* (~252 ka) tephra correlates with the undated pumice unit exposed in the *Opasny Canyon* below *DS2* and above lower welded tuffs (Table 5). *DS18* (~279 ka) correlates to the undated pumice tuff 74L-2014 in the *Opasny Canyon*.

Three of the welded tuff units dated near *Gorely caldera*—109L-2010 (227 ± 19 ka), 108L-2010 (324 ± 10 ka), and 107L-2010 (332 ± 6 ka) (Seligman et al., 2014)—do not have matches in the Detroit tephra sequence. The second one may have been derived from a source other than *Gorely* based on its too low K<sub>2</sub>O contents (Figure 15f). *DS27* (~351 ka) correlates to the oldest dated *Gorely* welded tuff (2005L-19, 361 ± 8 ka). The oldest tephra of the *Gorely* composition in the Detroit sequence is *DS33* (~450 ka)—pyroclastic deposits of such old age are not exposed in known outcrops around *Gorely*.

In total, eight tephra in the Detroit sequence and three more dated welded tuffs near the volcano provide evidence of 11 large eruptions from *Gorely* within the last ~450 ka (Table 5). These major eruptions were separated by 7–100 ka long repose periods. No tephra with the *Gorely* characteristics have been found earlier than 450 ka,

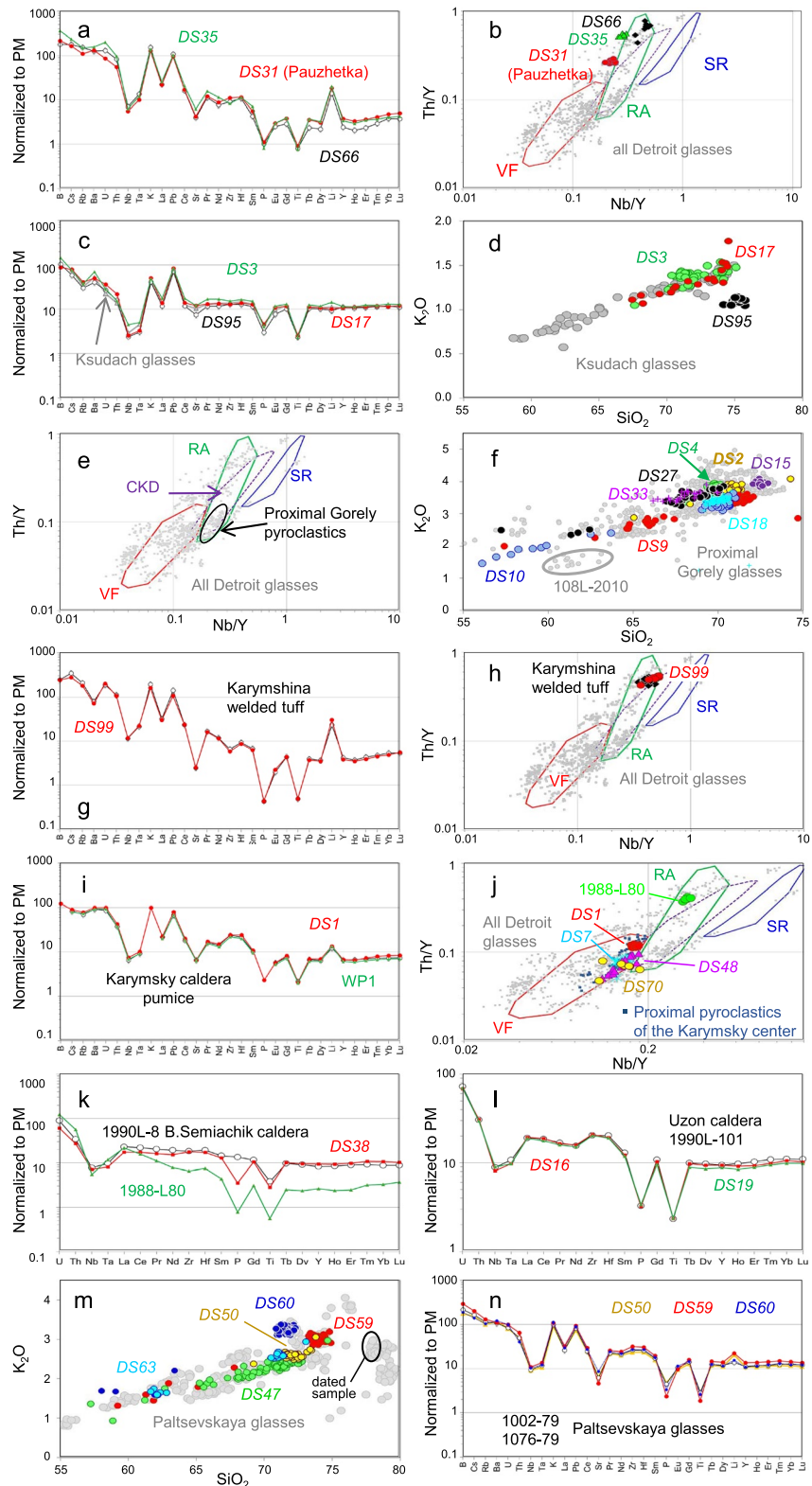


**Figure 15.** Correlations of the Detroit tephra to the Kamchatka volcanic centers.  $\text{SiO}_2$  and  $\text{K}_2\text{O}$  concentrations are given in wt%, trace elements—in ppm. Spider diagrams are drawn using trace elements concentrations normalized to primitive mantle (PM) after McDonough and Sun (1995).

**Table 5**

*Correlation of Tephra From the Composite Detroit Sequence to Compositionally Similar Proximal Pyroclastic Units From the Gorely Eruptive Center and to Distal Tephra From Other Sites*

Detroit tephra ID	Modeled age (ka)	Error 2σ (ka)	Dated proximal units	Ages of proximal units (ka)	Error 2σ (ka)	Compositionally identical distal tephra
DS2	50	2.8	“Dacite pumice”	33.9	0.4	WP4, D2, numerous on-land samples
DS4	77.5	9.0	77L-144 <sup>a</sup>	<100	-	WP5
DS9	150.9	6.4	Spokoiny Creek welded tuff and pumices	-	-	DL1
DS10	158.2	7.0				WP9
No matching tephra			109L-2010 <sup>a</sup>	227	19	-
DS15	251.7	5.6	K12-01-4b <sup>a</sup> , 36L-2015 <sup>a</sup> , Vvp01 <sup>a</sup>	-	-	-
DS18	278.9	11.8	74L-2014? <sup>a</sup>	-	-	-
No matching tephra			108L-2010 <sup>a</sup>	324	10	-
No matching tephra			107L-2010 <sup>a</sup>	332	6	-
DS27	350.6	10.0	2005L-19 <sup>a</sup>	361	-	-
DS33	450.0	13.6	Interval not exposed	-	-	-

*Note.* In column 5, the youngest date is calibrated radiocarbon age (Ponomareva et al., 2021); the other dates were obtained by <sup>40</sup>Ar/<sup>39</sup>Ar method (Bindeman et al., 2010; Seligman et al., 2014).

<sup>a</sup>Stratigraphically ordered samples from the Opasny Canyon, 3.5 km SE from the Gorely caldera rim (Portnyagin et al., 2020). Welded tuff sample 108L-2010 deemed as Gorely eruptive based on its position close to the Gorely caldera (Seligman et al., 2014) has too low K<sub>2</sub>O contents for Gorely so may belong to another volcanic center (Figure 15f).

which suggests the age of inception of the explosive activity from this eruptive center and gives an estimate of the longevity of the individual eruptive centers in Kamchatka.

The RA of South Kamchatka farther north of the Gorely caldera hosts tens of meters thick ignimbrite packages supposedly related to the *Karymshina caldera* complex (Figure 1b) (Leonov & Rogozin, 2007). The ages of different intra-caldera ignimbrite units were estimated at ~990, 1,390, and 1,780 ka while the age of the extra-caldera ignimbrite was estimated at 3,620–3,850 ka (Bindeman et al., 2010, 2019). In the Detroit sequence, we were not able to identify any tephra compositionally matching three intra-caldera ignimbrite units. However, we found a robust compositional and age match between the extra-caldera welded tuff (samples 13L-2015 and 139L-2013; Bindeman et al., 2019; Portnyagin et al., 2020) and DS99 tephra (Figures 15g and 15h) directly dated in this study at 3,900 ± 90 ka (<sup>40</sup>Ar/<sup>39</sup>Ar, Table 4) or at ~3,773 ± 20.6 ka (modeled age, Table 3).

A suite of mafic ignimbrites related to *Verkhneavachinskaya caldera* in the Kamchatka volcanic front was dated at 5,580 ± 30 and 5,780 ± 220 ka (Bergal-Kuvikas et al., 2019). The Detroit tephra sequence documents a number of explosive eruptions between 5,100 and 5,700 ka, however, no mafic tephra have been found within this interval (DS104-DS114).

The only Holocene tephra expressed in the Detroit sequence, DS1 (KRM), comes from the *Karymsky caldera* (EVB, Figures 1b and 15i). Its onshore age was estimated at ~8.5 ka (calibrated from an average radiocarbon age of 7,889 ± 67 <sup>14</sup>C BP; Braitseva et al., 1997). Cryptotephra from this eruption was found in Greenland ice cores and dated at 9,045 ± 64 b2k. In addition to Karymsky caldera, the *Karymsky eruptive center* includes a number of older calderas and hosts a stratigraphically complex package of numerous ignimbrite and pumice fall units (Leonov & Grib, 2004; Masurenkov, 1980). Three major ignimbrite units have been dated with the help of <sup>40</sup>Ar/<sup>39</sup>Ar method yielding the ages of ~70 (Odnoboky), ~400 (Polovinka), and ~1,200 ka (Stena-Soboliny) (Bindeman et al., 2010). We have not found geochemical/age matches for any of these eruptions in the Detroit sequence, however, three tephra compositionally resembling the Karymsky eruptive center pyroclastic deposits have been found in different time periods: DS7 (~101 ka), DS48 (~838 ka), and DS70 (~1,620 ka) (Figure 15j).

The next eruptive center to the north is the *Bolshoi Semiachik* nested caldera. Welded tuff dated at ~524 ka (sample 1990L-8 in Bindeman et al., 2010) is compositionally and temporally close to tephra DS38 tephra with an age of ~532 ka (Figure 15k, Table 2). No matches for the second welded tuff (sample 1988-L80, Bindeman

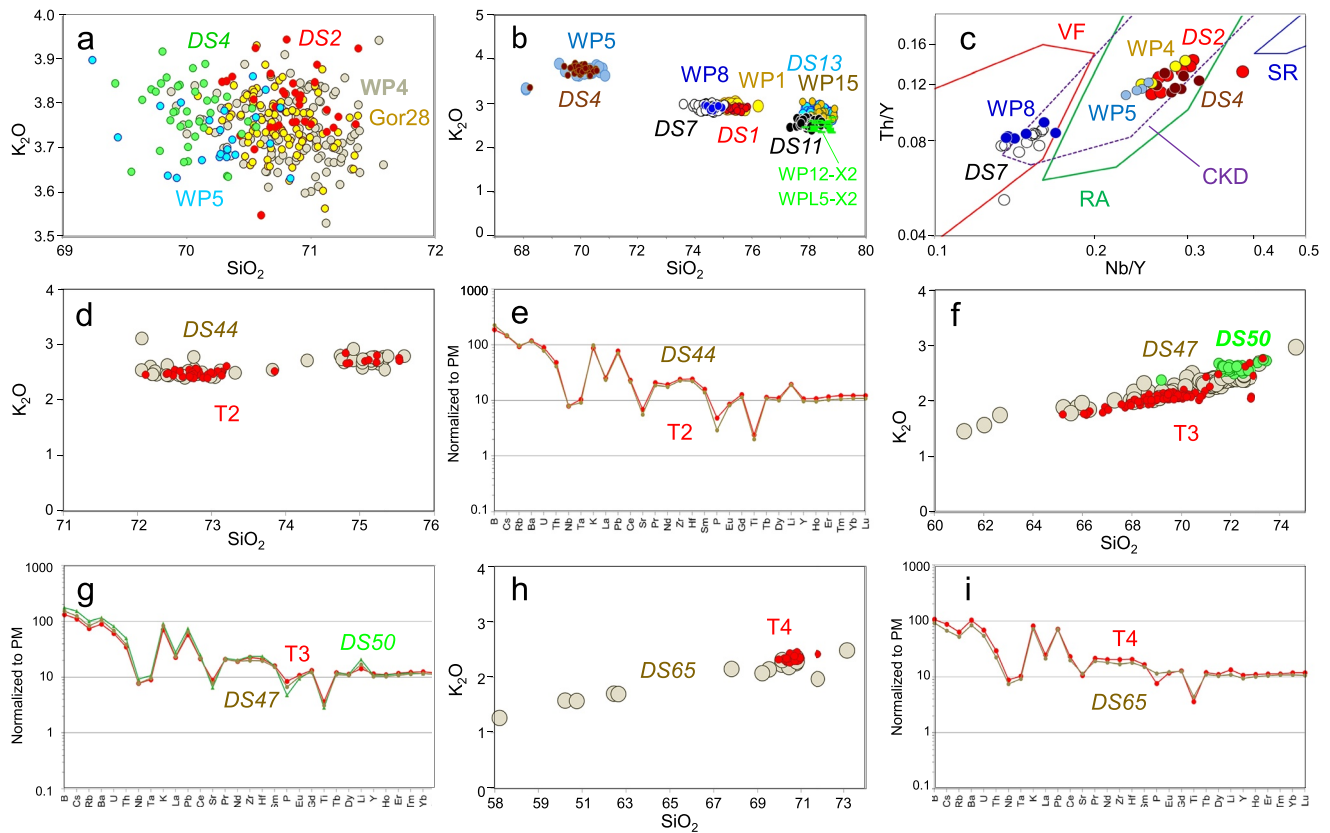


**Figure 16.** Correlations of the Detroit tephra to those from core SO201-2-40 (Meiji Seamount), Lv-4-2 (Detroit Seamount, Eastern slope), and the El'gygytgyn Lake core.  $\text{SiO}_2$  and  $\text{K}_2\text{O}$  concentrations are given in wt%, trace elements—in ppm. Spider diagrams are drawn using trace elements concentrations normalized to primitive mantle (PM) after McDonough and Sun (1995).

et al., 2010) assigned to Bolshoi Semiachik and dated at  $\sim 560$  ka have been found around this time. Based on the diagrams for the Kamchatka glasses in Portnyagin et al. (2020), this older sample comes from RA rather than from the VF, so it might belong to a different eruptive center. One of the welded tuff units related to the Uzon caldera and dated at  $\sim 278$  ka (Bindeman et al., 2010) geochemically matches *DS19* tephra with an age of  $\sim 281$  ka (Figure 15l). In addition, tephra *DS16* ( $\sim 263$  ka) is also compositionally close to the Uzon tuff.

The northernmost caldera in the Kamchatka VF is *Paltsevskaia caldera* surrounded by up to 160 m thick packages of welded tuffs, cinders and pumices. The caldera and surrounding deposits were described only once (Shantser & Kraevaya, 1980) and never studied in detail. Erosional contacts between the pyroclastic units suggest multiple explosive eruptions roughly assigned to two different age groups. The only available date of  $1,290 \pm 10$  ka was obtained for the lower ignimbrite within the younger age group (Bindeman et al., 2010). We did not find a geochemical match for the dated sample in the Detroit tephra sequence, however, for some pyroclastic units from the same younger group, there are matching tephra dated within the interval of 800–1,300 ka: *DS47*, *DS50*, *DS59*, *DS60*, and *DS63* (e.g., Figures 15m, 15n, and 16f). In addition, a suite of compositionally similar tephra was found between 2,100 and 2,500 ka (*DS84*, *DS87*, and *DS91*), which may represent the older group of proximal pyroclastic deposits from the Paltsevskaia area.

In *Sredinny Range*, welded tuffs from four eruptive centers (from south to north: Khangar, Nosichan, Uksichan, and Tekletunup) were dated with  $^{40}\text{Ar}/^{39}\text{Ar}$  (Bindeman et al., 2010). At the *Khangar eruptive center*, one of the ignimbrites, presumably the oldest of the sequence, was dated at  $398 \pm 8$  ka. We were not able to identify any matching tephra in the Detroit sequence. However, three *DS* tephra (*DS12*, *DS23*, and *DS24*) fall into the Khangar field. Three SR ignimbrites yielded late Pliocene ages: *Uksichan caldera*  $3,560 \pm 500$  ka, *Nosichan*— $4,020 \pm 120$  ka, and *Tekletunup*— $5,700 \pm 160$  ka (Bindeman et al., 2010). No exact matches have been found in the Detroit tephra sequence within the appropriate time intervals; however, tephra *DS106* and *DS108* with ages of  $5074.9 \pm 120.2$  ka and  $5132.5 \pm 119$  ka, respectively, have  $\text{Ba}/\text{Nb} > 30$  and are the most

similar to those from Tekletunup volcano among Miocene ignimbrites in the available database (Portnyagin et al., 2020). For the rest of the Detroit tephra, the preliminary identification of their source zones was performed using the discrimination diagrams developed by Portnyagin et al. (2020) (Tables 2 and 3).

The Detroit tephra sequence shows that glass from each tephra is compositionally unique. Even tephra from the same eruptive center, for example, Gorely, while quite similar in composition, can still be distinguished on the detailed binary plots. The unique characteristics of each tephra reflect the many variables involved in magma generation and ascent.

Since many Detroit tephra can be correlated to known Kamchatka eruptions and volcanic centers, an important question arises of whether the Detroit tephra record is representative of the Kamchatka volcanism in general. First of all, we are confident that the Detroit sequence is not representative for non- or weakly explosive but voluminous mafic volcanics in Kamchatka, composing several hundred-meter-thick lava piles in the basement of the Eastern and Central Kamchatka volcanoes and in the Sredinny Range (Churikova et al., 2015; Dorendorf et al., 2000; Volynets et al., 2010). The Detroit record can more readily pretend to be the most complete documented record of explosive volcanism of Kamchatka because this record consists of about 10 times more eruptions with  $M \sim 7.5$  than it was known before from the onshore record. On the other hand, the Detroit record cannot be considered complete because many voluminous ignimbrites of Kamchatka (e.g., Bergal-Kuvikas et al., 2019; Bindeman et al., 2010; Portnyagin et al., 2020) left no visible tephra layer in the Detroit section. Reconstruction of a complete history of Kamchatka volcanism will require integration of all available data from on-land or off-shore records. Making up such a composite record is hardly accessible goal in the close future because of the complex nature and low accessibility of the onshore pyroclastic sequences and scarcity of absolute age determinations for volcanic rocks in Kamchatka.

#### 5.4. Correlations to Distal Tephra Sequences

Existing pre-Holocene tephra inventories for the NW Pacific area include the following sites: (a) onshore tephra sequence in the Central Kamchatka Depression (CKD) (~30 ka; Ponomareva et al., 2021); (b) offshore cores SO201-2-40 on Meiji Seamount (~214 ka; Derkachev et al., 2020) and Lv63-4-2 on the eastern slope of the Detroit Seamount (~245 ka; Derkachev et al., 2023); (c) El'gygytgyn Lake cores drilled in the frames of the International Continental Scientific Drilling Program (2,800 ka; van den Bogaard et al., 2014); (d) a number of cores in the Okhotsk Sea (e.g., ~1,100 ka core MD01-2415; Derkachev et al., 2016) (Figure 1a).

Two tephra from the Detroit sequence occur in two or three of these inventories. The first one is *DS2* from the Gorely eruptive center. *DS2* tephra is similar to Gor28 from the onshore CKD sequence, to prevailing glass population in the WP4 tephra from the Meiji Seamount core (Derkachev et al., 2020), and to D2 ash from core Lv63-4-2 (Derkachev et al., 2023) (Figures 16a and 16b). In addition, compositionally identical tephra was also found in core ODP145-883D on the Detroit Seamount (Bigg et al., 2008) and in the Ledovy Bluff outcrop (Chukotka), ~1,500 km north of the Detroit (Figure 17; Ponomareva et al., 2021). Earlier known age estimates for this tephra ranged from 28 to 40 ka (Ponomareva et al., 2021) and are 47–53 ka in our age model (Table 2). The reasons for such a large array of age estimates for the Gorely tephra need further investigation and may arise from discrepancies in the age models based on different methods and proxies. Gorely *DS2* is the only tephra in the Detroit sequence belonging to the supposed 30–40 ka Kamchatka flare of caldera-forming eruptions (other calderas are Uzon, Krasheninnikov, and Opala) (Braitseva et al., 1995). The second tephra, *DS14* has two glass populations: one of those matches WP17 tephra from core SO201-2-40 and to D7 tephra from core Lv63-4-2.

Core SO201-2-40 is located ~200 km closer to Kamchatka than the Detroit cores (Figure 1a), so it contains more tephra for the same time period (~214 ka) compared to the Detroit sequence. Twenty-five visible tephra layers and lenses were found in the core and 21 of them were geochemically characterized; about half of those have mixed compositions with two or more glass populations likely indicating either bioturbation or closely spaced in time eruptions (Derkachev et al., 2020). Besides Gorely tephra *DS2* (WP4) and *DS14* (WP17), we found five more tephra compositionally matching certain Detroit tephra with close age estimates (Table 6, Figures 16a–16d). Tephra *DS1*, *DS4*, and *DS7* were correlated to WP1, WP5, and WP8 tephra in core SO201-2-40, respectively, based on both major and trace element compositions (Figures 15i and 16a–16d). The other core SO201-2-40 tephra (WPL5, WP12, and WP15) have not been analyzed for trace element composition, so their correlations to the Detroit tephra are tentative. *DS11* tephra is compositionally similar to one of the glass populations in two

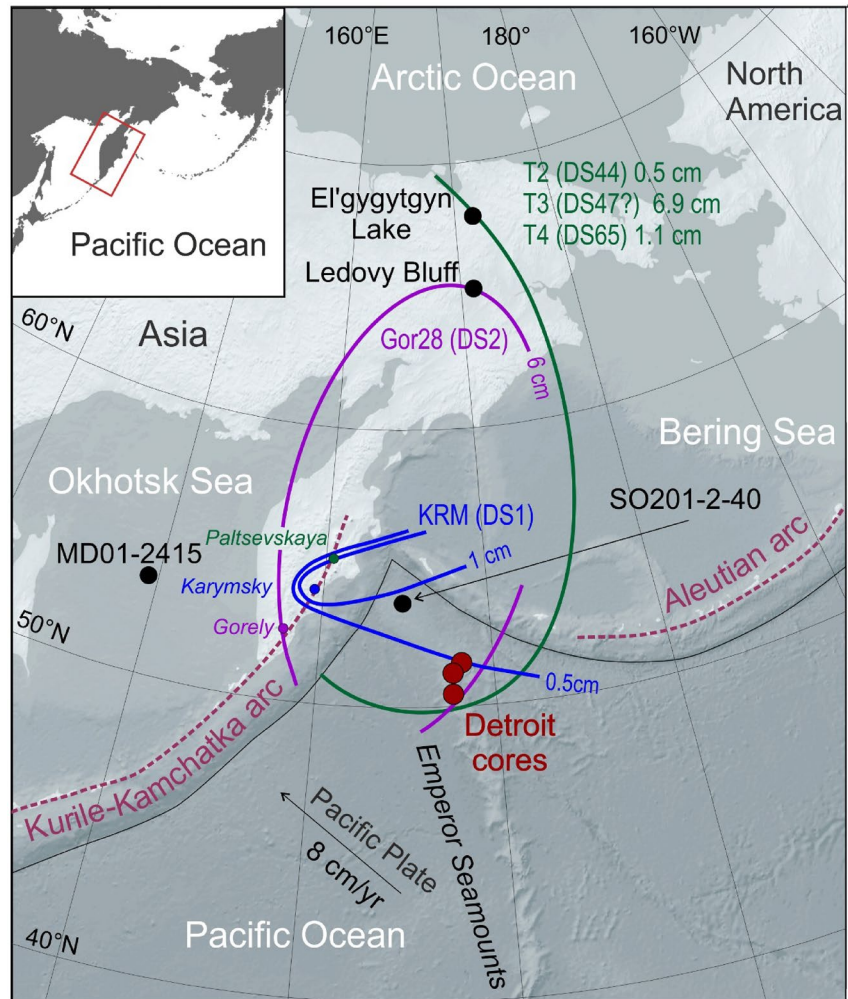


**Figure 17.** Dispersal areas for some widespread tephra found in the Detroit Seamount sediments (see explanations in the text).

mixed tephra (WPL5 and WP12) (Figure 16b). These identical populations come from stratigraphically close tephra, and may represent the same layer but deformed due to bioturbation or coring (Derkachev et al., 2020). *DS13* tephra is similar to WP15 (Table 6).

*Core Lv63-4-2* (~245 ka) is located ~42 km northwest of Site 884B (Figure 1a; Derkachev et al., 2023). Besides Gorely *DS2* (D2) and *DS14* (D7) tephra, considered above, there are four more tephra linking Detroit sequence to Lv63-4-2 (Table 6). These are *DS8* (D5); *DS9* (DL1); *DS12* (DL2); and *DS16* (D8) (Figure S2 in Supporting Information S1).

*El'gygytgyn Lake core* located ~1,900 km NNE of the Detroit Seamount (Figure 1a) contains eight visible tephra layers (T0-T7) with ages ranging between 58 and 2,225 ka (van den Bogaard et al., 2014). One of the layers, T1 (~177 ka), was earlier correlated to the Rauchua tephra on the Arctic coast and to layer WP14 in core SO201-2-40 (Ponomareva et al., 2013b). Three more layers—T2, T3, and T4—have tentative correlations to the Detroit sequence (Table 6, Figures 16d–16i). T2 (~674 ka) with its two glass populations coming from a single tephra is similar to *DS44* (~678 ka) (Figures 16d and 16e). T3 (~918 ka) resembles *DS47* (797 ka) (Figures 16f and 16g); however, the age estimates for these two tephra differ by about 100 ka. An older *DS50* tephra (~894 ka) which is closer in age to T3, is rather similar to the silicic part of the latter (Figures 16f and 16g); however, *DS50* glasses have slightly higher  $K_2O$  contents. Based on glass composition, we would favor T3-*DS47* correlation; in this case, ages for this eruption should be refined in further studies. In any case, T3, *DS47*, and *DS50* tephra likely

**Table 6**

Correlation of Tephra From the Composite Detroit Sequence to Those From the Onshore Central Kamchatka Depression Sequence, El'gygytyn Lake Core (Chukotka), and Marine Cores SO201-2-40 (Meiji Seamount) and Lv63-8-2 (Detroit Seamount)

Detroit tephra ID	Modeled age (ka)	Error $2\sigma$ (ka)	Compositionally similar tephra	Core/onshore site	Location	Previous age estimates (ka)	Source zone/volcano
DS1	9.0	0.2	WP1 (KRM)	SO201-2-40	Meiji Seamount	8.7	VF, Karymsky caldera
DS2	50.0	2.8	Gor28	CKD sequence	Kamchatka	28–40	RA, Gorely caldera
			WP4-X1	SO201-2-40	Meiji Seamount		
			D2	Lv63-4-2	Detroit Seamount, E flank		
DS4	77.5	9.0	WP5-X3	SO201-2-40	Meiji Seamount	80	RA, Gorely caldera
DS7	101.4	4.4	WP8	SO201-2-40	Meiji Seamount	107	VF, Karymsky center?
DS8	121.8	9.4	D5	Lv63-4-2	Detroit Seamount, E flank	123	Aleutian arc?
DS9	150.9	6.4	DL1	Lv63-4-2	Detroit Seamount, E flank	138	RA, Gorely caldera
DS11	159.0	6.6	WPL5-X2?	SO201-2-40	Meiji Seamount	162	VF
			WP12-X2?			167	
DS12	195.0	8.4	DL2	Lv63-4-2	Detroit Seamount, E flank	170	SR
DS13	208.4	5.4	WP15?	SO201-2-40	Meiji Seamount	195	VF
DS14	213.6	8.4	D7	Lv63-4-2	Detroit Seamount, E flank	210	VF
DS16	262.5	6.4	D8	Lv63-4-2	Detroit Seamount, E flank	245	VF
DS44	677.6	13.2	T2	5011-1B	El'gygytyn Lake, Chukotka	674	VF, Paltsevskaya caldera?
DS47	796.9	24.6	T3?	-"	-"	918	VF, Paltsevskaya caldera?
DS65	1432.6	13.6	T4	5011-1A	-"	1411	VF

Note. Gor28, WP, and D tephra according to Ponomareva et al. (2021) and Derkachev et al. (2020, 2023), respectively. T2, T3, and T4 tephra according to van den Bogaard et al. (2014). Correlations to WPL5, WP12, and WP15 and all Lv63-4-2 tephra are based on age and major element compositions as no trace element data for these tephra are available. KRM—tephra related to the Karymsky caldera (Braitseva et al., 1997).

represent the same eruptive flare up related to the Paltsevskaya caldera. T4 (~1,411 ka) glass composition is similar to DS65 with an age of ~1,432 ka (Figures 16h and 16i) suggesting that this is the same tephra.

We did not find any matches between the Detroit tephra sequence and Okhotsk Sea visible tephra identified by Derkachev et al. (2016). Only one of the Detroit tephra, DS31 (Pauzhetka) was found also in the Okhotsk Sea cores MD01-2415 and LV28-41-4, however, it was detected there as cryptotephra (Bubenschikova et al., 2023; Ponomareva et al., 2018).

### 5.5. Tephra Volumes and Eruption Magnitudes

Most tephra layers from the Detroit Seamount cores range in thickness from 0.5 to 20 cm (Tables 2 and 3; Table S1). Only 10 tephra layers, all of them from Site 884B, are thicker; of these, seven tephra have thicknesses between 22 and 46 cm, and three ones, DS49, DS69, and DS70, have thicknesses 84–182 cm. The last three tephra occur also in core 882A, where their thickness varies between 1 and 8.5 cm. Cao et al. (1995) who studied tephra in Sites 882, 883, and 884 also described such thick layers only in Site 884 (B and C holes). This site is located on the Meiji Drift deposit, which likely formed by deep ocean currents flowing mainly from the Bering Sea (Figure 1c) (VanLaningham et al., 2009). This suggests that the extraordinary high tephra thicknesses in Site 884B might result from their redeposition by these currents.

For most of the Detroit tephra, available data do not permit accurate estimates of volume and eruption size. However, conservative estimates can be made based on the single-isopach approach of Legros (2000). For a 1-cm-thick layer, even a narrow isopach striking from the Kamchatka volcanic front to the Detroit Seamount yields a minimum tephra volume ( $V$ ) of  $7 \text{ km}^3$  and  $M = 5.8$  (assumed density  $800 \text{ kg/m}^3$ ) (Pyle, 1995). Taking

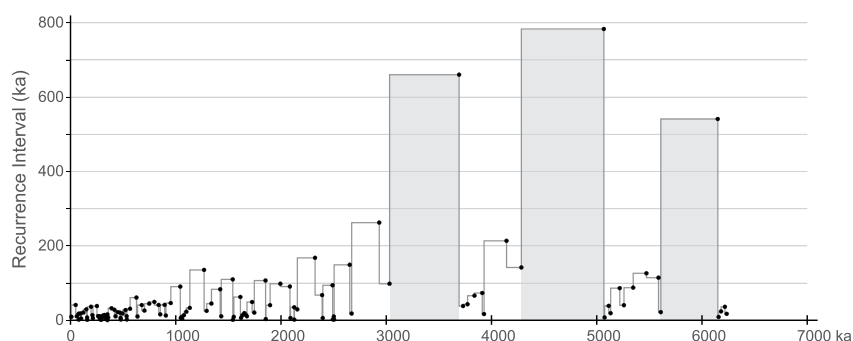


**Figure 18.** Recurrence of ash-falls at the Detroit Seamount during the last 6.2 Ma. Individual eruptions are shown with black dots. The three longest time gaps (540–780 ka) are shown with gray shade.

motion of the Pacific plate ( $\sim 8$  cm/yr; Gorbatov et al., 1997) into account, the oldest tephra were transported  $\sim 480$  km farther, so that a 1-cm-thick layer means at least  $10 \text{ km}^3$  of erupted tephra,  $M = 5.9$ . As a single-isopach estimate is a linear function of thickness, increase in thickness affects the volume, so that the thickest layers were deposited from at least  $700 \text{ km}^3$  ash-falls related to  $M = 7.8$  eruptions. Note that all the numbers above are based on most compact isopachs and any offset of an ash-fall axis from the Detroit Seamount sites will dramatically increase the volume and magnitude of the eruption. In addition, our volume estimates refer only to air-borne ash and do not include proximal ignimbrites or caldera fill, so they constitute only a part of the total eruptive volumes. For example, minimal volume of airfall ash from the Pauzhetka (*DS31*) eruption, was estimated at  $\sim 200 \text{ km}^3$ , which corresponds to  $M = 7.2$  while the total eruptive volume was almost twice larger ( $330\text{--}360 \text{ km}^3$ ) and corresponds to  $M = 7.60\text{--}7.65$  (Ponomareva et al., 2018).

Similar to the Pauzhetka (*DS31*) tephra, more precise volume estimates could be provided for a few more tephra correlated among several disparate sites based on rough dispersal area outlines and the same method by Legros (2000) (Figure 17). *DS1* (KRM) tephra yields  $V = 4.3 \text{ km}^3$  and  $M = 5.5$  based both on the 0.5 and 1 cm isopachs. Based on a 6 cm isopach, *DS2* (Gor28) tephra has  $V = 236 \text{ km}^3$  and  $M = 7.3$ . Tephra *DS44* (T2), *DS47* (T3), and *DS65* (T4) correlated to the corresponding tephra in the Elgygytgyn Lake core yield  $V > 95 \text{ km}^3$  and  $M = 6.9$ ,  $V > 426 \text{ km}^3$  and  $M = 7.5$ , and  $V > 61 \text{ km}^3$ ,  $M = 6.7$ , respectively. Our calculations suggest that the eruptions recorded in the Detroit tephra sequence had conservative magnitudes between 5.8 and 7.8, in other words, they were in the range of the Changbaishan Millennium Eruption and Campanian Ignimbrite Eruption (Silleni et al., 2020; Yang et al., 2021) or larger. It is clear that tephra from these eruptions were dispersed significantly farther than the Detroit Seamount and might have caused environmental changes.

### 5.6. Occurrence of Tephra Falls in the NW Pacific

The Detroit tephra sequence provides a 6.2 Ma long record including 119 explosive eruptions, most of which likely occurred in the Kamchatka Peninsula. As this sequence is located in favorable direction for ash-falls, it likely captures most of the largest events (Figures 2–5 and 18). Detailed analysis of the temporal patterns in the eruption sequence and their relation to the climate change will be considered in a separate paper. Here we will describe only main features of the eruption flux (Figure 18). The description of tephra layers in Sites 882 and 883B and 883C allowed Prueher and Rea (2001) to conclude that episodes of explosive volcanism from the Kamchatka arc occurred at approximately 2,650–2,500, 1,700–1,500, 900–700, and 500–200 ka. Later, Prueher (2004) omitted the third episode (900–700 ka) leaving three other peaks. These authors suggested a link between the great enhancement of explosive volcanism and the onset of large-scale Northern Hemisphere glaciation at 2,650 ka (Prueher & Rea, 1998; Rea et al., 1993). Our data indicates episodes of explosive activity at  $\sim 6,200$ ; 5,600–5,000; 4,300–3,700, and almost continuous activity since  $\sim 3,000$  ka (Figure 18). Within the latter 3,000 ka long episode, the most active intervals can be identified at 1,700–1,600, 1,150–1,050, and 600–500 ka (with a peak at 360–250 ka) (Figure 18).

It is usually the peaks of explosive activity that attract the most attention. However, the periods without explosive eruptions are equally fascinating. For example, our studied record of explosive eruptions was preceded by a  $\sim 30$  Ma long period, when no tephra were deposited in the Detroit Seamount sediments (Cao et al., 1995).

The reasons for such a long gap in the explosive activity are not clear. In our record, there are breaks as long as 0.78 Ma when no tephra was deposited (Figure 18). These irregularities in the eruption flux need further attention and explanations.

Episodes of enhanced explosive activity are known both on regional and even global scales (e.g., Cambray & Cadet, 1994, 1996; Cambray et al., 1995; Sigurdsson, 2000). For example, the abrupt increase of the amount of tephra layers around 2,600 ka was identified in many Pacific arcs (Prueher and Rea, 2001). The reasons for near-synchronous global and circum-Pacific episodicity are not clear. During the last decades, most studies link this episodicity to climate change and glacial stages, in particular (review of these studies is provided by Kutterolf et al., 2019). For example, Jellinek et al. (2004), Nowell et al. (2006), Kutterolf et al. (2013), and Schindlbeck, Kutterolf, Freundt, et al. (2018) consistently obtained data that place the peaks in volcanism in the deglaciation periods. According to our results for core MD01-2416 whose tephras were tied to marine isotope stage (MIS) events over the last 1,100 ka (Figures 3 and 4 and Table 2), large explosive eruptions in Kamchatka took place both during interglacials and glacial stages including most of the glacial terminations (deglaciations) in that time interval.

However, Kutterolf et al. (2019) rightly remarks that too many uncertainties involved in the calculations can hardly ensure robust conclusions. For example, Cao et al. (1995) counted 69 ash layers in the upper 394 m of Site 882A, which is close to our 66 layers within the same depth interval. At the same time, Prueher and Rea (2001) counted 182 ash layers in the upper 254 m in Hole B of the same Site 882. The cause for such large discrepancies in ash count at the same site might lie in different count methods (visual inspection of the cores, examination of images, inspection of the on-board sediment descriptions, etc.) and/or redeposition in one of the holes (as, e.g., noted for different holes of Site 881 by Cao et al., 1995). We tried to compensate for the differences between sites in the same area by combining three individual tephra sequences (Figures 2–5; Tables 2 and 3).

The patterns we see in the time series of large eruptions undoubtedly resulted from the interference of many local, regional and maybe global processes. The tendency of the large explosive eruptions to cluster and occur within the overall periods of enhanced volcanic activity was shown by statistical methods (Gusev, 2008; Gusev et al., 2003). Without dismissing the role of glacial loading/unloading and sea level change, we think that the subduction process has the leading role in the increase of magma supply to the surface.

### 5.7. Detroit Tephra Layers as Potential Markers for Paleoenvironmental Research

All studied Detroit tephra layers are derived from large eruptions and have the potential to be excellent markers for linking and dating disparate depositional sequences, providing an opportunity to compare their paleoenvironmental records. For example, tephra from the Karymsky caldera (Greenland GICC05 ice core age  $9,045 \pm 64$  a b2k) was mostly dispersed toward the ocean, east of the source, and was found on Bering Island (Kyle et al., 2011), in core SO201-2-40 (Derkachev et al., 2020), and in core 884B (Figure 17). Three tephra layers, *DS44*, *DS47*, and *DS65*, link the marine Detroit sedimentary sequence to the onshore El'gygytyn Lake core (Figure 17). Tephra layers from the Gorely eruptive center also have great potential as markers, as demonstrated by the *DS2* (Gor28) tephra. All these tephra layers can be used as markers over large areas and may allow comparison of age models and climate records in these distant locations. In addition, some tephra layers mark specific paleomagnetic and paleoclimate events (Figures 2–5; Tables 2 and 3), which permits immediate identification of these events in other onshore and offshore records. Undoubtedly, as more cores are described in the future, more marker tephra layers of regional significance will be identified.

## 6. Conclusions

The study of tephra layers buried in marine sediments is an effective method of identifying and dating the largest eruptions and reconstructing a continuous and long record of past explosive activity. The tephra sequence from sediments on the Detroit Seamount studied in this paper provides a 6.2 Ma long and continuous record of explosive volcanism from the NW Pacific arcs. Based on their geochemical make-up, the majority of the Detroit tephra layers were likely derived from Kamchatka with only a minor addition of tephra layers from the Kuril and Aleutian sources. Some tephra layers exhibit geochemical characteristics unknown thus far for any onshore erupted products in the NW Pacific. We did not find any clear geochemical trend, which could be correlated with the regional tectonic evolution of the volcanic arc subduction systems or involvement of different magma sources.

For all tephtras, except *DS1* one, the sedimentation rates (SRs)-based ages were calculated with the help of published and refined core age models. *DS99*, *DS103*, *DS112* and *DS114* tephtras were dated using the  $^{40}\text{Ar}/^{39}\text{Ar}$  technique. A Detroit age model for *DS1-DS119* tephtras was constructed with the help of the Bayesian approach using all relevant tephtra ages and tie-points. The Detroit age model may be revised in the subsequent studies once new data become available.

The eruptions recorded in the Detroit tephtra sequence had conservative magnitudes between 5.8 and 7.8, roughly the range from the Changbaishan Millennium Eruption to the Campanian Ignimbrite eruption (Campi Flegrei). A number of tephtras were correlated to their proximal counterparts and to other distal tephtras from marine and continental deposits. The most active explosive volcanic centers, which repetitively sent their tephtras as far as the Detroit Seamount, were Gorely and Paltsevskaia caldera complexes. Sredinny Range tephtras were surprisingly rare in the record. Our data indicate that episodes of explosive activity took place at  $\sim 6,200$ ;  $5,600\text{--}5,000$ ;  $4,300\text{--}3,700$  ka, and almost continuous activity took place since  $\sim 3,000$  ka. The eruptive flux was irregular with up to 600 ka long quiescent periods within the first 3,200 ka long period and shorter but well expressed breaks in the later record.

The largest tephtras such as Gorely *DS2* as well as the three tephtras *DS44* (T2), *DS47* (T3) and *DS65* (T4) linking the Detroit Seamount cores to the El'gygytgyn one across the distance of  $\sim 1,800$  km are excellent markers, which allow the comparison of disparate paleoenvironmental archives and of their age models. The *DS2* ash layer is the best studied tephtra from the whole Detroit sequence identified thus far in numerous onshore and offshore records providing their correlation. At the same time, the causes of a large range of its age estimates (28–50 ka) with the systematically older offshore ages is still unclear.

Our 6.2 Ma long and continuous record of the largest eruptions offers the basis for further research on the temporal patterns of explosive volcanism as well as on geochemical characteristics of the erupted magmas.

## Data Availability Statement

Geochemical and age data acquired in this study are provided in Tables S1–S7. CQL code for the Bayesian age modeling is provided in Supporting Information S2. All the data is archived at the Mendeley Data repository at Portnyagin (2023).

## Acknowledgments

VP, NB, EZ, and AD gratefully acknowledge support from the Russian Science Foundation (RSF) Grant 22-17-00074, <https://rscf.ru/en/project/22-17-00074/>, which funded data analysis and our work on the manuscript. Sampling was partially supported by the RSF Grant 22-17-00118. We acknowledge GEOMAR (Kiel, Germany) funding for the electron microprobe and LA-ICP-MS analyses. We thank Michael Sarnthein (GEOMAR) for sharing his data on core MD01-2416, Mario Thöner (GEOMAR) and Ulrike Westernströer (CAU Kiel) for their assistance with electron probe and LA-ICP-MS analyses. This research used samples and data provided by the Ocean Drilling Program (ODP). We highly appreciate efficient work of the Gulf Coast Repository (Texas, USA) personnel, and Phil Rumford and Helen Evans, in particular, who made our 2016 sampling campaign highly productive. The ice core work of EC was funded by the European Research Council ice2ice project #610055. We are thankful to the anonymous reviewer for constructive comments. Open Access funding enabled and organized by Projekt DEAL.

## References

- Avdeiko, G. P., Antonov, A. J., Volynets, O. N., Bondarenko, V. I., Rashidov, V. A., Gladkov, N. G., et al. (1992). *Submarine volcanism and zonality of the Kurile island arc* (p. 528). Nauka Publishers. p. [in Russian].
- Avdeiko, G. P., Saveleyev, D. P., Palueva, A. A., & Popruzenko, S. V. (2007). Evolution of the Kurile-Kamchatkan volcanic arcs and dynamics of the Kamchatka-Aleutian junction. In J. Eichelberger, E. Gordeev, M. Kasahara, P. Izbekov, & J. Lees (Eds.), *Volcanism and subduction: The Kamchatka region* (Vol. 172, pp. 37–55). American Geophysical Union.
- Ballouard, C., Massuyeau, M., Elburg, M. A., Tappe, S., Viljoen, F., & Brandenburg, J.-T. (2020). The magmatic and magmatic-hydrothermal evolution of felsic igneous rocks as seen through Nb-Ta geochemical fractionation, with implications for the origins of rare-metal mineralizations. *Earth-Science Reviews*, 203, 103115. <https://doi.org/10.1016/j.earscirev.2020.103115>
- Bergal-Kuvikas, O., Leonov, V., Rogozin, A., Bindeman, I., Kliapitskiy, E., & Churikova, T. (2019). Stratigraphy, structure and geology of Late Miocene Verkhnevachinskaya caldera with basaltic-andesitic ignimbrites at Eastern Kamchatka. *Journal of Geosciences*, (64), 229–250. <https://doi.org/10.3190/jgeosci.295>
- Bigg, G. R., Clark, C. D., & Hughes, A. L. C. (2008). A last glacial ice sheet on the Pacific Russian coast and catastrophic change arising from coupled ice-volcanic interaction. *Earth and Planetary Science Letters*, 265(3–4), 559–570. <https://doi.org/10.1016/j.epsl.2007.10.052>
- Bindeman, I. N., Leonov, V. L., Colón, D. P., Rogozin, A. N., Shipley, N., Jicha, B., et al. (2019). Isotopic and petrologic investigation, and a thermomechanical model of genesis of large-volume rhyolites in arc environments: Karymshina Volcanic Complex, Kamchatka, Russia. *Frontiers in Earth Science*, 6, 238. <https://doi.org/10.3389/feart.2018.00238>
- Bindeman, I. N., Leonov, V. L., Izbekov, P. E., Ponomareva, V. V., Watts, K. E., Shipley, N. K., et al. (2010). Large-volume silicic volcanism in Kamchatka:  $^{40}\text{Ar}/^{39}\text{Ar}$  and U-Pb ages, isotopic, and geochemical characteristics of major pre-Holocene caldera-forming eruptions. *Journal of Volcanology and Geothermal Research*, 189(1–2), 57–80. <https://doi.org/10.1016/j.jvolgeores.2009.10.009>
- Blaauw, M., & Christen, J. A. (2011). Flexible paleoclimate age-depth models using an autoregressive gamma process. *Bayesian Analysis*, 6(3), 457–474. <https://doi.org/10.1214/11-BA618>
- Blockley, S. P., Ramsey, C. B., & Pyle, D. M. (2008). Improved age modelling and high-precision age estimates of late Quaternary tephtras, for accurate palaeoclimate reconstruction. *Journal of Volcanology and Geothermal Research*, 177(1), 251–262. <https://doi.org/10.1016/j.jvolgeores.2007.10.015>
- Blundy, J., & Cashman, K. (2008). Petrologic reconstruction of magmatic system variables and processes. *Reviews in Mineralogy and Geochemistry*, 69(1), 179–239. <https://doi.org/10.2138/rmg.2008.69.6>
- Braitseva, O. A., Melekestsev, I. V., Ponomareva, V. V., & Sulerzhitsky, L. D. (1995). Ages of calderas, large explosive craters and active volcanoes in the Kuril-Kamchatka region, Russia. *Bulletin of Volcanology*, 57(6), 383–402. <https://doi.org/10.1007/BF00300984>

- Braitseva, O. A., Ponomareva, V. V., Sulerzhitsky, L. D., Melekestsev, I. V., & Bailey, J. (1997). Holocene key-marker tephra layers in Kamchatka, Russia. *Quaternary Research*, 47(2), 125–139. <https://doi.org/10.1006/qres.1996.1876>
- Bronk Ramsey, C. (2009a). Bayesian analysis of radiocarbon dates. *Radiocarbon*, 51(1), 337–360. <https://doi.org/10.1017/s0033822200033865>
- Bronk Ramsey, C. (2009b). Dealing with outliers and offsets in radiocarbon dating. *Radiocarbon*, 51(3), 1023–1045. <https://doi.org/10.1017/s0033822200034093>
- Bronk Ramsey, C. B., Housley, R. A., Lane, C. S., Smith, V. C., & Pollard, A. M. (2015). The RESET tephra database and associated analytical tools. *Quaternary Science Reviews*, 118, 33–47. <https://doi.org/10.1016/j.quascirev.2014.11.008>
- Bryant, C. J., Arculus, R. J., & Eggins, S. M. (2003). The geochemical evolution of the Izu-Bonin arc system: A perspective from Tephra recovered by deep-sea drilling. *Geochemistry, Geophysics, Geosystems*, 4(11), 1094. <https://doi.org/10.1029/2002GC000427>
- Bubenshchikova, N., Ponomareva, V., Portnyagin, M., Nürnberg, D., ChaoLembke-Jene, W.-S. L., & Tiedemann, R. (2023). The Pauzhetka tephra (South Kamchatka): A key middle Pleistocene isochron for the Northwest Pacific and Okhotsk Sea sediments. *Quaternary Geochronology*, 79, 101476. <https://doi.org/10.1016/j.quageo.2023.101476>
- Cambay, H., & Cadet, J. P. (1994). Testing global synchronism in peri-Pacific arc volcanism. *Journal of Volcanology and Geothermal Research*, 63(3–4), 145–164. [https://doi.org/10.1016/0377-0273\(94\)90071-X](https://doi.org/10.1016/0377-0273(94)90071-X)
- Cambay, H., & Cadet, J.-P. (1996). Synchronisme de l'activité volcanique d'arc: mythe ou réalité? *Comptes rendus de l'Académie des sciences. Série 2. Sciences de la terre et des planètes*, 322, 237–244.
- Cambay, H., Pubellier, M., Jolivet, L., Pouclet, A., Taylor, B., & Natland, J. (1995). Volcanic activity recorded in deep-sea sediments and the geodynamic evolution of western Pacific island arcs. In B. Taylor & J. Natland (Eds.), *Active margins and marginal basins of the Western Pacific, geophysical monograph series*, 88 (pp. 97–124). American Geophysical Union.
- Cao, L. Q., Arculus, R. J., & McKelvey, B. C. (1995). Geochemistry and petrology of volcanic ashes recovered from sites 881 through 884: A temporal record of Kamchatka and Kurilee volcanism. In D. K. Rea, I. A. Basov, D. W. Scholl, & J. F. Allan (Eds.), *Proceedings of Ocean Drilling Program Science Results*. 145 (pp. 345–381). Ocean Drilling Program. <https://doi.org/10.2973/odp.proc.sr.145.126.1995>
- Channell, J. E., Singer, B. S., & Jicha, B. R. (2020). Timing of Quaternary geomagnetic reversals and excursions in volcanic and sedimentary archives. *Quaternary Science Reviews*, 228, 106114. <https://doi.org/10.1016/j.quascirev.2019.106114>
- Churikova, T., Dorendorf, F., & Wörner, G. (2001). Sources and fluids in the mantle wedge below Kamchatka, evidence from across-arc geochemical variation. *Journal of Petrology*, 42(8), 1567–1593. <https://doi.org/10.1093/ptrology/42.8.1567>
- Churikova, T. G., Gordeychik, B. N., Iwamori, H., NakamuraIshizuka, H. O., Nishizawa, T., Haraguchi, S., et al. (2015). Petrological and geochemical evolution of the Tolbachik volcanic massif, Kamchatka, Russia. *Journal of Volcanology and Geothermal Research*, 307, 156–181. <https://doi.org/10.1016/j.jvolgeores.2015.10.026>
- Cook, E., Portnyagin, M. V., Ponomareva, V. V., Bazanova, L. I., Svensson, A., & Garbe-Schönberg, D. (2018). First identification of cryptotephra from the Kamchatka Peninsula in a Greenland ice core: Implications of a widespread marker deposit that links Greenland to the Pacific northwest. *Quaternary Science Reviews*, 181, 200–206. <https://doi.org/10.1016/j.quascirev.2017.11.036>
- Derkachev, A., Gorbarenko, S., Portnyagin, M., Zhong, Y., Nikolaeva, N. A., Shi, X., & Liu, Y. (2023). Tephrostratigraphy of Pleistocene-Holocene deposits from the Detroit Rise eastern slope (northwestern Pacific). *Frontiers in Earth Science*, 10, 2535. <https://doi.org/10.3389/feart.2022.971404>
- Derkachev, A. N., Gorbarenko, S. A., Ponomareva, V. V., Portnyagin, M. V., Malakhova, G. I., & Liu, Y. (2020). Middle to late Pleistocene record of explosive volcanic eruptions in marine sediments offshore Kamchatka (Meiji Rise, NW Pacific). *Journal of Quaternary Science*, 35(1–2), 362–379. <https://doi.org/10.1002/jqs.3175>
- Derkachev, A. N., Nikolaeva, N. A., Gorbarenko, S. A., Harada, N., Sakamoto, T., Iijima, K., et al. (2012). Characteristics and ages of tephra layers in the central Okhotsk Sea over the last 350 kyr. *Deep Sea Research Part II: Topical Studies in Oceanography*, 61, 179–192. <https://doi.org/10.1016/j.dsr2.2011.05.015>
- Derkachev, A. N., Nikolaeva, N. A., Gorbarenko, S. A., Portnyagin, M. V., Ponomareva, V. V., Nürnberg, D., et al. (2016). Tephra layers of in the Quaternary deposits of the Sea of Okhotsk: Distribution, composition, age and volcanic sources. *Quaternary International*, 425, 248–272. <https://doi.org/10.1016/j.quaint.2016.07.004>
- Derkachev, A. N., Ponomareva, V. V., Portnyagin, M. V., Gorbarenko, S. A., Nikolaeva, N. A., Malakhov, M. I., et al. (2018). Widespread tephra layers in the Bering Sea sediments: Distal clues to large explosive eruptions from the Aleutian volcanic arc. *Bulletin of Volcanology*, 80(11), 1–17. <https://doi.org/10.1007/s00445-018-1254-9>
- Derkachev, A. N., & Portnyagin, M. V. (2013). Marker tephra layers in the late quaternary deposits of the Sea of Okhotsk as evidence of catastrophic eruptions in the Nemo caldera complex (Onekotan Island, Kuril Islands). *Stratigraphy and Geological Correlation*, 21(5), 553–571. <https://doi.org/10.1134/s0869593813040035>
- Dorendorf, F., Churikova, T., Koloskov, A., & Wörner, G. (2000). Late Pleistocene to Holocene activity at Bakening volcano and surrounding monogenetic centers (Kamchatka): Volcanic geology and geochemical evolution. *Journal of Volcanology and Geothermal Research*, 104(1–4), 131–151. [https://doi.org/10.1016/s0377-0273\(00\)00203-1](https://doi.org/10.1016/s0377-0273(00)00203-1)
- Gebhardt, H., Sarnthein, M., Grootes, P. M., Kiefer, T., Kuehn, H., Schmieder, F., & Röhl, U. (2008). Paleonutrient and productivity records from the subarctic North Pacific for Pleistocene glacial terminations I to V. *Paleoceanography*, 23(4), PA4212. <https://doi.org/10.1029/2007PA001513>
- Global Volcanism Program. (2023). Smithsonian Institution. Retrieved from <https://volcano.si.edu/>
- Gorbatov, A., Kostoglodov, V., Suárez, G., & Gordeev, E. I. (1997). Seismicity and structure of the Kamchatka subduction zone. *Journal of Geophysical Research*, 102(B8), 17883–17898. <https://doi.org/10.1029/96jb03491>
- Gusev, A. A. (2008). Temporal structure of the global sequence of volcanic eruptions: Order clustering and intermittent discharge rate. *Physics of the Earth and Planetary Interiors*, 166(3–4), 203–218. <https://doi.org/10.1016/j.pepi.2008.01.004>
- Gusev, A. A., Ponomareva, V. V., Braitseva, O. A., Melekestsev, I. V., & Sulerzhitsky, L. D. (2003). Great explosive eruptions on Kamchatka during the last 10,000 years: Self-similar irregularity of the output of volcanic products. *Journal of Geophysical Research*, 108/B2(B2), 2126. <https://doi.org/10.1029/2001JB000312>
- Holbourn, A., Kiefer, T., Pflaumann, U., & Rothe, S. (2002). *WEPAMA cruise MD 122/IMAGES VII, Rapp. Campagnes Mer OCE/2002/01*. Inst. Polaire Fr. Paul Emile Victor (IPEV).
- Hora, J. M., Singer, B. S., Jicha, B. R., Beard, B. L., Johnson, C. M., de Silva, S., & Salisbury, M. (2010). Volcanic biotite-sanidine <sup>40</sup>Ar/<sup>39</sup>Ar age discordances reflect Ar partitioning and pre-eruption closure in biotite. *Geology*, 38(10), 923–926. <https://doi.org/10.1130/g31064.1>
- Hughes, G. R., & Mahood, G. A. (2008). Tectonic controls on the nature of large silicic calderas in volcanic arcs. *Geology*, 36(8), 627–630. <https://doi.org/10.1130/g24796a.1>
- Ishikawa, T., Tera, F., & Nakazawa, T. (2001). Boron isotope and trace element systematics of the three volcanic zones in the Kamchatka arc. *Geochimica et Cosmochimica Acta*, 65(24), 4523–4537. [https://doi.org/10.1016/s0016-7037\(01\)00765-7](https://doi.org/10.1016/s0016-7037(01)00765-7)

- Jaccard, S. L., Galbraith, E. D., Sigman, D. M., & Haug, G. H. (2010). A pervasive link between Antarctic ice core and subarctic Pacific sediment records over the past 800 kyrs. *Quaternary Science Reviews*, 29(1–2), 206–212. <https://doi.org/10.1016/j.quascirev.2009.10.007>
- Jellinek, A. M., Manga, M., & Saar, M. O. (2004). Did melting glaciers cause volcanic eruptions in eastern California? Probing the mechanics of dike formation. *Journal of Geophysical Research*, 109(B9), B09206. <https://doi.org/10.1029/2004jb002978>
- Jensen, B. J., Davies, L. J., Nolan, C., Pyne-O'Donnell, S., Monteath, A. J., Ponomareva, V., et al. (2021). A latest Pleistocene and Holocene composite tephrostratigraphic framework for northeastern North America. *Quaternary Science Reviews*, 272, 107242. <https://doi.org/10.1016/j.quascirev.2021.107242>
- Jicha, B. R., Scholl, D. W., Singer, B. S., Yagodinski, G. M., & Kay, S. M. (2006). Revised age of Aleutian Island Arc formation implies high rate of magma production. *Geology*, 34(8), 661–664. <https://doi.org/10.1130/g22433.1>
- Jicha, B. R., Singer, B. S., & Sobol, P. (2016). Re-evaluation of the ages of  $^{40}\text{Ar}/^{39}\text{Ar}$  sanidine standards and supereruptions in the western U.S. using a Noblesse multi-collector mass spectrometer. *Chemical Geology*, 431, 54–66. <https://doi.org/10.1016/j.chemgeo.2016.03.024>
- Kawabe, M., & Fujio, S. (2010). Pacific ocean circulation based on observation. *Journal of Oceanography*, 66(3), 389–403. <https://doi.org/10.1007/s10872-010-0034-8>
- Kay, S. M., & Kay, R. W. (1994). Aleutian magmas in space and time. In G. Plafker & H. C. Berg (Eds.), *The geology of Alaska*. Geological Society of America. <https://doi.org/10.1130/DNAG-GNA-G1.687>
- Kelemen, P. B., Yagodinski, G. M., & Scholl, D. W. (2003). Along-strike variations in the Aleutian island arc: Genesis of high Mg# andesite and implications for continental crust. In *Inside the subduction factory, geophysical monograph 138* (pp. 223–276). American Geophysical Union.
- Konstantinovskaia, E. A. (2001). Arc–continent collision and subduction reversal in the Cenozoic evolution of the Northwest Pacific: An example from Kamchatka (NE Russia). *Tectonophysics*, 333(1–2), 75–94. [https://doi.org/10.1016/s0040-1951\(00\)00268-7](https://doi.org/10.1016/s0040-1951(00)00268-7)
- Krashennikov, S. P., Bazanova, L. I., Ponomareva, V. V., & Portnyagin, M. V. (2020). Detailed tephrochronology and composition of major Holocene eruptions from Avachinsky, Kozelsky, and Koryaksky volcanoes in Kamchatka. *Journal of Volcanology and Geothermal Research*, 408, 107088. <https://doi.org/10.1016/j.jvolgeores.2020.107088>
- Kuehn, S. C., Froese, D. G., & Shane, P. A. R. (2011). The INTAV intercomparison of electron-beam microanalysis of glass by tephrochronology laboratories: Results and recommendations. *Quaternary International*, 246(1–2), 19–47. <https://doi.org/10.1016/j.quaint.2011.08.022>
- Kuiper, K. F., Deino, A., Hilgen, F. J., Krijgsman, W., Renne, P. R., & Wijbrans, J. R. (2008). Synchronizing rock clocks of Earth history. *Science*, 320(5875), 500–504. <https://doi.org/10.1126/science.1154339>
- Kutterolf, S., Freundt, A., & Pérez, W. (2008). Pacific offshore record of plinian arc volcanism in Central America: 2. Tephra volumes and erupted masses. *Geochemistry, Geophysics, Geosystems*, 9(2), Q02S02. <https://doi.org/10.1029/2007gc001791>
- Kutterolf, S., Freundt, A., Pérez, W., Mörz, T., Schacht, U., Wehrmann, H., & Schmincke, H. U. (2008). Pacific offshore record of plinian arc volcanism in Central America: 1. Along-arc correlations. *Geochemistry, Geophysics, Geosystems*, 9(2), Q02S01. <https://doi.org/10.1029/2007gc001631>
- Kutterolf, S., Jegen, M., Mitrovica, J. X., Kwasnitschka, T., Freundt, A., & Huybers, P. J. (2013). A detection of Milankovitch frequencies in global volcanic activity. *Geology*, 41(2), 227–230. <https://doi.org/10.1130/G33419.1>
- Kutterolf, S., Schindlbeck, J. C., Jegen, M., Freundt, A., & Straub, S. M. (2019). Milankovitch frequencies in tephra records at volcanic arcs: The relation of kyr-scale cyclic variations in volcanism to global climate changes. *Quaternary Science Reviews*, 204, 1–16. <https://doi.org/10.1016/j.quascirev.2018.11.004>
- Kyle, P. R., Ponomareva, V. V., & Rourke Schlupe, R. (2011). Geochemical characterization of marker tephra layers from major Holocene eruptions, Kamchatka Peninsula, Russia. *International Geology Review*, 53(9), 1059–1097. <https://doi.org/10.1080/00206810903442162>
- Lander, A. V., & Shapiro, M. N. (2007). *The origin of the modern Kamchatka subduction zone* (Vol. 172, pp. 57–64). Washington DC American Geophysical Union Geophysical Monograph Series.
- Larsen, J. F., Neal, C., Schaefer, J., Beget, J., & Nye, C. (2007). *Late Pleistocene and Holocene caldera-forming eruptions of Okmok caldera, Aleutian islands, Alaska* (Vol. 172, pp. 343–364). Washington DC American Geophysical Union Geophysical Monograph Series.
- Lee, J. M., Stern, R. J., & Bloomer, S. H. (1995). Forty million years of magmatic evolution in the Mariana arc: The tephra record. *Journal of Geophysical Research*, 100(B9), 17671–17687. <https://doi.org/10.1029/95jb01685>
- Legros, F. (2000). Minimum volume of a tephra fallout deposit estimated from a single isopach. *Journal of Volcanology and Geothermal Research*, 96(1–2), 25–32. [https://doi.org/10.1016/S0377-0273\(99\)00135-3](https://doi.org/10.1016/S0377-0273(99)00135-3)
- Le Maitre, R. W., Streckeisen, A., Zanetti, B., Le Bas, M. J., Bonin, B., Bateman, P., et al. (Eds.) (2002). *Igneous rocks. A classification and glossary of terms* (p. 236). Cambridge University Press.
- Leonov, V. L., & Grib, E. N. (2004). The structural position and volcanism of the Quaternary Kamchatka calderas. In V. I. Belousov (Ed.), *Vladivostok* (p. 189). Dalnauka Publisher. (in Russian).
- Leonov, V. L., & Rogozin, A. N. (2007). Karymshina, a giant supervolcano caldera in Kamchatka: Boundaries, structure, volume of pyroclastics. *Journal of Volcanology and Seismology*, 1(5), 296–309. <https://doi.org/10.1134/S0742046307050028>
- Lisiecki, L. E., & Raymo, M. E. (2005). A Pliocene–Pleistocene stack of 57 globally distributed benthic  $\delta^{18}\text{O}$  records. *Paleoceanography*, 20(1), PA1003. <https://doi.org/10.1029/2004PA001071>
- Lourens, L., Hilgen, F. J., Shackleton, N. J., Laskar, J., & Wilson, D. (2004). The Neogene period. In F. M. Gradstein, J. G. Ogg, & A. G. Smith (Eds.), *A geologic time scale 2004* (pp. 409–440). Cambridge University Press.
- Masurenkov, Yu.P. (Ed.) (1980). *Volcanic center: Structure, dynamics, and erupted material (Karymsky Structure)* (p. 300). Nauka Publishers. [In Russian].
- McCarron, A. P., Bigg, G. R., Brooks, H., Leng, M. J., Marshall, J. D., Ponomareva, V., et al. (2021). Northwest Pacific ice-rafted debris at 38° N reveals episodic ice-sheet Change in late quaternary Northeast Siberia. *Earth and Planetary Science Letters*, 553, 116650. <https://doi.org/10.1016/j.epsl.2020.116650>
- McDonough, W. F., & Sun, S.-S. (1995). The composition of the Earth. *Chemical Geology*, 120(3–4), 223–253. [https://doi.org/10.1016/0009-2541\(94\)00140-4](https://doi.org/10.1016/0009-2541(94)00140-4)
- Miller, T. P., & Smith, R. L. (1987). Late Quaternary caldera-forming eruptions in the eastern Aleutian arc, Alaska. *Geology*, 15(5), 434–438. [https://doi.org/10.1130/0091-7613\(1987\)15<434:lqceit>2.0.co;2](https://doi.org/10.1130/0091-7613(1987)15<434:lqceit>2.0.co;2)
- Min, K., Mundil, R., Renne, P. R., & Ludwig, K. R. (2000). A test for systematic errors in  $^{40}\text{Ar}/^{39}\text{Ar}$  geochronology through comparison with U/Pb analysis of a 1.1-Ga rhyolite. *Geochimica et Cosmochimica Acta*, 64(1), 73–98. [https://doi.org/10.1016/s0016-7037\(99\)00204-5](https://doi.org/10.1016/s0016-7037(99)00204-5)
- Nowell, D. A., Jones, M. C., & Pyle, D. M. (2006). Episodic quaternary volcanism in France and Germany. *Journal of Quaternary Science*, 21(6), 645–675. <https://doi.org/10.1002/jqs.1005>
- Nye, C. J., Begét, J. E., Layer, P. W., Mangan, M. T., McConnell, V. S., McGimsey, R. G., et al. (2018). Geochemistry of some quaternary lavas from the Aleutian arc and Mt Wrangell: Alaska division of geological & geophysical surveys raw data. File 2018–1, 29. <https://doi.org/10.14509/29843>

- Ogg, J. G. (2012). Geomagnetic polarity time scale. In *The geologic time scale* (pp. 85–113).
- Pearce, J. (1996). Sources and settings of granitic rocks. *Episodes. Journal of International Geoscience*, 19(4), 120–125. <https://doi.org/10.18814/epiugs/1996/v19i4/005>
- Pearce, J. A., Harris, N. B., & Tindle, A. G. (1984). Trace element discrimination diagrams for the tectonic interpretation of granitic rocks. *Journal of Petrology*, 25(4), 956–983. <https://doi.org/10.1093/ptrology/25.4.956>
- Pearce, J. A., & Peate, D. W. (1995). Tectonic implications of the composition of volcanic arc magmas. *Annual Review of Earth and Planetary Sciences*, 23(1), 251–285. <https://doi.org/10.1146/annurev.ea.23.050195.001343>
- Ponomareva, V., Bubenshchikova, N., Portnyagin, M., Zelenin, E., Derkachev, A., Gorbarenko, S., et al. (2018). Large-magnitude Pauzhetka caldera-forming eruption in Kamchatka: Astrochronologic age, composition and tephra dispersal. *Journal of Volcanology and Geothermal Research*, 366, 1–12. <https://doi.org/10.1016/j.jvolgeores.2018.10.006>
- Ponomareva, V., Pendea, I. F., Zelenin, E., Portnyagin, M., Gorbach, N., Pevzner, M., et al. (2021). The first continuous late Pleistocene tephra record from Kamchatka Peninsula (NW Pacific) and its volcanological and paleogeographic implications. *Quaternary Science Reviews*, 257, 106838. <https://doi.org/10.1016/j.quascirev.2021.106838>
- Ponomareva, V., Portnyagin, M., & Davies, S. (2015). Tephra without borders: Far-reaching clues into past explosive eruptions. *Frontiers in Earth Science*, 3. <https://doi.org/10.3389/feart.2015.00083>
- Ponomareva, V. V., Kyle, P. R., Melekestsev, I. V., Rinkleff, P. G., Dirksen, O. V., Sulerzhitsky, L. D., et al. (2004). The 7600 (<sup>14</sup>C) year BP Kuril Lake caldera-forming eruption, Kamchatka, Russia: Stratigraphy and field relationships. *Journal of Volcanology and Geothermal Research*, 136(3–4), 199–222. <https://doi.org/10.1016/j.jvolgeores.2004.05.013>
- Ponomareva, V. V., Portnyagin, M. V., Derkachev, A. N., Juschus, O., Garbe-Schönberg, D., & Nürnberg, D. (2013a). Identification of a widespread Kamchatkan tephra: A middle Pleistocene tie-point between Arctic and Pacific paleoclimatic records. *Geophysical Research Letters*, 40(14), 3538–3543. <https://doi.org/10.1002/grl.50645>
- Ponomareva, V. V., Portnyagin, M. V., Derkachev, A. N., Pendea, I. F., Bourgeois, J., Reimer, P. J., et al. (2013b). Early Holocene M–6 explosive eruption from Plosky volcanic massif (Kamchatka) and its tephra as a link between terrestrial and marine paleoenvironmental records. *International Journal of Earth Sciences*, 102/6(6), 1673–1699. <https://doi.org/10.1007/s00531-013-0898-0>
- Ponomareva, V. V., Portnyagin, M. V., Pendea, I. F., Zelenin, E. A., Bourgeois, J., Pingina, T. K., & Kozhurin, A. I. (2017). A full Holocene tephrochronology for the Kamchatsky Peninsula region: Applications from Kamchatka to North America. *Quaternary Science Reviews*, 168, 101–122. <https://doi.org/10.1016/j.quascirev.2017.04.031>
- Ponomareva, V. V., Portnyagin, M. V., Pevzner, M. M., Blaauw, M., Kyle, P. R., & Derkachev, A. N. (2015). Tephra from andesitic Shiveluch volcano, Kamchatka, NW Pacific: Chronology of explosive eruptions and geochemical fingerprinting of volcanic glass. *International Journal of Earth Sciences*, 104(5), 1459–1482. <https://doi.org/10.1007/s00531-015-1156-4>
- Portnyagin, M. (2023). Detroit tephra dataset, *Mendeley data*, V1. <https://doi.org/10.17632/zckyw7rjkh.1>
- Portnyagin, M., Duggen, S., Hauff, F., Mironov, N., Bindeman, I., Thirlwall, M., & Hoernle, K. (2015). Geochemistry of the late Holocene rocks from the Tolbachik volcanic field, Kamchatka: Quantitative modelling of subduction-related open magmatic systems. *Journal of Volcanology and Geothermal Research*, 307, 133–155. <https://doi.org/10.1016/j.jvolgeores.2015.08.015>
- Portnyagin, M. V., Ponomareva, V. V., Zelenin, E. A., Bazanova, L. I., Pevzner, M. M., Plechova, A. A., et al. (2020). TephraKam: Geochemical database of glass compositions in tephra and welded tuffs from the Kamchatka volcanic arc (northwestern Pacific). *Earth System Science Data*, 12(1), 469–486. <https://doi.org/10.5194/essd-12-469-2020>
- Prueher, L. (2004). Tephrochronology of North Pacific volcanic arcs—data from ODP leg 145. *AGU Fall Meeting Abstracts*, 2004, V21C-V04.
- Prueher, L. M., & Rea, D. K. (1998). Rapid onset of glacial conditions in the subarctic North Pacific region at 2.67 Ma: Clues to causality. *Geology*, 26(11), 1027–1030. [https://doi.org/10.1130/0091-7613\(1998\)026<1027:roogci>2.3.co;2](https://doi.org/10.1130/0091-7613(1998)026<1027:roogci>2.3.co;2)
- Prueher, L. M., & Rea, D. K. (2001). Tephrochronology of the Kamchatka–Kurile and Aleutian arcs: Evidence for volcanic episodicity. *Journal of Volcanology and Geothermal Research*, 106(1–2), 67–84. [https://doi.org/10.1016/S0377-0273\(00\)00266-3](https://doi.org/10.1016/S0377-0273(00)00266-3)
- Pyle, D. M. (1995). Assessment of the minimum volume of tephra fall deposits. *Journal of Volcanology and Geothermal Research*, 69(3–4), 379–382. [https://doi.org/10.1016/0377-0273\(95\)00038-0](https://doi.org/10.1016/0377-0273(95)00038-0)
- Rea, D. K., Basov, I. A., Janecek, T. R., Palmer-Julson, A., & the Shipboard Scientific Party. (1993). *Proceedings of Ocean Drilling Program Initial Reports 145*. Ocean Drilling Program. <https://doi.org/10.2973/odp.proc.ir.145.1993>
- Rostov, I. D., Yurasov, G. I., Rudyh, N. I., Dmitrieva, E. V., & Rostov, V. I. (2002). Oceanographic Atlas of the Bering Sea, Okhotsk Sea and Japan/eaast sea. In *Information resources of V.I. Il'ichev Pacific Oceanological Institute* (Vol. 2). (CD-ROM) (in Russian).
- Rudnick, R. L., & Gao, S. (2003). Composition of the continental crust. In *Treatise on geochemistry*, vol 3 (pp. 1–64). Elsevier Ltd.
- Schindlbeck, J. C., Kutterolf, S., Freundt, A., Alvarado, G. E., Wang, K.-L., Straub, S. M., et al. (2016). Late Cenozoic tephrostratigraphy offshore the southern Central American volcanic arc: 1. Tephra ages and provenance. *Geochemistry, Geophysics, Geosystems*, 17(11), 4641–4668. <https://doi.org/10.1002/2016GC006503>
- Schindlbeck, J. C., Kutterolf, S., Freundt, A., Eisele, S., Wang, K.-L., & Frische, M. (2018). Miocene to Holocene marine tephrostratigraphy offshore northern Central America and southern Mexico: Pulsed activity of known volcanic complexes. *Geochemistry, Geophysics, Geosystems*, 19(11), 4143–4173. <https://doi.org/10.1029/2018GC007832>
- Schindlbeck, J. C., Kutterolf, S., Straub, S. M., Andrews, G. D. M., Wang, K.-L., & Mleneck-Vautravers, M. J. (2018). One million years tephra record at IODP Sites U1436 and U1437: Insights into explosive volcanism from the Japan and Izu arcs. *Island Arc*, 27(3), 12244. <https://doi.org/10.1111/iar.12244>
- Schlitzer, R. (2022). *Ocean data view* [Software]. Retrieved from <https://odv.awi.de/>
- Scholl, D. W., Hein, J. R., Marlow, M., & Buffington, E. C. (1977). Meiji sediment tongue: North Pacific evidence for limited movement between the Pacific and North American plates. *Geological Society of America Bulletin*, 88(11), 1567–1576. [https://doi.org/10.1130/0016-7606\(1977\)88<1567:mstnpe>2.0.co;2](https://doi.org/10.1130/0016-7606(1977)88<1567:mstnpe>2.0.co;2)
- Seligman, A., Bindeman, I., Jicha, B., Ellis, B., Ponomareva, V., & Leonov, V. (2014). Multi-cyclic and isotopically diverse silicic magma generation in an arc volcano: Gorely eruptive center, Kamchatka, Russia. *Journal of Petrology*, 55(8), 1561–1594. <https://doi.org/10.1093/ptrology/egu034>
- Seliverstov, N. I., Torokhov, P. V., & Baranov, B. V. (1995). Submarine Piip Volcano; structural-tectonics control, geological setting, and hydrothermal activity. *Journal of Volcanology and Seismology*, 2, 50–71.
- Selyangin, O. B., & Ponomareva, V. V. (1999). Gorelovsky volcanic center, South Kamchatka: Structure and evolution. *Journal of Volcanology and Seismology*, 21, 163–194.
- Shane, P., & Wright, I. C. (2011). Late quaternary tephra layers around Raoul and Macauley islands, Kermadec arc: Implications for volcanic sources, explosive volcanism and tephrochronology. *Journal of Quaternary Science*, 26(4), 422–432. <https://doi.org/10.1002/jqs.1468>

- Shantser, A. E., & Kraevaya, T. S. (1980). Tumrok range. In K. N. Rudich (Ed.), *Formation series of terrestrial volcanic belt (Late Cenozoic in Kamchatka)* (pp. 33–64). Nauka Publishers. [In Russian].
- Sigurdsson, H. (2000). Volcanic episodes and rates of volcanism. *Encyclopedia of Volcanoes*, 271–279.
- Silleni, A., Giordano, G., Isaia, R., & Ort, M. H. (2020). The magnitude of the 39.8 ka Campanian Ignimbrite eruption, Italy: Method, uncertainties and errors. *Frontiers in Earth Science*, 8, 543399. <https://doi.org/10.3389/feart.2020.543399>
- Singer, B. S., Jicha, B. R., Leeman, W. P., Rogers, N. W., Thirlwall, M. F., Ryan, J., & Nicolaysen, K. E. (2007). Along-strike trace element and isotopic variation in Aleutian Island arc basalt: Subduction melts sediments and dehydrates serpentine. *Journal of Geophysical Research*, 112(B6), B06206. <https://doi.org/10.1029/2006JB004897>
- Straub, S. M. (2003). The evolution of the Izu Bonin-Mariana volcanic arcs (NW Pacific) in terms of major element chemistry. *Geochemistry, Geophysics, Geosystems*, 4(2), 1018. <https://doi.org/10.1029/2002GC000357>
- Straub, S. M., & Layne, G. D. (2003). The systematics of chlorine, fluorine, and water in Izu arc front volcanic rocks: Implications for volatile recycling in subduction zones. *Geochimica et Cosmochimica Acta*, 67(21), 4179–4203. [https://doi.org/10.1016/s0016-7037\(03\)00307-7](https://doi.org/10.1016/s0016-7037(03)00307-7)
- Straub, S. M., Woodhead, J. D., & Arculus, R. J. (2015). Temporal evolution of the Mariana Arc: Mantle wedge and subducted slab controls revealed with a tephra perspective. *Journal of Petrology*, 56(2), 409–439. <https://doi.org/10.1093/ptrology/egv005>
- Tiedemann, R., & Haug, G. H. (1995). Astronomical calibration of cycle stratigraphy for Site 882 in the northwest Pacific. In D. K. Rea, I. A. Basov, D. W. Scholl, & J. F. Allan (Eds.), *Proc. ODP, Sci. Results. 145* (pp. 283–292). Ocean Drilling Program. <https://doi.org/10.2973/odp.proc.sr.145.124.1995>
- van den Bogaard, C., Jensen, B. J. L., Pearce, N. J. G., Froese, D. G., Portnyagin, M. V., Ponomareva, V. V., & Wennrich, V. (2014). Volcanic ash layers in lake El'gygytyn: Eight new regionally significant chronostratigraphic markers for western Beringia. *Climate of the Past*, 10(3), 1041–1062. <https://doi.org/10.5194/cp-10-1041-2014>
- VanLaningham, S., Piasis, N. G., Duncan, R. A., & Clift, P. D. (2009). Glacial–interglacial sediment transport to the Meiji Drift, Northwest Pacific Ocean: Evidence for timing of Beringian outwashing. *Earth and Planetary Science Letters*, 277(1–2), 64–72. <https://doi.org/10.1016/j.epsl.2008.09.033>
- Volynets, A., Churikova, T., Wörner, G., Gordeychik, B., & Layer, P. (2010). Mafic Late Miocene–Quaternary volcanic rocks in the Kamchatka back arc region: Implications for subduction geometry and slab history at the Pacific–Aleutian junction. *Contributions to Mineralogy and Petrology*, 159(5), 659–687. <https://doi.org/10.1007/s00410-009-0447-9>
- Volynets, O. N. (1994). Geochemical types, petrology, and genesis of late Cenozoic volcanic rocks from the Kuril-Kamchatka Island-arc system. *International Geology Review*, 36(4), 373–405. <https://doi.org/10.1080/00206819409465467>
- Volynets, O. N., Ponomareva, V. V., Braitseva, O. A., Melekestsev, I. V., & Chen, C. H. (1999). Holocene eruptive history of Ksudach volcanic massif, South Kamchatka: Evolution of a large magmatic chamber. *Journal of Volcanology and Geothermal Research*, 91(1), 23–42. [https://doi.org/10.1016/s0377-0273\(99\)00049-9](https://doi.org/10.1016/s0377-0273(99)00049-9)
- Wang, W., von Dobeneck, T., Frederichs, T., Zhang, Y., Lembke-Jene, L., Tiedemann, R., et al. (2021). Dating North Pacific Abyssal sediments by geomagnetic paleointensity: Implications of magnetization carriers, plio-pleistocene climate change, and benthic redox conditions. *Frontiers in Earth Science*, 9, 683177. <https://doi.org/10.3389/feart.2021.683177>
- Weeks, R. J., Roberts, A. P., Verosub, K. L., Okada, M., & Dubuisson, G. J. (1995). Magnetostratigraphy of upper Cenozoic sediments from leg 145, North Pacific Ocean. In D. K. Rea, I. A. Basov, D. W. Scholl, & J. F. Allan (Eds.), *Proceedings of the Ocean Drilling Program Scientific results* (Vol. 145, pp. 491–521). Texas A & M University Ocean Drilling Program.
- Werner, R., Hoernle, K., Hauff, F., Portnyagin, M., Yagodinski, G., & Ziegler, A. (2016). *RV SONNE Fahrtbericht/cruise report SO249 BERING–origin and evolution of the Bering Sea: An integrated Geochronological, Volcanological, Petrological and geochemical approach, Leg 1: Dutch Harbor (USA)-Petropavlovsk-Kamchatsky (Russia), 05.06. 2016-15.07. 2016, Leg 2: Petropavlovsk-Kamchatsky (Russia)-Tomakomai (Japan), 16.07. 2016-14.08. 2016. GEOMAR report, N. Ser. 030.* (p. 451). GEOMAR Helmholtz-Zentrum für Ozeanforschung. [https://doi.org/10.3289/GEOMAR\\_REP\\_NS\\_30\\_2016](https://doi.org/10.3289/GEOMAR_REP_NS_30_2016)
- Xiong, X. L., Keppler, H., Audetat, A., Ni, H. W., Sun, W. D., & Li, Y. A. (2011). Partitioning of Nb and Ta between rutile and felsic melt and the fractionation of Nb/Ta during partial melting of hydrous metabasalt. *Geochimica et Cosmochimica Acta*, 75(7), 1673–1692. <https://doi.org/10.1016/j.gca.2010.06.039>
- Yang, Q., Jenkins, S. F., Lerner, G. A., Li, W., Suzuki, T., McLean, D., et al. (2021). The Millennium eruption of Changbaishan Tianchi volcano is VEI 6, not 7. *Bulletin of Volcanology*, 83(11), 1–10. <https://doi.org/10.1007/s00445-021-01487-8>
- Yagodinski, G. M., Brown, S. T., Kelemen, P. B., Vervoort, J. D., Portnyagin, M., Sims, K. W. W., et al. (2015). The role of subducted basalt in the source of island arc magmas: Evidence from Seafloor lavas of the western Aleutians. *Journal of Petrology*, 56(3), 441–492. <https://doi.org/10.1093/ptrology/egv006>

## References From the Supporting Information

- Bassinot, F. C., Labeyrie, L. D., Vincent, E., Quidelleur, X., Shackleton, N. J., & Lancelot, Y. (1994). The astronomical theory of climate and the age of the Brunhes-Matuyama magnetic reversal. *Earth and Planetary Science Letters*, 126(1–3), 91–108. [https://doi.org/10.1016/0012-821x\(94\)90244-5](https://doi.org/10.1016/0012-821x(94)90244-5)
- Berger, A., & Loutre, M. F. (1991). Insolation values for the climate of the last 10 million years. *Quaternary Science Reviews*, 10(4), 297–317. [https://doi.org/10.1016/0277-3791\(91\)90033-q](https://doi.org/10.1016/0277-3791(91)90033-q)
- Channell, J. E. T., Xuan, C., & Hodell, D. (2009). Stacking paleointensity and oxygen isotope data for the last 1.5 Myr (PISO-1500). *Earth and Planetary Science Letters*, 283(1–4), 14–23. <https://doi.org/10.1016/j.epsl.2009.03.012>
- Galbraith, E. D., Kienast, M., Jaccard, S. L., Pedersen, T. F., Brunelle, B. G., Sigman, D. M., & Kiefer, T. (2008). Consistent relationship between global climate and surface nitrate utilization in the western subarctic Pacific throughout the last 500 ka. *Paleoceanography*, 23(2), PA2212. <https://doi.org/10.1029/2007PA001518>
- Dreyfus, G. B., Parrenin, F., Lemieux-Dudon, B., Durand, G., Masson-Delmotte, V., Jouzel, J., et al. (2007). Anomalous flow below 2700 m in the EPICA Dome C ice core detected using  $\delta^{18}\text{O}$  of atmospheric oxygen measurements. *Climate of the Past*, 3(2), 341–353. <https://doi.org/10.5194/cp-3-341-2007>
- Jouzel, J., Masson-Delmotte, V., Cattani, O., Dreyfus, G., Falourd, S., Hoffmann, G., et al. (2007). Orbital and millennial Antarctic climate variability over the past 800,000 years. *Science*, 317(5839), 793–796. <https://doi.org/10.1126/science.1141038>